Retinal photoreceptor patterning during the larval to juvenile transition in Atlantic halibut (*Hippoglossus hippoglossus*)

by

Kennedy Bolstad

BSc. (Hons.), University of Victoria, 2020

Thesis Submitted in Partial Fulfillment of the
Requirements for the Degree of
Master of Science

in the
Department of Biological Sciences
Faculty of Science

SIMON FRASER UNIVERSITY
Fall 2022

Declaration of Committee

Name:	**Kennedy Bolstad**
Degree:	**Master of Science**
Title:	**Retinal photoreceptor patterning during the larval to juvenile transition in Atlantic halibut (*Hippoglossus hippoglossus*)**
Committee:	**Chair: Jenny Cory** Professor, Biological Sciences
	Iñigo Novales Flamarique Supervisor Professor, Biological Sciences
	Julian Christians Committee Member Professor, Biological Sciences
	Norbert Haunerland Committee Member Professor, Biological Sciences
	Gerhard Gries Examiner Professor, Biological Sciences

Abstract

Indirectly developing teleosts, such as flatfishes, have different visual requirements during their larval and juvenile stages. As such, the organization and spectral sensitivity of their retinal photoreceptors differ before and after metamorphosis, yet this transition had not been previously examined. I used Atlantic halibut (*Hippoglossus hippoglossus*) to characterize the spatiotemporal rearrangement and opsin (photosensitive protein) expression of photoreceptors during metamorphosis. The complex reorganization of the larval photoreceptors shifted the area of greatest visual acuity from the ventrotemporal to the dorsotemporal retina. Genome queries followed by immunohistochemistry experiments respectively examined the opsin repertoire of Atlantic halibut, and the distribution of short- and long-wavelength sensitive opsins during this developmental transition. These experiments confirmed that the opsin repertoire of Atlantic halibut is consistent with that of other flatfishes and suggest opsin switching as a mechanism to create new photoreceptor phenotypes during metamorphosis.

Keywords: photoreceptor mosaic; opsin repertoire; retina development; flatfish; metamorphosis

Acknowledgements

I would like to thank Lisa Grebinsky for assistance with data analysis, Ilaria Savelli and the staff previously employed by Scotian Halibut Ltd for raising and collecting the flatfish used in this project, and lab of Dr. John Taylor (University of Victoria) for allowing me to work alongside them.

I would also like to thank the labs of Dr. James Fadool (Florida State University), Dr. Catarina Oliveira (Centro de Ciências do Mar), and Dr. José A. Muñoz-Cueto (University of Cádiz) for welcoming me as a visiting researcher during my degree and for providing feedback on my scientific ideas.

Lastly, I would like to thank my supervisor, Dr. Iñigo Novales Flamarique, whose mentorship, enthusiasm, and wit were invaluable for the completion of this research.

Table of Contents

List of Tables

List of Figures

Chapter 1.

General Introduction

Parts of this chapter have been adapted from the two publications that comprise this thesis:

(1) Bolstad, K., & Novales Flamarique, I. (2022a). Photoreceptor distributions, visual pigments and the opsin repertoire of Atlantic halibut (*Hippoglossus hippoglossus*). *Scientific Reports, 12*: 8062.

(2) Bolstad, K., & Novales Flamarique, I. (2022b). Chromatic organization of retinal photoreceptors during eye migration of Atlantic halibut (*Hippoglossus hippoglossus*). *Journal of Comparative Neurology*, 1-25.

1.1. Spectral sensitivity of the teleost retina

Teleosts can inhabit a broad range of photic environments and display a wide range of foraging preferences; the consequences of this diversity are the demands placed upon their visual systems. As such, their retinas are often specialized to reflect the diversity of their life histories. For example, a common trade-off in the specialization of the retina is between rod photoreceptor and cone photoreceptor densities; the former functions in dim-light environments and its density is often correlated with maximum habitat depth (Hunt *et al*., 2015). Cone photoreceptors allow for vision in brightly lit environments, and their spectral sensitivity can facilitate color discrimination (Ebrey & Koutalos, 2001; Carleton *et al*., 2020).

Photoreceptor spectral sensitivity is primarily modulated through alteration of the dominant visual pigment contained in their outer segments (Ebrey & Koutalos, 2001). These visual pigments are composed of a chromophore (vitamin A_1 or A_2 derivative) and an opsin (G-coupled protein receptor); both can confer spectral sensitivity, however, in teleosts, most variation in light sensitivity is due to opsin type (Hárosi, 1994; Bowmaker, 1995). Within cones, teleost opsins fall into four main classes: short wavelength-sensitive or UV-sensitive (SWS1; λ_{max} = 347- 383 nm) and blue-sensitive (SWS2; λ_{max} = 397- 482 nm), middle wavelength or green-sensitive (RH2, λ_{max} = 452- 537 nm), and

long wavelength or red-sensitive (LWS; λ_{max} = 501- 573 nm). Rhodopsin (RH1; λ_{max} = 447- 525 nm) is only present within rods, however, some deep-sea fishes have multiple copies of the rhodopsin gene (Ebrey & Koutalos, 2001; Musilova *et al*., 2019).

The repertoire of cone opsins in the retinas of fishes differs between species and may change with development and retinal location. For instance, salmonid fishes (genus *Oncorhynchus*) start switching opsin expression in the single cones from SWS1 to SWS2 around the time of first feeding, and this switch progresses from ventral to dorsal retina (Cheng *et al*., 2006; Cheng *et al*., 2007; Cheng & Novales Flamarique, 2007; Novales Flamarique, 2019b). Other opsins (such as RH2, located in one member of double cones) also change over with a preponderance of longer wavelength absorbing subtypes expressed as a function of growth (Novales Flamarique, 2013; Temple et al., 2008). This trend toward expression of longer wavelength-associated opsins with growth is also a feature of development in other fishes including cichlids (Carleton *et al*., 2008; Torres-Dowdall *et al*., 2017), zebrafish (*Danio rerio*) (MacKin *et al*., 2019), and flatfishes (Kasagi et al., 2015; Sato et al., 2021; Savelli et al., 2018). In addition, many species show regional variation in the expression of opsins or their retinal transcripts (Cheng et al., 2006; Cheng & Novales Flamarique, 2007; Dalton *et al*., 2017; Novales Flamarique, 2017; Savelli & Novales Flamarique, 2018; Takechi & Kawamura, 2005; Torres-Dowdall *et al*., 2021), and this is thought to enhance different aspects of vision such as chromatic or achromatic discrimination of targets over different backgrounds.

Further modulation of spectral sensitivity can occur through tandem duplication of opsin genes and subsequent diversification of tuning sites through amino acid substitutions at key protein residues (Yokoyama 2008; Rennison *et al*., 2012; Cortesi *et al*., 2015). This mechanism is widespread throughout teleosts, across freshwater fishes (Chinen *et al*., 2003; Matsumoto *et al*., 2006; Escobar-Camacho *et al*., 2020), pelagic and migratory fishes (Nakamura *et al*., 2013), and even coral reef fishes (Mitchell *et al*., 2021).

1.2. Morphological complexity of the teleost retina

Morphological complexity of the retina is determined through the abundance of single and double cones, the latter of which are formed by two cones apposed together (Lyall, 1957; Ahlbert, 1973). In general, single cones contain a short-wavelength

sensitive opsins (either SWS1 or SWS2), and double cones will either have both cones contain a middle wavelength sensitive opsin (RH2), or one member expressing a long-wavelength sensitive opsin (LWS) (Hárosi, 1994; Yokoyama, 2008).

Light in natural water bodies is reduced in both intensity and spectrum along the horizontal and upwelling directions compared to the downwelling direction (Novales Flamarique & Hawryshyn, 1993; Savelli *et al*., 2018). Small targets, such as unicellular organisms or the zooplankton that many small fish prey upon, would appear as bright targets (reflecting downwelling light) over the horizontal (darker) background in surface waters (Johnsen *et al*., 2011; Novales Flamarique, 2019a; Yoshimatsu *et al*., 2020). This is the basis for the longstanding hypothesis that “offset pigments” improve contrast detection of objects over the veiling background (Lythgoe & Partridge, 1989). As such, single cones with their shorter wavelength visual pigments (which are offset from the dominant background wavelengths) would detect objects of interest over the background, the latter predominantly sensed by double cones. Double cones have therefore been primarily associated with achromatic tasks, such as detection of silhouettes (Novales Flamarique & Wachowiak, 2015), or forming the main inputs to motion perception as shown for zebrafish and goldfish, *Carassius auratus* (Orger & Baier, 2005).

Single and double cones are often arranged in lattice formations with most teleosts that have been examined having a square mosaic lattice. The repeating unit in the square mosaic consists of four double cones surrounding a single (center) cone, with accessory (corner) cones facing the double cone partitions when present (Engström, 1963; Frau *et al*., 2020; Lyall, 1957). Another arrangement is the row mosaic, as exemplified by the retina of the zebrafish, whereby double and single cones form alternating rows (Frau *et al*., 2020; Suliman & Novales Flamarique, 2014). Both intraretinally and between species, the square mosaic can vary in its regularity (Frau *et al*., 2020). Regularity in mosaics has been associated with increased achromatic sensitivity (van der Meer, 1992) if cone packing is enhanced over random mosaics (Frau *et al*., 2020), improved chromatic contrast discrimination if spectral cone phenotypes are also regularly organized (Fernald, 1981; van der Meer, 1992), motion detection (Lyall, 1957; Ahlbert, 1973; Wagner, 1990; van der Meer, 1992) and enhanced visual acuity (Engström, 1963, Frau *et al*., 2020). Despite the importance of these mosaics, the developmental mechanisms governing their formation are largely unknown.

1.3. Flatfishes: indirectly developing species as a model for the developing retina

Fishes with indirect development (i.e., species that undergo a pronounced metamorphosis where the larva and adult have very different form) that experience a transition from pelagic to demersal habitats (Evans & Fernald, 1990) can have pronounced retinal transformations, often involving changes in the spectral absorbance of photoreceptors and their spatial re-organization (Shand *et al.*, 1999, 2001; Evans & Fernald, 1993; Evans *et al*., 1993; Hoke *et al*., 2006). During the larval stages of these fishes, single cones dominate the retina and are arranged in a honeycomb mosaic (i.e., a centre single cone surrounded by six other single cones) (Kvenseth *et al*., 1996; Shand *et* al., 1999; Hoke *et al*., 2006). As development progresses, these fishes transform their retinas into their juvenile retinal mosaics (e.g., square mosaic). Due to this transition, these fishes can provide evidence for mechanisms governing the formation of these diverse retinal organizations. Flatfishes (order Pleuronectiformes), an indirectly developing species, are therefore powerful models for understanding the dynamics of a developing retina- both in terms of morphological transformations and chromatic organization.

In this thesis, I use Atlantic halibut (*Hippoglossus hippoglossus*) as a model for flatfish retinal development. I examine the spatiotemporal organization of photoreceptors and their chromatic organization during their developmental transition.

In Chapter 2, I examine the spatiotemporal organization of photoreceptors during their developmental transition and predict an opsin repertoire for this species. In Chapter 3, I describe the chromatic organization of these photoreceptors as they progress from larval to juvenile stages and hypothesize mechanisms for square mosaic formation.

1.4. References

Ahlbert, I. (1973). Ontogeny of double cones in the retina of perch fry (*Perca fluviatilis*, Teleostei). *Acta Zoologica*, *54*(4), 241–254.

Bowmaker, J. (1995). The visual pigments of fish. *Progress in Retinal and Eye Research*, *15*(1), 1–31.

Carleton, K. L., Spady, T. C., Streelman, J. T., Kidd, M. R., McFarland, W. N., & Loew, E. R. (2008). Visual sensitivities tuned by heterochronic shifts in opsin gene expression. *BMC Biology*, *6*, 22.

Carleton, K. L., Escobar-Camacho, D., Stieb, S. M., Cortesi, F., & Marshall, N. J. (2020). Seeing the rainbow: Mechanisms underlying spectral sensitivity in teleost fishes. *Journal of Experimental Biology*, *223*(8), jeb193334.

Cheng, C. L., & Flamarique, I. N. (2007). Chromatic organization of cone photoreceptors in the retina of rainbow trout: Single cones irreversibly switch from UV (SWS1) to blue (SWS2) light sensitive opsin during natural development. *Journal of Experimental Biology*, *210*(23), 4123–4135.

Cheng, C. L., Flamarique, I. N., Hárosi, F. I., Rickers-Haunerland, J., & Haunerland, N. H. (2006). Photoreceptor layer of salmonid fishes: Transformation and loss of single cones in juvenile fish. *Journal of Comparative Neurology*, *495*(2), 213–235.

Cheng, C. L., Gan, K. J., & Flamarique, I. N. (2007). The ultraviolet opsin is the first opsin expressed during retinal development of salmonid fishes. *Investigative Ophthalmology & Visual Science*, *48*(2), 866–873.

Chinen, A., Hamaoka, T., Yamada, Y., & Kawamura, S. (2003). Gene duplication and spectral diversification of cone visual pigments of zebrafish. *Genetics*, *163*(2), 663–675.

Cortesi, F., Musilová, Z., Stieb, S. M., Hart, N. S., Siebeck, U. E., Malmstrøm, M., Tørresen, O. K., Jentoft, S., Cheney, K. L., & Marshall, N. J. (2015). Ancestral duplications and highly dynamic opsin gene evolution in percomorph fishes. *Proceedings of the National Academy of Sciences*, *112*(5), 1493–1498.

Dalton, B. E., De Busserolles, F., Marshall, N. J., & Carleton, K. L. (2017). Retinal specialization through spatially varying cell densities and opsin coexpression in cichlid fish. *Journal of Experimental Biology*, *220*(2), 266–277.

Ebrey, T., & Koutalos, Y. (2001). Vertebrate photoreceptors. *Progress in Retinal and Eye Research*, *20*(1), 49–94.

Engström, K. (1963). Cone types and cone arrangements in teleost retinae. *Acta Zoologica*, 44, 179–243.

Escobar-Camacho, D., Carleton, K. L., Narain, D. W., & Pierotti, M. E. (2020). Visual pigment evolution in Characiformes: The dynamic interplay of teleost whole-genome duplication, surviving opsins and spectral tuning. *Molecular Ecology*, *29*(12), 2234–2253.

Evans, B. I., & Fernald, R. D. (1990). Metamorphosis and fish vision. *Journal of Neurobiology*, *21*(7), 1037–1052.

Evans, B. I., Hárosi, F. I., & Fernald, R. D. (1993). Photoreceptor spectral absorbance in larval and adult winter flounder (*Pseudopleuronectes americanus*). *Visual Neuroscience*, *10*(6), 1065–1071.

Frau, S., Novales Flamarique, I., Keeley, P. W., Reese, B. E., & Muñoz-Cueto, J. A. (2020). Straying from the flatfish retinal plan: Cone photoreceptor patterning in the common sole (*Solea solea*) and the Senegalese sole (*Solea senegalensis*). *Journal of Comparative Neurology*, *528*(14), 2283–2307.

Hárosi, F. I. (1994). An analysis of two spectral properties of vertebrate visual pigments. *Vision Research*, *34*(11), 1359–1367.

Hoke, K. L., Evans, B. I., & Fernald, R. D. (2006). Remodeling of the cone photoreceptor mosaic during metamorphosis of flounder (*Pseudopleuronectes americanus*). *Brain, Behavior and Evolution*, *68*(4), 241–254.

Hunt, D., Rawlinson, N., Thomas, G., & Cobcroft, J. M. (2015). Investigating photoreceptor densities, potential visual acuity, and cone mosaics of shallow water, temperate fish species. *Vision Research*, *111*, 13–21.

Johnsen, S., Marshall, N. J., & Widder, E. A. (2011). Polarization sensitivity as a contrast enhancer in pelagic predators: Lessons from in situ polarization imaging of transparent zooplankton. *Philosophical Transactions of the Royal Society B: Biological Sciences*, *366*, 655–670.

Kasagi, S., Mizusawa, K., Murakami, N., Andoh, T., Furufuji, S., Kawamura, S., & Takahashi, A. (2015). Molecular and functional characterization of opsins in barfin flounder (*Verasper moseri*). *Gene*, *556*(2), 182–191.

Lythgoe, J. N., & Partridge, J. C. (1989). Visual pigments and the acquisition of visual information. *Journal of Experimental Biology*, *146*, 1–20.

Mackin, R. D., Frey, R. A., Gutierrez, C., Farre, A. A., Kawamura, S., Mitchell, D. M., & Stenkamp, D. H. (2019). Endocrine regulation of multichromatic color vision. *Proceedings of the National Academy of Sciences of the United States of America*, *116*, 16882–16891.

Matsumoto, Y., Fukamachi, S., Mitani, H., & Kawamura, S. (2006). Functional characterization of visual opsin repertoire in Medaka (*Oryzias latipes*). *Gene*, *371*(2), 268–278.

Mitchell, L. J., Cheney, K. L., Lührmann, M., Marshall, J., Michie, K., & Cortesi, F. (2021). Molecular evolution of ultraviolet visual opsins and spectral tuning of photoreceptors in anemonefishes (Amphiprioninae). *Genome Biology and Evolution*, *13*(10), evab184.

Musilova, Z., Cortesi, F., Matschiner, M., Davies, W. I., Patel, J. S., Stieb, S. M., de Busserolles, F., Malmstrøm, M., Tørresen, O. K., & Brown, C. J. (2019). Vision using multiple distinct rod opsins in deep-sea fishes. *Science*, *364*(6440), 588–592.

Nakamura, Y., Mori, K., Saitoh, K., Oshima, K., Mekuchi, M., Sugaya, T., Shigenobu, Y., Ojima, N., Muta, S., & Fujiwara, A. (2013). Evolutionary changes of multiple visual pigment genes in the complete genome of Pacific bluefin tuna. *Proceedings of the National Academy of Sciences*, *110*(27), 11061–11066.

Novales Flamarique, I. (2017). A vertebrate retina with segregated colour and polarization sensitivity. *Proceedings of the Royal Society B: Biological Sciences*, *284*, 20170759.

Novales Flamarique, I. (2019a). Swimming behaviour tunes fish polarization vision to double prey sighting distance. *Scientific Reports*, *9*(1), 1–8.

Novales Flamarique, I. (2019b). Light exposure during embryonic and yolksac alevin development of Chinook salmon *Oncorhynchus tshawytscha* does not alter the spectral phenotype of photoreceptors. *Journal of Fish Biology*, *95*, 214–221.

Novales Flamarique, I., & Hawryshyn, C. W. (1993). Spectral characteristics of salmonid migratory routes from southern Vancouver Island (British Columbia). Canadian Journal of Fisheries and Aquatic Sciences, *50*, 1706–1716.

Novales Flamarique, I., &Wachowiak, M. (2015). Functional segregation of retinal ganglion cell projections to the optic tectum of rainbow trout. *Journal of Neurophysiology*, *114*, 2703–2717.

Orger,M. B., & Baier, H. (2005). Channeling of red and green cone inputs to the zebrafish optomotor response. *Visual Neuroscience*, *22*, 275–281.

Rennison, D. J., Owens, G. L., & Taylor, J. S. (2012). Opsin gene duplication and divergence in ray-finned fish. *Molecular Phylogenetics and Evolution*, *62*(3), 986–1008.

Sato, I., Kasagi, S., Takahashi, A., & Mizusawa, K. (2021). Expression dynamics of visual opsin genes in marbled sole *Pseudopleuronectes yokohamae* during metamorphosis from the larval to the juvenile stage. *Gene*, *787*, 145622.

Savelli, I., & Flamarique, I. N. (2018). Variation in opsin transcript expression explains intraretinal differences in spectral sensitivity of the northern anchovy. *Visual Neuroscience*, *35,* E005.

Savelli, I., Flamarique, I. N., Iwanicki, T., & Taylor, J. S. (2018). Parallel opsin switches in multiple cone types of the starry flounder retina: Tuning visual pigment composition for a demersal life style. *Scientific Reports*, *8*(1), 1–10.

Shand, J., Archer, M. A., & Collin, S. P. (1999). Ontogenetic changes in the retinal photoreceptor mosaic in a fish, the black bream, *Acanthopagrus butcheri*. *Journal of Comparative Neurology*, *412*(2), 203–217.

Shand, J., Archer, M.A., Thomas, N., & Cleary, J. (2001). Retinal development of West Australian dhufish, *Glaucosoma hebraicum*. *Visual Neuroscience*, *18*(5), 711.

Takechi, M., & Kawamura, S. (2005). Temporal and spatial changes in the expression pattern of multiple red and green subtype opsin genes during zebrafish development. *Journal of Experimental Biology*, *208*(7), 1337–1345.

Temple, S., Veldhoen, K., Phelan, J., Veldhoen, N., & Hawryshyn, C. (2008). Ontogenetic changes in photoreceptor opsin gene expression in coho salmon (*Oncorhynchus kisutch*, Walbaum). *Journal of Experimental Biology*, *211*(24), 3879–3888.

Torres-Dowdall, J., Pierotti, M. E. R., Härer, A., Karagic, N.,Woltering, J. M., Henning, F., Elmer, K. R., & Meyer, A. (2017). Rapid and parallel adaptive evolution of the visual system of neotropical midas cichlid fishes. *Molecular Biology & Evolution*, *34*, 2469–485.

Torres-Dowdall, J., Karagic, N., Härer, A., & Meyer, A. (2021). Diversity in visual sensitivity across Neotropical cichlid fishes via differential expression and intraretinal variation of opsin genes. *Molecular Ecology*, *30*(8), 1880–1891.

Yoshimatsu, T., Schröder, C., Nevala, N. E., Berens, P., & Baden, T. (2020). Fovea-like photoreceptor specializations underlie single UV cone driven prey-capture behavior in zebrafish. *Neuron*, *107*(2), 320–337.

Chapter 2.

Photoreceptor distributions, visual pigments and the opsin repertoire of Atlantic halibut (*Hippoglossus hippoglossus*)

This chapter was adapted from Bolstad, K., & Novales Flamarique, I. (2022a). Photoreceptor distributions, visual pigments and the opsin repertoire of Atlantic halibut (*Hippoglossus hippoglossus*). *Scientific Reports, 12*: 8062.

The microspectrophotometry data used in this thesis was obtained from Dr. Novales Flamarique.

Abstract

Fishes often have cone photoreceptors organized in lattice-like mosaic formations. In flatfishes, these lattices undergo dramatic changes during metamorphosis whereby a honeycomb mosaic of single cones in the larva is replaced by a square mosaic of single and double cones in the adult. The spatiotemporal dynamics of this transition are not well understood. Here, we describe the photoreceptors and mosaic formations that occur during the larva to juvenile transition of Atlantic halibut from the beginning of eye migration to its completion. To gauge the possibility of colour vision, visual pigments in juveniles were measured by microspectrophotometry and the opsin repertoire explored using bioinformatics. At the start of eye migration, the larva had a heterogeneous retina with honeycomb mosaic in the dorsonasal and ventrotemporal quadrants and a square mosaic in the ventronasal and dorsotemporal quadrants. By the end of metamorphosis, the square mosaic was present throughout the retina except in a centrodorsotemporal area where single, double and triple cones occurred randomly. Six cone visual pigments were found with maximum absorbance (λmax, in nm) in the short [S(431) and S(457)], middle [M(500), M(514) and M(527)], and long [L(559)] wavelengths, and a rod visual pigment with λmax at 491 nm. These pigments only partially matched the opsin repertoire detected by query of the Atlantic halibut genome. We conclude that the Atlantic halibut undergoes a complex re-organization of photoreceptors at metamorphosis resulting in a multi-mosaic retina adapted for a demersal lifestyle.

2.1. Introduction

Flatfishes are peculiar among teleosts in that they undergo a pronounced metamorphosis whereby a bilaterally symmetric, pelagic larva transforms into a flattened, demersal juvenile with both eyes on the same side of the head (Bao *et al*., 2011; Suzuki & Tanaka 2015). During this period of transformation, which can last from days to weeks depending on the species (Geffen *et al*., 2007), the animal experiences a progressive change in the perception of its surroundings resulting from the shifting visual fields of both eyes and increasing proximity to the ocean floor. In parallel, the diet changes from a preponderance of pelagic plankton consumed by pre-metamorphic larvae to small benthic invertebrates favoured by post-metamorphic juveniles (Geffen *et al*., 2007).

Despite these profound alterations to the anatomy and ecology of flatfishes, their visual system during metamorphosis has seldom been examined and is poorly understood. Morphological investigations into the larval retina of winter flounder, *Pseudopleronectes americanus*, and Atlantic halibut have shown the presence of a single morphological type of cone photoreceptor prior to the start of eye migration, arranged in a honeycomb mosaic (Evans & Fernald, 1993; Kvenseth *et al*., 1996). Post-metamorphosis, retinas from both species contain rod photoreceptors and two morphological cone photoreceptor types (single, double), the latter of which are arranged in a square mosaic (Evans & Fernald, 1993; Kvenseth *et al*., 1996).

To determine the origination of double cones during retina development of winter flounder, tritiated (^{3}H) thymidine was used to label dividing cells prior to photoreceptor rearrangement (Hoke *et al*., 2006). These authors concluded that double cones central to the peripheral growth zone should form from coalescing single cones (Hoke *et al*., 2006). As such, two mechanisms of square mosaic formation would exist during metamorphosis of flatfishes: one operating at the peripheral growth zone producing a square mosaic from differentiation of progenitor cells, and the other more centrally, requiring the re-arrangement of pre-existing, differentiated single cones.

Like other teleosts, flatfishes have several duplicated opsins; for example, barfin flounder (*Verasper moseri*), marbled sole (*Pseudopleuronectes yokohamae*), and Japanese flounder (*Paralichthys olivaceus*) all have two copies of the *sws2* gene (i.e.,

sws2a and *sws2b*) (Kasagi *et al*., 2015; Kasagi *et* al., 2018; Sato *et al*., 2021). Interestingly, a subtype of the *rh2* gene, *rh2a*, is not present across all flatfishes: turbot (*Scophthalmus maximus*) and Japanese flounder have two copies of the *rh2a* gene, marbled sole has one copy, barfin flounder has a *rh2a* pseudogene, and the gene is entirely absent in spotted halibut (*Verasper variegatus*) (Wang *et al*., 2021; Sato *et al*., 2021; Kasagi *et al*., 2015; Kasagi *et al*., 2018). The published opsin repertoire for Atlantic halibut stands out from other flatfishes, as it does not have any reported opsin duplicates (Helvik *et al*., 2001b), yet it is not known if this is due to sampling method (i.e., identification of opsin sequences prior to a published genome) or if this has biological significance. Once the full opsin repertoire of Atlantic halibut is identified, we can better understand how the chromatic expression of photoreceptors may change during metamorphosis (Chapter 3).

This study was undertaken to reveal the morphological organization of photoreceptors during the larval to juvenile transition of Atlantic halibut, from the start of eye migration to its completion. Combining these observations and morphometric measures of the lens, the spatial resolving power was derived for different regions of the retina. Microspectrophotometric measurements of visual pigment absorbance from post-metamorphic fish and opsin bioinformatic analyses were also undertaken to gain insight into photoreceptor chromatic diversity and opsin evolution with respect to other flatfishes.

2.2. Methods

2.2.1. Fish husbandry and collections

Atlantic halibut were reared from the fertilized egg in 100 L recirculating saltwater indoor tanks at a temperature of 7.5 ± 1.6°C and maintained under artificial illumination (λ range: 350-750 nm, irradiance: 1.2 x 1015 photons $m^{-2}s^{-1}$) provided by tungsten-halogen tubes (Scotian Halibut Ltd, Nova Scotia, Canada). Peak hatching occurred at 14 days post-fertilization [~ 90 Accumulated Temperature Units (ATUs), calculated as the product of days from fertilization and mean water temperature]. Hatched larvae had a prominent yolk sac which was fully absorbed around 50 days post-hatching (~ 320 ATUs). Pre-metamorphic larvae were fed a combination of freeze-dried Gemma Diamond, 0.5 and 0.8 mm pellets (Skretting), added every 30 minutes throughout the

day at a density of 2 pellets per fish, and *Artemia* nauplii, added twice a day at a density of 10-15 metanauplii $ml^{-1}day^{-1}$. Fish nearing complete metamorphosis, or having completed it, were fed a mixture of Gemma Diamond 0.8, 1.0 and 1.2 mm every hour at a density of 3 pellets per fish and *Artemia* nauplii twice a day at a density of 5 to 10 metanauplii $ml^{-1}day^{-1}$. Clay was added to the tanks every day to recreate the turbid water conditions found in nature.

Collections of specimens took place at 82, 89, 96 and 103 days post-hatching, corresponding to 720, 773, 825 and 878 ATU. At each stage, fish were collected in the light-adapted state for *in-situ* hybridization analyses and, separately, for morphological observations. At 720 ATU, eye migration had just started in the majority of fish examined and, by 878 ATU, metamorphosis was complete (Fig. 2.1). In addition to these collections at the aquaculture facility, post-metamorphic juvenile fish were flown live to the University of Victoria aquatic facility (British Columbia, Canada) for measurements of visual pigment absorbance by microspectrophotometry. The study is reported in accordance with ARRIVE guidelines.

All holding and experimental procedures were carried out in accordance with Canadian Council for Animal Care guidelines and were approved by the Animal Care committees of Simon Fraser University (protocol # 1126B-10) and the University of Victoria (protocol # 2017-005).

2.2.2. Histology

Fish were euthanized and the entire bodies fixed in primary fixative (2.5% glutaraldehyde, 1% paraformaldehyde in 0.08 M PBS, pH = 7.4) at 4ºC for a minimum of 72 hrs. The retina from the migrating and non-migrating eye was individually extracted, rinsed in 0.08 M PBS, and cut into four quadrants (ventrotemporal, VT; ventronasal, VN; dorsonasal, DN; and dorsotemporal, DT). The quadrants were post-fixed in secondary fixative (1% osmium tetroxide in 0.08 M PBS) for 1 hr at 4ºC. Following a brief rinse in distilled water, the tissue was dehydrated through a series of solutions of increasing ethanol concentration, infiltrated with mixtures of propylene oxide and EPON resin, and embedded in 100% EPON resin. Retinal blocks were cut tangentially, in 1-2 µm steps, and stained with Richardson's solution (1:1 mixture of 1% Azure II in dH_2O and 1% Methylene blue in 1% NaB_4O_7) to reveal the cone mosaic (de Busserolles *et al*., 2021;

Hárosi, 1994). Digital images of sections were acquired with an E-600 Nikon microscope equipped with a DXM-100 digital camera. Photographs were obtained using a Plan/Apo 60X/1.40 objective and further amplified 1.5x with an optical tourette on the microscope (total magnification 90x). Observations of mosaic types in different sectors were carried out on 10 retinas (5 each from migrating and non-migrating eyes). From these, four retinas with the largest tangential mosaic area (0.0106 mm^{-2}) spanning the region of widest cone ellipsoid cross sections to the bases of the outer segments were selected for density determinations and spatial analyses.

2.2.3. Morphometric analysis

Digital micrographs of tangential sections, each covering a 52 x 52 μm^2 area, were analyzed with Photoshop (Adobe Systems) to extract the X-Y coordinates (centroids) of every morphological cone type in the field of view. The coordinates were then imported into a customized Matlab program that computed the Delauney tessellation of the field, from which the nearest neighbour distance of each individual cell was determined, as was their Voronoi domain area (i.e., the area surrounding each cell that encloses the territory closer to that cell than to any of the neighbours) (Reese and Keeley, 2015). Each analysis excluded “border cells”, i.e., those with uncertain nearest neighbour distances or Voronoi domain areas. In each case, the regularity index was defined as the mean divided by the standard deviation.

To assess whether the cone distributions analyzed had higher order (lattice-like) periodicity, a spatial auto-correlation analysis was carried out that examined the positioning of each cell with respect to all other cells across the mosaic. The Density Recovery Profile was derived from each autocorrelogram, providing a plot of the mean density of cells as a function of distance from each cell. The autocorrelogram permits the detection of higher order patterning and the Density Recovery Profile provides a measure of the exclusion zone surrounding each cell where other homotypic cells are less likely to be found than at further distances (Reese & Keeley, 2015).

To assess whether cell distributions with low regularity indices were different from random distributions, their spatial statistics were compared to those of simulated random fields of cells matched for density and constrained by soma size. Non-random retinal mosaics of cells show greater regularity indices and exclusion zones to those

from corresponding random simulations resulting in effective radii that are larger than if determined by soma size alone (Keeley *et al*., 2020).

Statistical analyses to assess differences in mosaic regularity and cone density between retinal sectors were based on analysis of variance (ANOVA) with post-hoc grouping tests (Student-Neuman-Keuls, Tukey HSD) evaluated at $\alpha = 0.05$ level of significance.

2.2.4. Visual acuity

Theoretical determinations of spatial resolving power (in degrees of arc) were calculated as the inverse of the Nyquist frequency (f_N) (in cycles per degree) using the equation:

$$f_N = (\pi * PND/360^o) * (2*D/(3)^{1/2})^{1/2}$$

where D is the photoreceptor cell density (in mm^{-2}) and PND is the posterior nodal distance (in mm) (Fritsch *et al*., 2017). PND was approximated as the product of lens radius and 2.55 (the mean Matthiessen's ratio for teleost eyes (Shand *et al*., 1999a)). The photoreceptor cell density was computed from the sum of all cone types measured in a 0.0106 mm^{-2} area, with each double cone and triple cone contributing two and three cells, respectively. Based on the resolving power, the distance at which a given region of the retina would detect a 0.5 mm size food item, such as the typical food pellet encountered in aquaculture conditions or prey copepod consumed in nature, was computed.

2.2.5. Microspectrophotometry

This analysis was performed on four post-metamorphic juveniles with mean weight ± SD and total length ± SD of 3.6 ± 0.8 g and 7.5 ± 0.5 cm, respectively. Individual fish were dark adapted for 8 hours, following which the fish was euthanized, and the retina extracted under infrared illumination. Small pieces of retina were teased apart and prepared for viewing with the dichroic microspectrophotometer (DMSP) as per previous studies (Hárosi, 1987; Novales Flamarique & Hárosi, 2000; Novales Flamarique & Hárosi, 2002). The DMSP is a computer-controlled, wavelength-scanning, single-beam photometer that simultaneously records average and polarized transmitted

light fluxes through microscopic samples (Hárosi, 1987; Novales Flamarique & Hárosi, 2002). The DMSP was equipped with ultrafluar (Zeiss) objectives: 32/0.4 for the condenser and 100/1.20 for the objective. With the aid of reference measurements recorded through cell-free areas, individual photoreceptor outer segments were illuminated sideways with a measuring beam of rectangular cross section of ca. 2 x 0.6 μm. Absolute absorbance spectra were computed in 2 nm increments from the obtained transmittances (each spectrum consisted of an average of 8 scans). The solid spectra (fits) were derived from experimental data by Fourier filtering (Novales Flamarique & Hárosi, 2000).

2.2.6. Analysis of spectra consisting of multiple visual pigments

Because the S(431) absorbance spectrum showed a “hump” in the range 450-550 nm, suggesting the presence of multiple visual pigments, the Simplex algorithm (Caceci *et al*., 1984) was used to fit the data with a combination of visual pigment absorbance curves using the equation (Sirovich *et al*., 1977):

$$R = [k_i A_i^p (\lambda)]^{1/p}$$

where R is the response (overall absorbance) function, A_i^p is the absorbance of pigment i at light of wavelength λ, and p is an exponent resulting from the mathematical requirement that the absorbance function to be fitted be differentiable at the origin (Sirovich *et al*., 1977). The variables k_i are coupling constants resulting from the best fit of the model to the data. The visual pigment absorbance values used in the model were generated with an eighth-order polynomial template (Palacios *et al*., 1996) based on the λ_{max} of visual pigments measured by microspectrophotometry. The use of templates ensures β-band representation of individual visual pigments, which is not always present in microspectrophotometry records.

2.2.7. Genomic analyses

Zebrafish visual opsins (Table A1) were used as query sequences to search predicted proteins from the reference genome of Atlantic halibut (Einfeldt *et al*., 2021) (NCBI *Hippoglossus hippoglossus* Annotation Release 100; GCF_009819705.1) using BLASTp (v.2.12.0). Predicted proteins with e-values < 1e-5 and percent identities ≥ 50%

were retained and duplicated results were filtered by accession number using R (v.4.1.0) (R Core Team, 2021) and RStudio (v.1.4.1717) (RStudio Team, 2021) (Table A2). Locations of the corresponding coding sequences and their immediate flanking genes were compared to those in the reference genomes of turbot (NCBI *Scophthalmus maximus* Annotation Release 100; GCF_013347765.1) (Figueras *et al*., 2016)[51] and zebrafish (NCBI *Danio rerio*, GRCz11, NCBI Annotation Release 106; GCF_000002035.6) and used to further narrow down the predicted opsins using the NCBI Genome Browser and Gene Graphics (Harrison *et al*., 2018). Coding sequences that were eliminated from further analysis can be found in Table A3 with the corresponding justification.

To confirm the assigned opsin classes of the predicted proteins, opsin sequences reported previously (Helvik *et al*., 2001b) were used to query the subset of predicted Atlantic halibut proteins using BLASTp, and sequences with an e-value < 1e-5 and a percent identity ≥ 70% were retained. To confirm that the predicted proteins were visual opsins, a multiple sequence alignment was performed that incorporated visual zebrafish opsins and non-visual zebrafish and Atlantic halibut opsins (Table A4). Visual opsins were distinguished from non-visual opsins by their identity at key amino acid sites (Davies *et al*., 2015). All multiple alignments were performed and edited using ClustalX (v.2.0) (Larkin *et al*., 2007) and Qiagen CLC Sequence Viewer (v.8.0) (www.qiagenbioinformatics.com). Amino acid residue numbers were standardized to bovine rhodopsin (Accession: NP_001014890.1) (Palczewski *et al*., 2000).

The predicted Atlantic halibut opsins were assigned to opsin subclasses using phylogenetic analyses and tuning sites from key amino acid residues for each of the visual opsins (Musilova *et al*, 2019; Wang *et al*., 2021; Yokoyama, 2008; Nakamura *et al*., 2013). Phylogenetic trees were constructed with MEGAX (Kumar *et al*., 2018) using maximum likelihood and boostrap analyses (n=100) and visualized using R and ggtree (R Core Team, 2021; R Studio Team, 2021; Yu *et al*., 2017). Sequences used in these analyses (Tables A1, A5) were obtained from GenBank (https://www-ncbi-nlm-nih-gov.proxy.lib.sfu.ca/genbank) and SoleaDB (Benzekri *et al*., 2014), with zebrafish VA opsins used as the outgroup.

2.3. Results

2.3.1. Eye morphology and migration

The youngest Atlantic halibut examined (96 days post-fertilization or 720 ATU) were bilaterally quasi-symmetrical with a compressed, oval shaped body and similar pigmentation on either side of the body (Fig. 2.1 A,E). In the majority of animals examined (6 of 10), one of the eyes (usually the left eye) had recently started migrating as evidenced by its slightly closer proximity to the midline with respect to the other eye (Fig. 2.1 E). Migration of the eye proceeded throughout the study period (Fig. 2.1 A-D) such that between 773 and 825 ATU (i.e., 103 and 110 days post-fertilization, respectively) the migrating eye had reached the mid-line (Fig. 2.1 C,F) or proceeded beyond, to the other side of the head. The oldest halibut examined (878 ATU, or 117 days post-fertilization) had both eyes on the same side of the head (the ocular side, Fig. 2.1 D,G) whereas the opposite side (the blind side) rested on the bottom and had reduced pigmentation.

All fish examined had elliptically shaped eyes and retinas (Fig. 2.1). The eye dimensions increased from a mean ± SD (n =10) of 1.6 ± 0.18 mm for the long axis and 1.3 ± 0.11 mm for the short axis at 720 ATU to 2.2 ± 0.13 mm and 1.6 ± 0.15 mm, respectively, at 878 ATU. The mean lens diameter ± SD (n =10) increased from 0.44 ± 0.04 mm to 0.64 ± 0.02 mm during the same time period. The extracted retinas showed an embryonic fissure that projected from the medial ventral periphery to the central retina (location of the optic nerve head) pointing slightly to the temporal retina. The optic nerve head was localized in the ventral half of the retina (Fig. 2.1 G), below the theoretical crossing of short and long retinal axes.

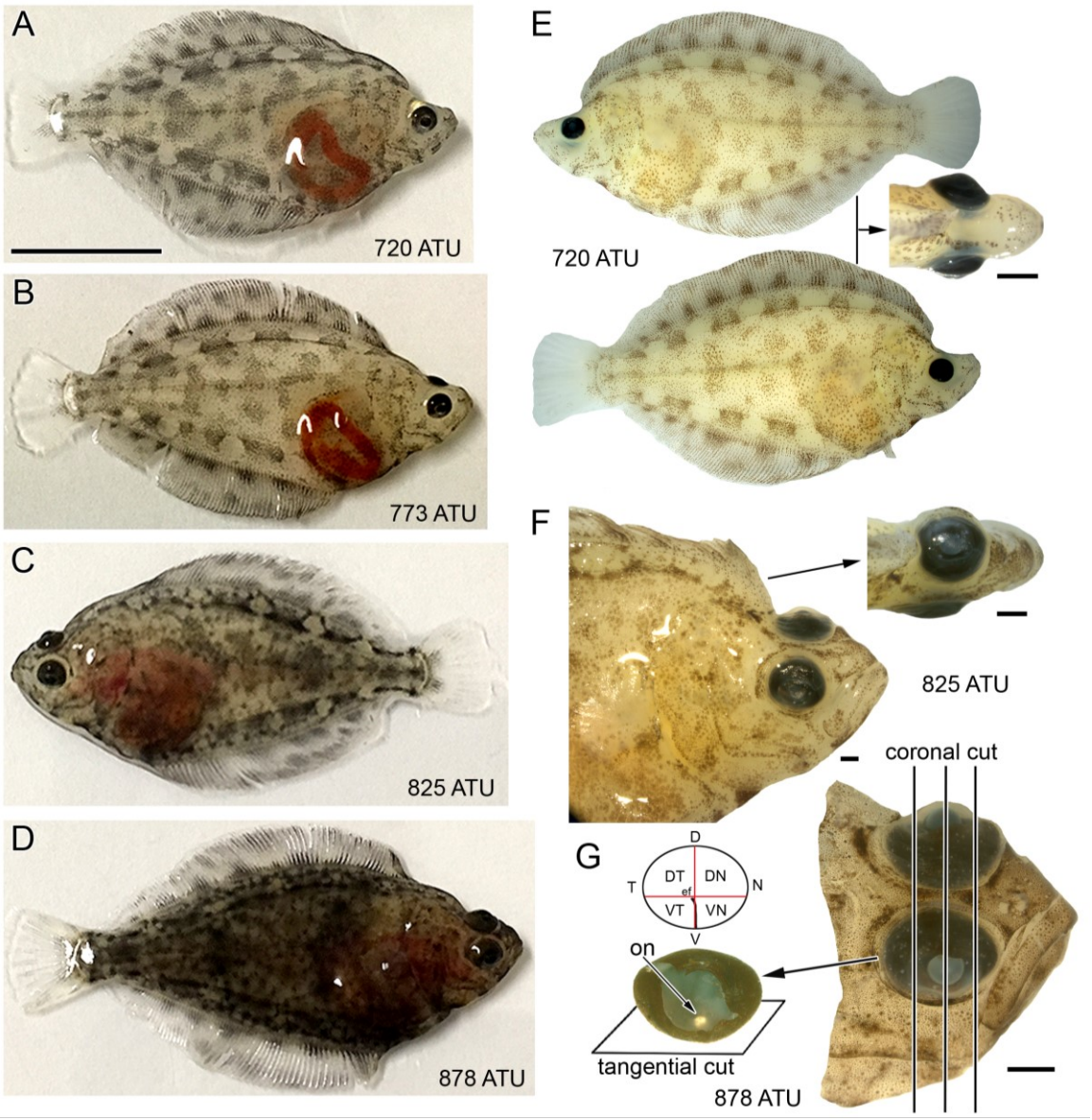

Figure 2.1. Developmental stages of Atlantic halibut examined illustrating eye migration and orientation of histological sectioning.

Note: (A-D) Body morphology of live fish at approximately 720 ATU (82 days post-hatching) (A), 773 ATU (89 days post-hatching) (B), 825 ATU (96 days post-hatching) (C), and 878 ATU (103 days post-hatching) (D). The left eye is migrating in all fish except for the one shown in (C), where the right eye is migrating. (E) Lateral and top views of a fixed specimen at 720 ATU. Migration of the left eye has just started. (F) Lateral and top views of a fixed specimen at 825 ATU. The left eye has migrated halfway between the blind side (bottom part of the fish following metamorphosis) and ocular side (top part of the fish following metamorphosis). (G) Head of fixed specimen at 878 ATU showing completed eye migration and the extracted right eye without lens. The optic nerve (on) exits the retina below the crossing of theoretical short and long ellipse axes that characterize this elliptically-shaped eye and retina. The optic nerve head coincides with the central end of the embryonic fissure (ef) which extends to the ventral periphery. The panel illustrates the direction of sectioning when full eyes were cut, revealing

tangential sections of central retina and more oblique sections toward the periphery, and coronal cuts when a head was sectioned, revealing radial views of the retina throughout the lens region and tangential views at the nasal and temporal ends. The schematic shows the division of a right eye retina into quarters (VT, ventrotemporal; VN, ventronasal; DT, dorsotemporal; DN, dorsonasal). Other abbreviations: V, ventral; D, dorsal; N, nasal; T temporal. Scale bar in (A) equals 1 cm and holds for (B-D) and the lateral views in (E); the other scale bars represent 1 mm and are associated with the figures closest to them.

2.3.2. Photoreceptor types and mosaics

The morphological trends were the same for the migrating and non-migrating eye. At 720 ATU, the retina had two main types of cone photoreceptors: single and double cones (Fig. 2.2 A,C,E,G). The single cones were round in cross section and formed a honeycomb mosaic in the ventrotemporal and dorsonasal regions of the retina (Fig. 2.2 C,E). The honeycomb mosaic consisted of six neighbouring cones flanking a single cone (Fig. 2.2 C; white contours) thereby forming a hexagon if the centres of neighbouring cones were to be connected. The inner segments of some single cones stained darker (Fig. 2.2 C,E; double black arrowheads) than the rest of the cone population, and an accessory outer segment was prominent at the base of the outer segments (Fig. 2.2 E; white arrowheads).

In the ventronasal and dorsotemporal quadrants, double cones were present as part of square mosaics of varying regularity (Fig. 2.2 A,G). The basic square mosaic unit consisted of four double cones surrounding a single (centre) cone (Fig. 2.2 A; white contours). There was, however, substantial deviation from a lattice formation (Fig. 2.2 A; white rectangle). Single (corner) cones, i.e., those facing the partitioning membranes of neighbouring double cones, were absent or extremely rare. Some double cone members in the ventronasal retina stained darker than their counterparts (Fig. 2.2 A; red arrow) and, in the dorsotemporal retina, accessory outer segments were prominent and appeared to make contact between cone types (Fig. 2.2 G; white arrowheads).

At 773 ATU, double cones were present in the centroventrotemporal retina forming a square mosaic region of varying disposition (Fig. 2.2 D). The honeycomb mosaic was restricted to the dorsonasal retina (Fig. 2.2 F). In regions with double cones, an arrangement consisting of a single cone flanked by three double cones was common (Fig. 2.2 B,D,H; white circles), as were irregular formations of single and double cones (Fig. 2.2 B, white rectangle).

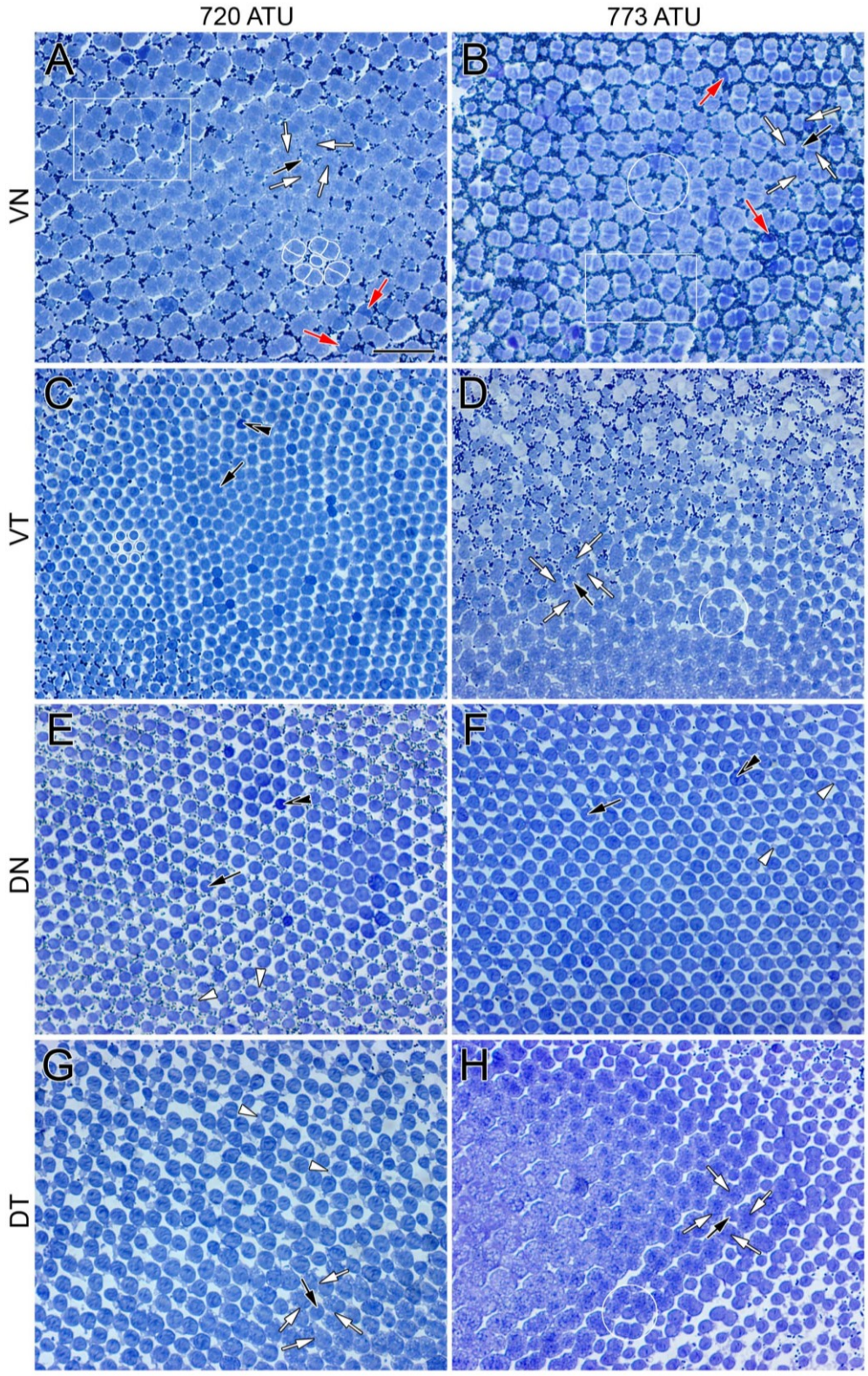

Figure 2.2. Micrographs of tangential EPON sections showing cone distributions at the level of largest ellipsoid cross section or near the base of the outer segments from various regions of the light adapted retina of Atlantic halibut undergoing metamorphosis.

(Continuation of Figure 2.2.) Note: (A,C,E,G) Central area from the ventronasal (A), ventrotemporal (C), dorsonasal (E) and dorsotemporal (G) retina at 720 ATU. (B,D,F,H) Equivalent central sectors to those in (A,C,E,G) but from a retina at 773 ATU. At 720 ATU, the ventronasal (A) and dorsotemporal (D) quadrants show cone square mosaics whereas honeycomb mosaics characterize the ventrotemporal (C) and dorsonasal (E) quadrants. (A) A square mosaic unit consisting of a single cone surrounded by four double cones is traced in white; white arrows point to the apposing partitions of double cone members surrounding a single cone (black arrow); red arrows indicate double cone members that stain darker than their counterparts. The area within the white rectangle illustrates a less regular arrangement of single and double cones. (C) A honeycomb mosaic unit consisting of one single cone surrounded by six others is shown in white; double black arrowheads point to a single cone that stains darker than most others in the field of view. (E, G) White arrowheads point to accessory outer segments of individual single cones. At 773 ATU (B,D,F,H), only the central region of the dorsonasal quadrant retains a honeycomb mosaic (F). The white rectangle in (B) illustrates an area with less regular disposition of single and double cones. (B,D,H) White circles encompass a single cone flanked by a triangular arrangement of three neighbouring double cones. Abbreviations as per Figure 2.1. Scale bar in (A) equals 10 μm and holds for all panels.

By the time eye migration was complete (878 ATU), the honeycomb mosaic was absent from the retina and other cone formations had emerged (Fig. 2.3- 2.5). A new cone type, the triple cone (t) (white contours), spanned the centrodorsotemporal retina (Fig. 2.3 A-D) abutting onto a lattice square mosaic of smaller cones closer to the periphery (Fig. 2.3 A,B,E; white rectangle in B). The triple cones were part of mosaic formations that also included single and double cones (Fig. 2.3 B-D) with ratios of double to single cone and double to triple cone that varied between 1.3 and 0.96, respectively, for the centrodorsotemporal retina, to 2.0 and 62 for the dorsonasal retina. The dorsonasal retina consisted primarily of square mosaic formations with larger cones in the central retina and smaller ones toward the periphery (Fig. 2.4). Although variation in regularity of the square lattice occurred in various areas (Fig. 2.4 B,D,E; white rectangle and circles), cones in the periphery were more tightly packed and the mosaic appeared more regular (Fig. 2.4 B). Cone distributions differed the most from a lattice formation in the region approaching the ventronasal retina, where double cone members with darker stain (red arrow) were present (Fig. 2.4 D).

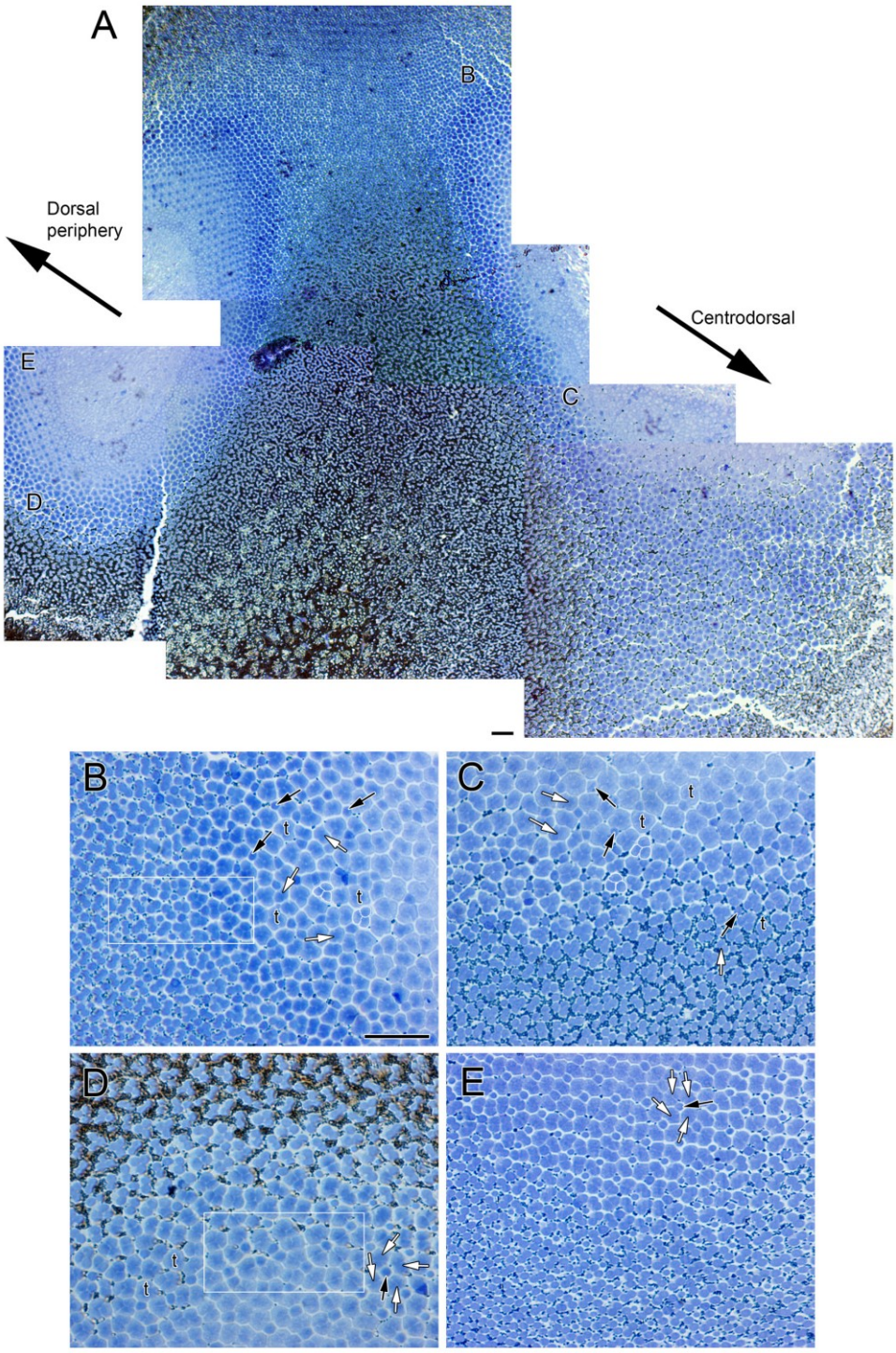

Figure 2.3. Micrographs of tangential EPON sections showing cone distributions from the dorsotemporal retinal quadrant at 878 ATU.

Note: (A) View stitched together from multiple micrographs spanning the central to peripheral retina. The centrotemporal retina comprises three different cone types (single, double and triple cones) arranged in various formations whereas the retinal periphery shows a square mosaic. (B-E) Cone distributions from different areas of the field shown

in (A) and indicated by the same letters (in A). (B,D) Cone distributions at interfaces between the more central, triple cone-occupied area and the peripheral, square mosaic area (white rectangles); triple cones (t, white contours) are common among double and single cones toward the central retina. (C) Area of central retina illustrating larger cells and prominent triple cone presence. (E) Square mosaic toward the periphery of the retina. Other symbols and abbreviations as per Figure 2.2. Scale bars in (A) and (B) equal 10 µm; scale bar in (B) holds for (C-E).

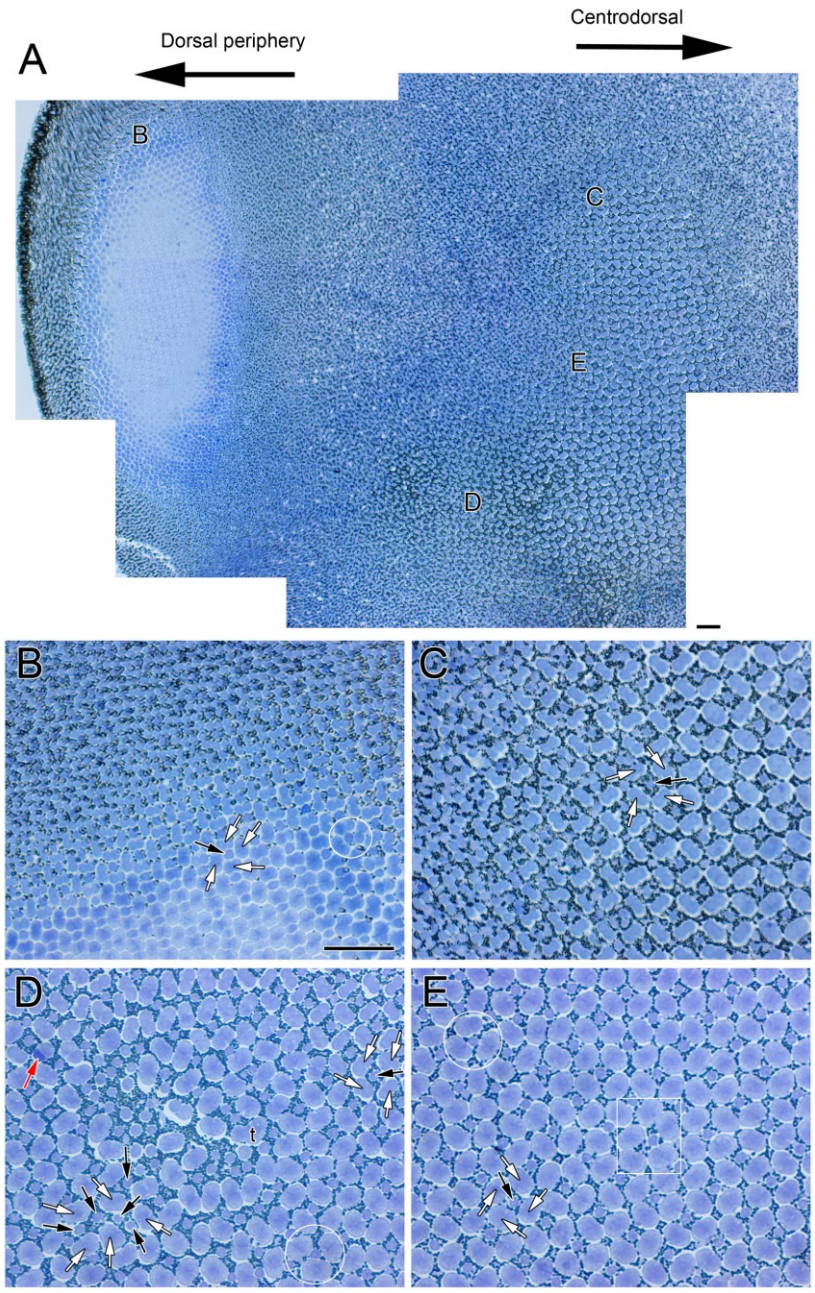

Figure 2.4. Micrographs of tangential EPON sections showing cone distributions from the dorsonasal retinal quadrant at 878 ATU.

(Continuation of Figure 2.3.) Note: (A) View stitched together from multiple micrographs spanning the central to peripheral retina. The primary cone formation is a square mosaic but there are other cone arrangements. (B-E) Cone distributions from different areas of the field shown in (A) and indicated by the same letters (in A). (B,D) White circles encompass a single cone flanked by three double cones. (E) The white rectangle shows an area where five double cones surround a single cone. Scale bars in (A) and (B) equal 10 μm; scale bar in (B) holds for (C-E).

As per the trends in the dorsonasal retina, the ventral retina at 878 ATU consisted of square mosaics with variable jitter in the lattice (Fig. 2.5 A,C,D; white rectangles and circle). Double cone members with darker stain (red arrows) than their counterparts were more frequent in the ventral retina than in other areas of the retina, as were single corner cones (double white arrowheads) (Fig. 2.5 A,B,D). At this developmental stage, rod photoreceptors were present; their outer segments were larger and displaced further into the retinal pigment epithelium with respect to those of cones (white closed contours, Fig. 2.5 E,F).

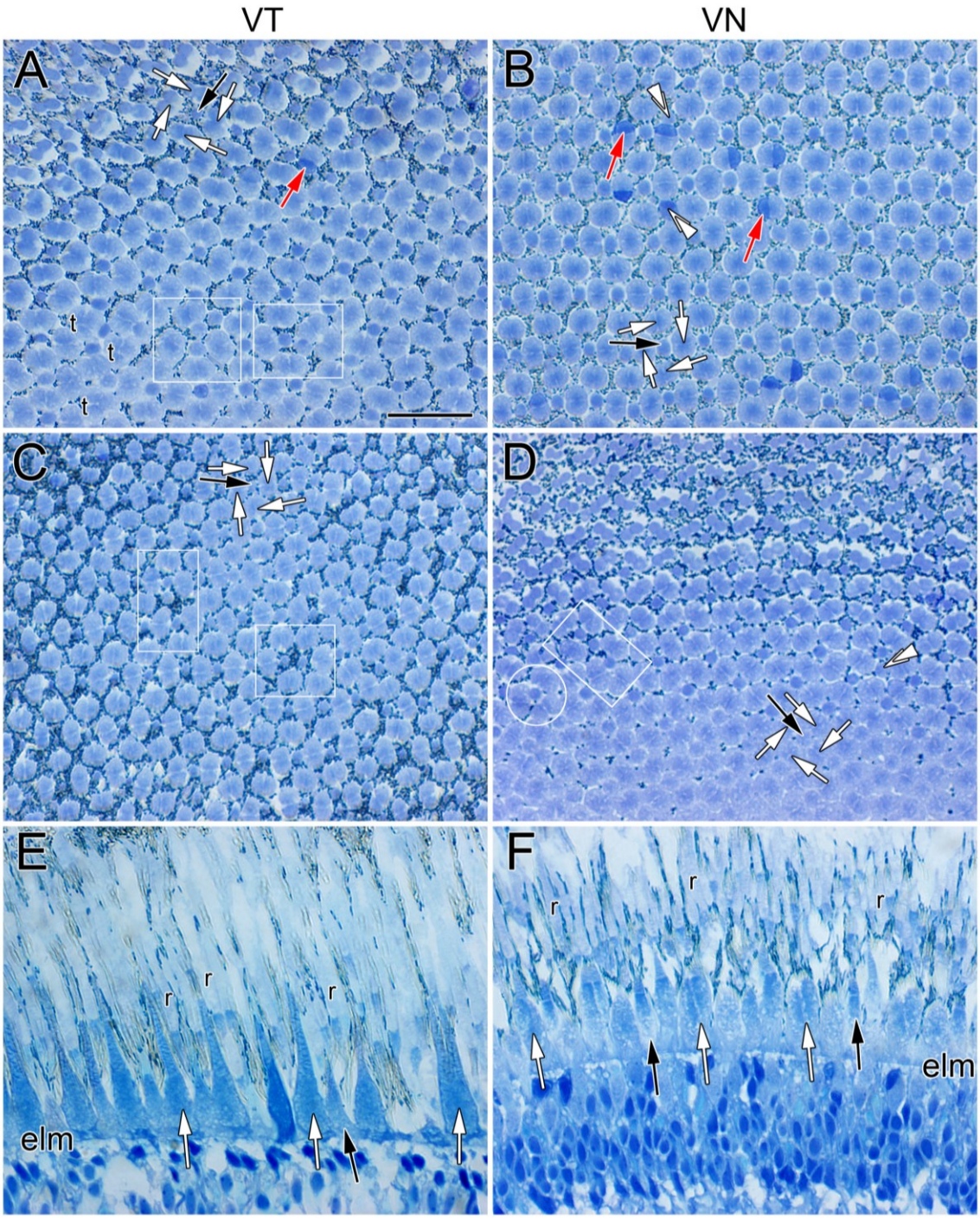

Figure 2.5. Micrographs of EPON sections showing cone distributions from the ventral retina at 878 ATU.

Note: (A-D) Tangential sections of central retina from the ventrotemporal (A) and ventronasal (B) quadrants and corresponding sections from the ventrotemporal (C) and ventronasal (D) periphery. White rectangles in (A,C,D) show cone arrangements that deviate from the square mosaic and the white circle in (D) illustrates a single cone surrounded by three double cones. The double white arrowheads in (B,D) point to single corner cones, which face the partitions of adjacent double cones. (E,F) Radial sections from the central regions of the ventrotemporal (E) and ventronasal (F) quadrants; white

contours depict rods Abbreviations: r, rod; elm, external limiting membrane. Other abbreviations as per Figure 2.2. Scale bar in (A) equals 10 μm and holds for (B-F).

2.3.3. Cone densities and measures of visual acuity

A summary topographical schematic showing mean cone densities in the Atlantic halibut retina at the two extreme developmental time periods examined (720 and 878 ATU) revealed profound retinal transformations (Fig. 2.6). At 720 ATU, the greatest cone density within the central retina was found in the ventrotemporal quadrant and the lowest in the dorsotemporal quadrant (Fig. 2.6 A). Correspondingly, the greatest theoretical spatial resolving power was found in the ventrotemporal quadrant and the lowest in the dorsotemporal quadrant (Fig. 2.6 B). This translated into a mean increase of 14 mm in the distance at which the ventrotemporal retina would resolve a 0.5 mm target with respect to the dorsotemporal retina (Fig. 2.6 B). Based on total density of cones (where each cell was counted individually), the greatest resolving power was found in an area devoid of double cones and square mosaics.

At 878 ATU, the region of the central retina with the greatest cone density had shifted to the dorsotemporal quadrant (Fig. 2.6 C). This region, with theoretical resolving power similar to that of the peripheral retina, also had the greatest density of triple cones (Fig. 2.6 D). Despite an overall reduction in cone density in the central retina during development from 720 to 878 ATU (Fig. 2.6 A,C), theoretical resolving power generally improved (Fig. 2.6 B,D) as a result of increased lens size.

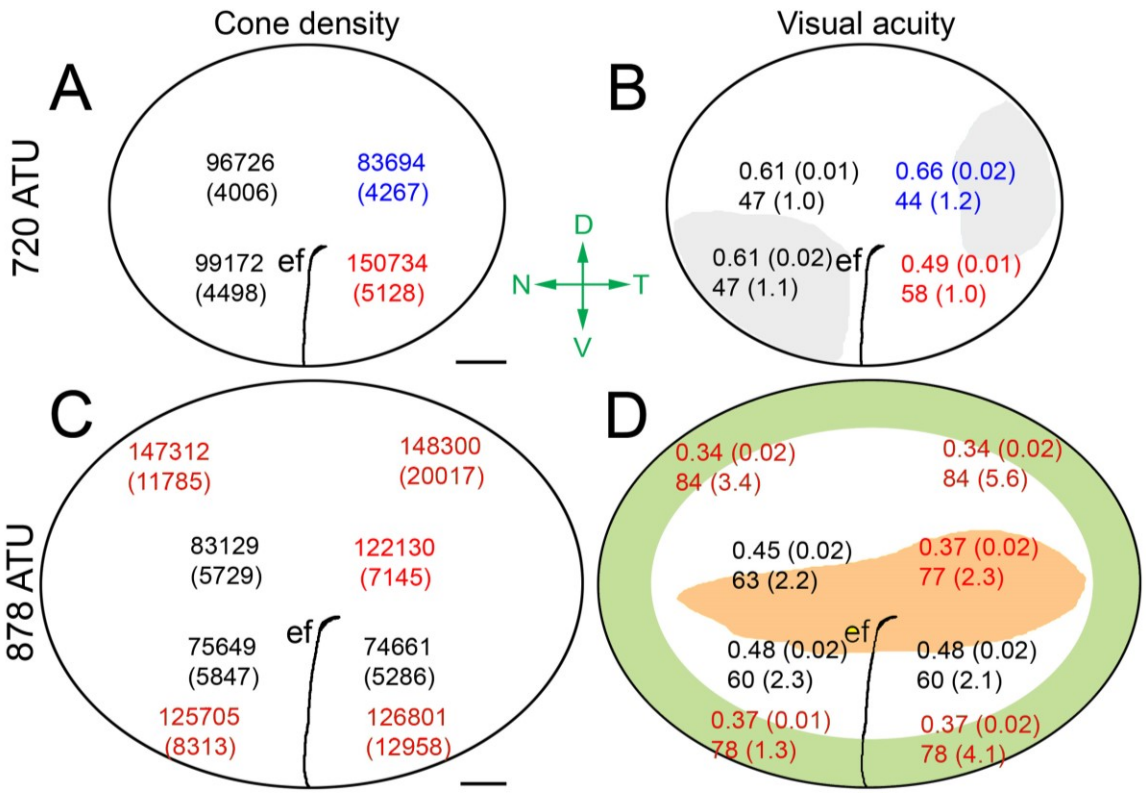

Figure 2.6. Diagrams illustrating topographic maps of cone densities and visual acuity-related variables extracted from the retinas of four Atlantic halibut at 720 ATU or 878 ATU.

Note: Each statistic is the mean (± SD). (A,C) Cone density per mm^2; gray zones in (C) delineate the approximate areas of square mosaic presence. (B,D) Minimum resolvable angle (º) (top number), and distance (in mm) (bottom number) at which a 0.5 mm target would be resolved. The green and pink zones in (D) denote the approximate areas associated with the peripheral square mosaic and triple cone presence, respectively. Means with different colour are statistically different across retinal quadrants at α=0.05 level of significance. The embryonic fissure (ef) runs from the ventral retina toward the centro-temporal retina. Abbreviations (axes in green): D, dorsal; V, ventral; N, nasal; and T, temporal. Scale bars in (A) and (C) equal 0.2 mm.

2.3.4. Visual pigments

Absorbance measurements from the outer segment of individual photoreceptors from four juvenile Atlantic halibut revealed six cone visual pigments and one rod visual pigment (Fig. 2.7). The cone visual pigments consisted of two short wavelength (S) types with maximum wavelength of absorbance (λ_{max}) ± SD at 431 ± 7 nm (n = 8) (Fig. 2.7 A) and 457 ± 6 nm (n = 7) (Fig. 2.7 B), three middle wavelength (M) types with λ_{max} ± SD at 500 ± 5 nm (n = 23) (Fig. 2.7 C), 514 ± 8 (n = 35) (Fig. 2.7 D), and 527 ± 6 (n = 19) (Fig. 2.7 E), and one long wavelength (L) type peaking at 550 ± 11 nm (n = 4) (Fig.

8G). The rod visual pigment had λ_{max} ± SD at 491 ± 7 nm (n = 25) (Fig. 2.7 F). The S visual pigments were located in the single cones, whereas the M and L visual pigments were mostly confined to the double cones, one per double cone member. The S(431) absorbance curve showed an increase ("hump") between 450 and 550 nm (Fig. 2.7 A). Fitting of this curve with combinations of visual pigment templates (Fig. 2.7 G) suggested that it consisted of the S(431) visual pigment and a smaller amount of either M(500) or M (514) visual pigment (Table 2.1). The majority of double cones measured were M/M pairs, either 500/514 (n = 18), 514/527 (n = 12), or 527/527 (n = 10), with a minority of M/L pairs (527/550, n= 4). The L/M pairs tended to be shorter size cones, which were more prevalent in the ventral retina.

Table 2.1. Best-fit Simplex derived parameters and corresponding least sum of squares (SS) for the spectral functions depicted in Figure 2.7H.

Note: The k_{431} and k_{other} coupling constants are the inputs of the visual pigments to the absorbance function [k_{431} corresponds to the S(431) visual pigment and K_{other} to the other pigment in a combination]. The λ_{max} of the visual pigments used in the fitting process are indicated in the first column. The SS statistic is derived from the sum of differences between mean absorbance data and the corresponding values predicted by the Simplex algorithm.

Visual pigments	K_{431}	K_{other}	p	SS
S (431)	1.124	0	1.025	0.333
S (431), S(457)	1.925	0.007	6.494	0.176
S (431), M (500)	1.398	0.061	5.523	0.056
S (431), M(514)	1.263	0.091	3.911	0.059
S (431), M (527)	0.992	0.355	1.689	0.173

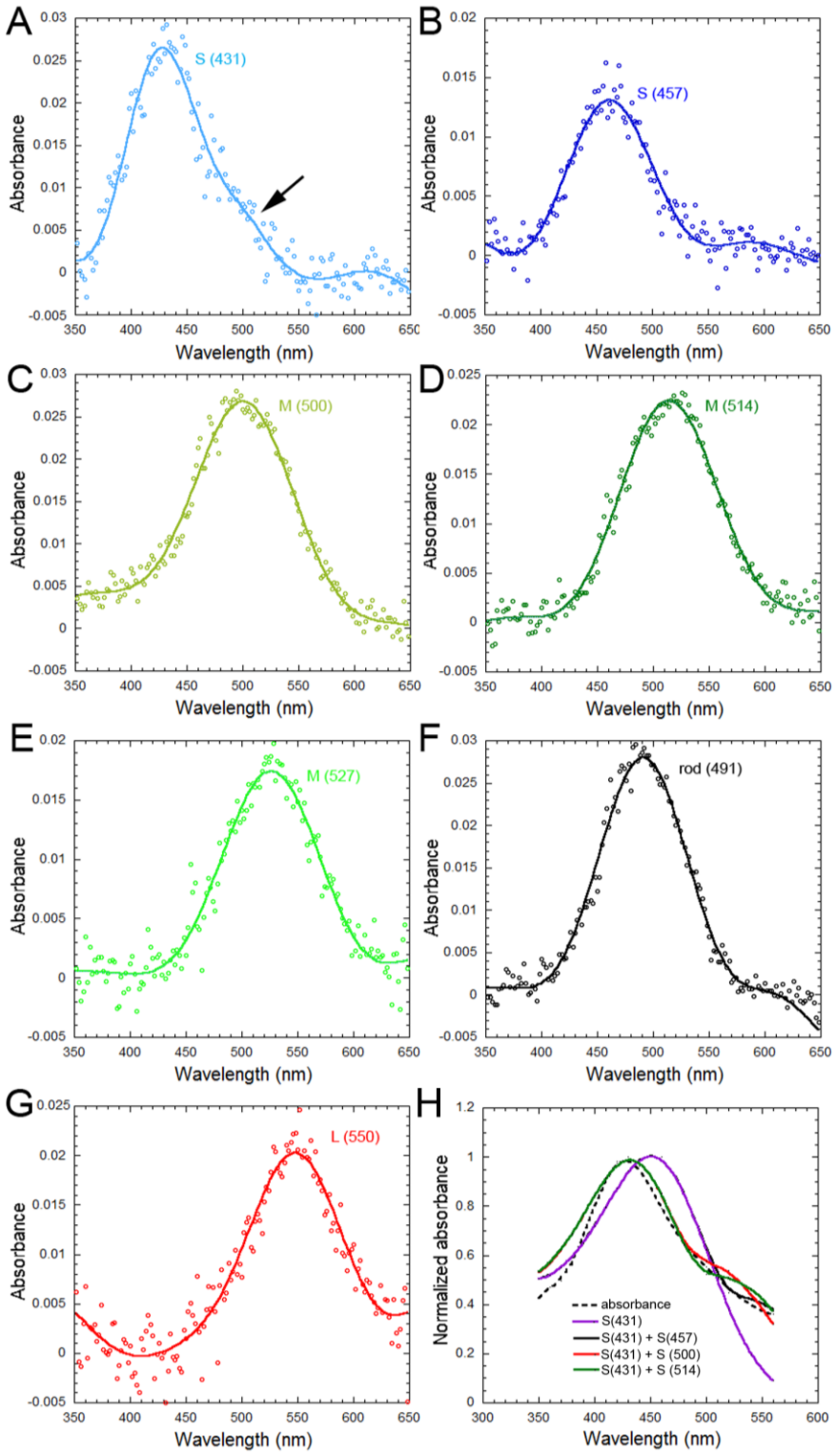

Figure 2.7. Representative visual pigment absorbance spectra from isolated photoreceptors in the retina of Atlantic halibut juvenile (each trace is the mean of 4-14 records from 4 fish).

Note: (A) Coexpression of a short wavelength sensitive [S (431)] visual pigment with another visual pigment (as revealed by the “hump” in absorbance at longer wavelengths,

black arrow). (B) Short wavelength sensitive [S(457)] visual pigment. (C) Middle wavelength [M (500)] visual pigment. (D) Middle wavelength [M (514)] visual pigment. (E) Middle wavelength [M (527)] visual pigment. (F) Rod (491) visual pigment. (G) Long wavelength sensitive [L(550)] visual pigment. The wavelength of maximum absorbance, λ_{max}, associated with each visual pigment type is in parenthesis. (H) Simplex-derived fits to the S(431) absorbance in (A) (dotted black function) using one [S(431)] or two visual pigment templates (see Table 1 for corresponding fit parameters).

2.3.5. Spatial analyses of cone distributions

Spatial analyses of the main cone distributions in the retina of Atlantic halibut undergoing metamorphosis revealed regularities that differed as a function of cone and mosaic type (Fig. 2.8-2.10). The greatest regularities were associated with lattice mosaics, which have characteristically high cone periodicity (Fig. 2.8 A-J; Fig. 2.9 A-E) and the lowest ones belonged to mosaics with triple cones (Fig. 2.8 K-O; Fig. 2.9 F-J; Fig. 2.10 A-E). With the exception of cones forming the honeycomb mosaic, which were positioned side-by-side with minute spaces between them (Fig. 2.8 A), single cones had greater nearest neighbour distances and Voronoi domain areas than their double or triple cone counterparts in the remaining mosaics (Fig. 2.8- 2.10). This might have been expected from their lower relative densities (Fig. 2.8 F,K; Fig. 2.9 A,F; Fig 2.10 A).

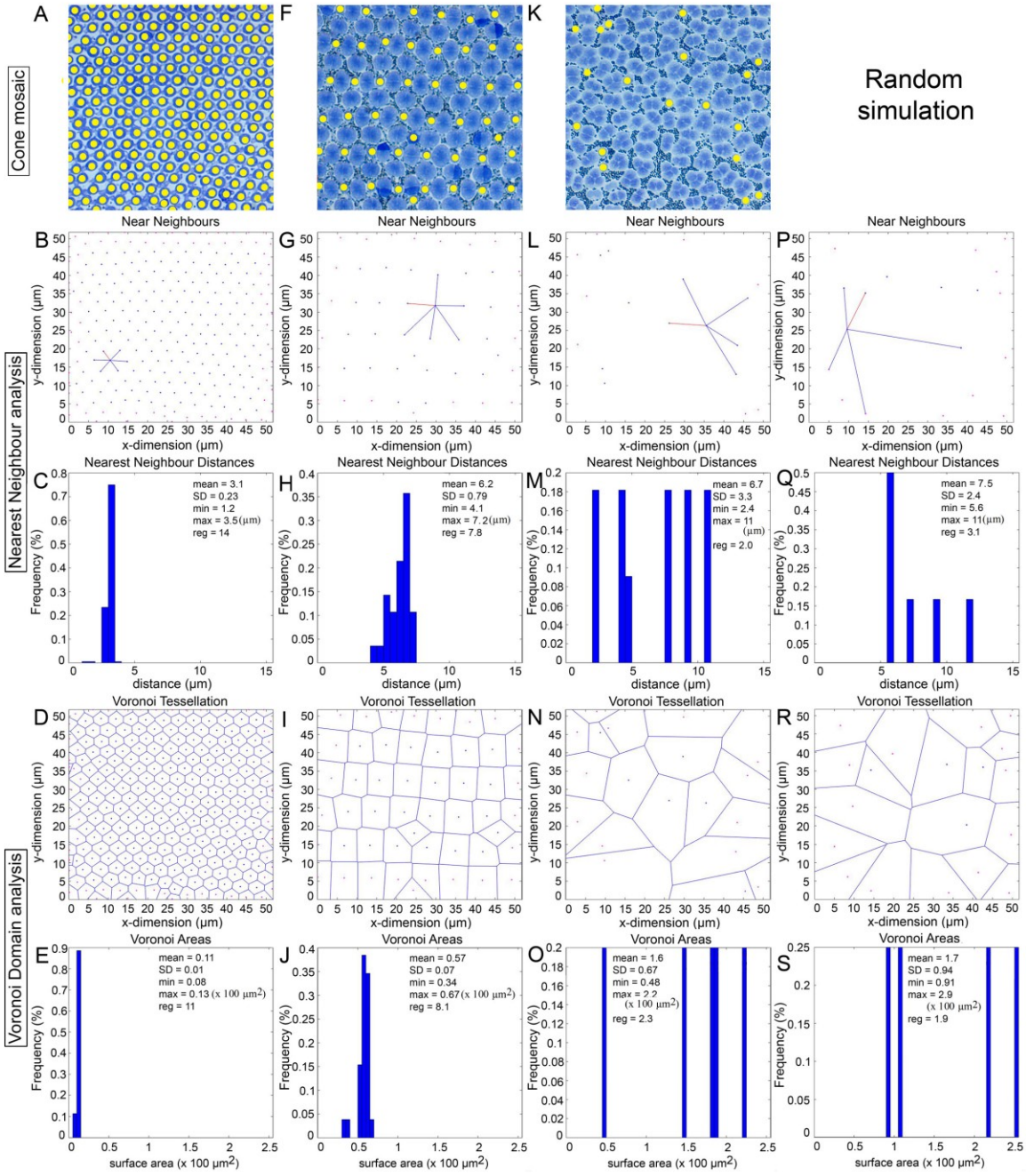

Figure 2.8. Spatial analysis of single cone distributions from representative mosaics in the retina of Atlantic halibut undergoing metamorphosis.

Note: Single cones are marked with yellow dots. (A-E) Cone mosaic from the centrodorsonasal retina at 773 ATU (A); Nearest neighbour analysis of double cone centroids, illustrating the near neighbours of a single cone, including its nearest neighbour in red (B) and their frequency distribution (C) [statistics (in μm) are the mean nearest neighbour distance, its standard deviation (SD), the minimum (min) and maximum (max) nearest neighbour distances, and the regularity index = mean/SD]; Voronoi tessellation of double cone domains (D) and their frequency distribution (E) [statistics (in 100 μm^2) are the mean area (domain), its standard deviation (SD), the minimum (min) and maximum (max) areas, and the regularity index = mean/SD]. (F-J)

Same presentation of data as per (A-E) but for the centroventronasal retina at 878 ATU. (K-O) Same presentation of data as per (A-E) but for the centrodorsotemporal retina at 878 ATU. (P-S) Same presentation of data as per (B-E) but for a random distribution of points matched for density with that in (K) and constrained by single cone soma size.

To assess whether cones in non-lattice mosaics had some level of organization, their spatial statistics were compared to those of twenty random distributions of corresponding mean density and constrained by soma size. The latter was the mean diameter of 2.2 μm for the single cone, mean short axis distance of 3.0 μm for the double cone, and mean median of 4.1 μm for the triple cone (n=30; Fig. 2.8 P-S; Fig. 2.9 K-N; Fig. 2.10 F-I). None of the comparisons to the random distributions were significantly different, or the means were greater for the random distributions. Thus, all cone types (single, double, and triple) in mixed cone areas with high triple cone density (i.e., where the proportion of triple cones was statistically similar to that of double cones; Fig. 2.8 K; Fig. 2.9 F; Fig. 2.10 A) were distributed randomly.

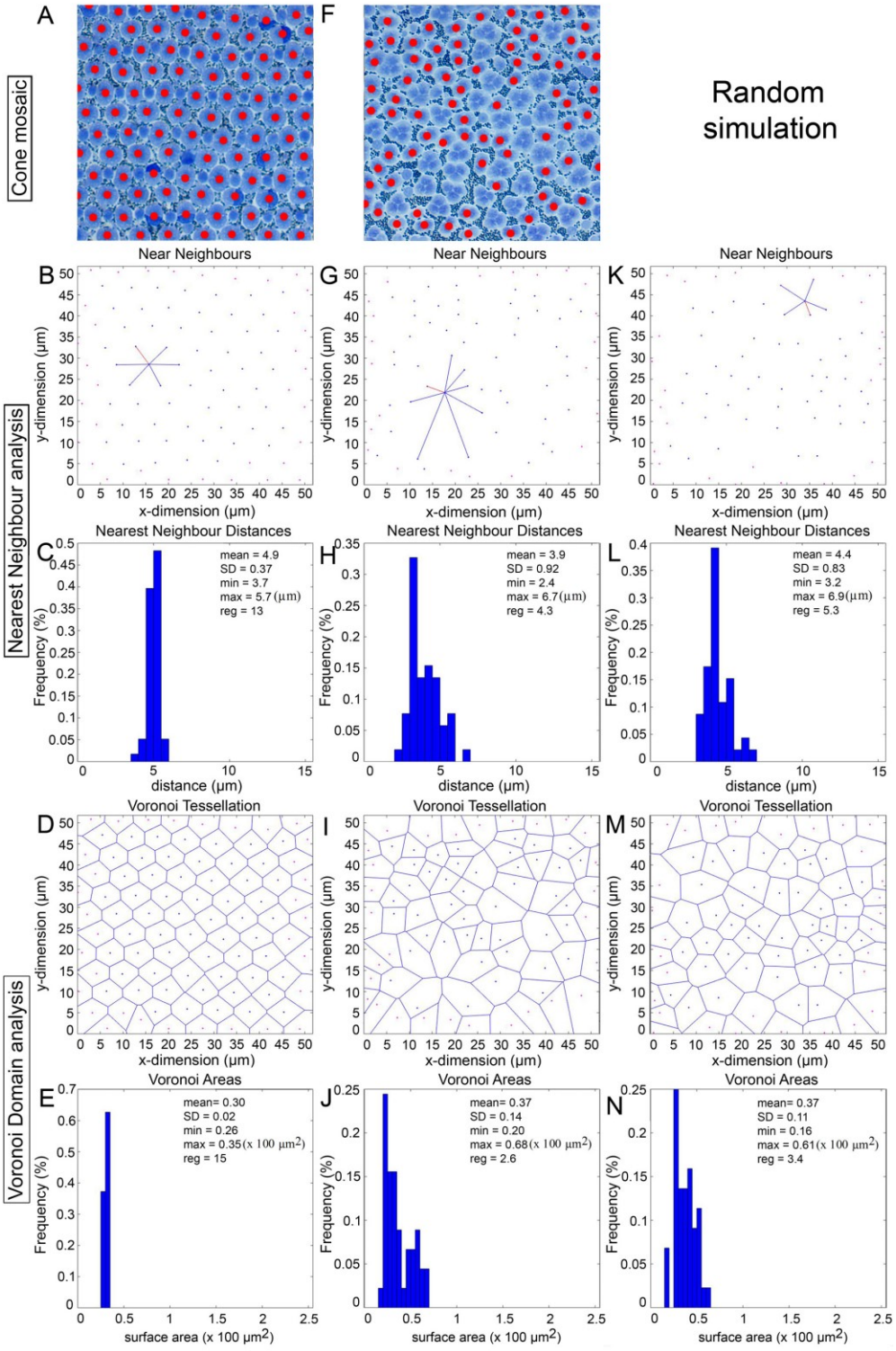

Figure 2.9. Spatial analysis of double cone distributions from the same mosaics shown in (A) and (F) of Figure 2.8.

Note: Double cones are marked with red dots. (K-N) Same presentation of data as per (G-J) but for a random distribution of points matched for density with that in (G) and constrained by double cone soma size. Presentation of data as in Figure 2.8.

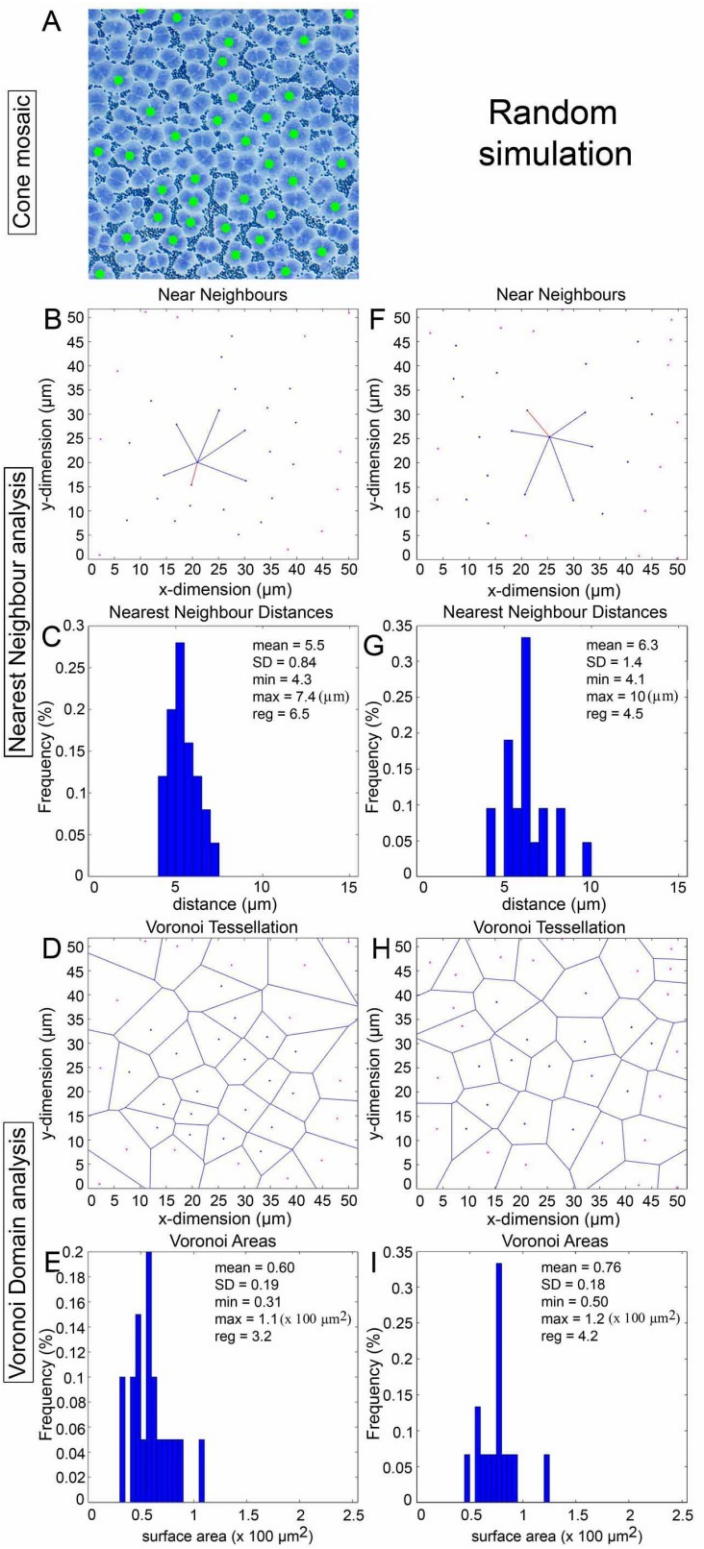

Figure 2.10. Spatial analysis of triple cone distributions from the same mosaics shown in (K) of Figure 2.8.

Note: Triple cones are marked with green dots. (F-I) Same presentation of data as per (B-E) but for a random distribution of points matched for density with that in (A) and constrained by triple cone soma size. Presentation of data as in Figure 2.8.

2.3.6. Autocorrelation and Density Recovery Profile analyses

The autocorrelograms of morphological cone types that were part of square or honeycomb mosaics revealed a variety of lattice-like arrangements characterized by periodic foci with variable jitter (Fig. 2.11; Fig. 2.12). The density recovery profile, derived from the aurocorrelogram, showed a region surrounding the origin (the effective radius) where like-type cones were absent (Fig. 2.11 B,C,J,K; Fig. 2.12 B,C). This exclusion zone for single cones in the honeycomb mosaic was slightly greater than the diameter of a single cone (Fig. 2.11 K). For double cones of the square mosaic, it approximated the size of the long axis of a double cone ellipsoid cross section (Fig. 2.12 C). These results reflect the tight packing of these cone types in their respective lattices. The greatest distance between single cones (compared to double cones) in the square mosaic resulted in a larger effective radius for this cone type (Fig. 2.11 C).

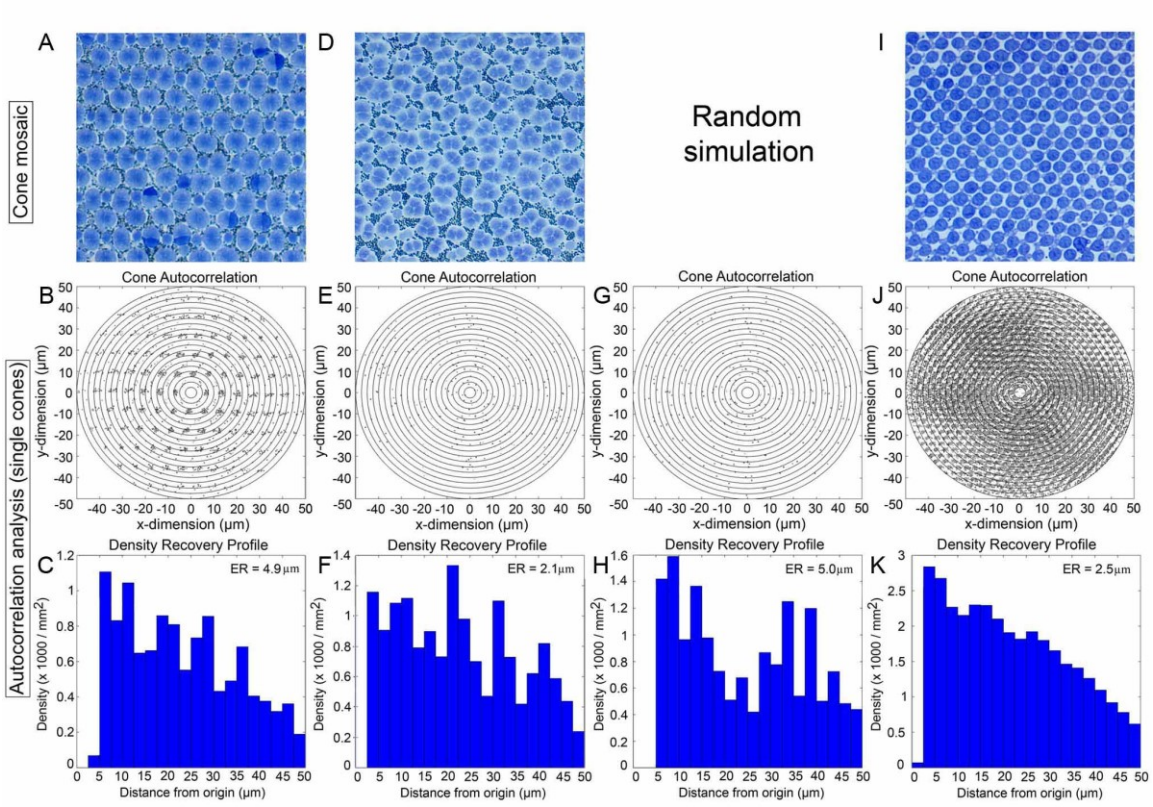

Figure 2.11. Autocorrelogram and density recovery profile for the single cone distributions (B,C,E,F,J,K) shown in Figure 2.8, as well as the random distribution associated with the single cone in the triple cone area (G,H).

Note: The ER is the effective radius (or exclusion zone) which represents the size of the null region at the centre of the autocorrelogram.

None of the autocorrelograms associated with cones in non-lattice distributions showed signs of periodicity (Fig. 2.11 E; Fig. 2.12 E,J). The density recovery profiles of cones in non-lattice mosaics (Fig. 2.11 F; Fig. 2.12 F,K) had effective radii that were statistically similar or lower than those obtained from simulations of random distributions (Fig. 2.11 G,H; Fig. 2.12 G,H,L,M).

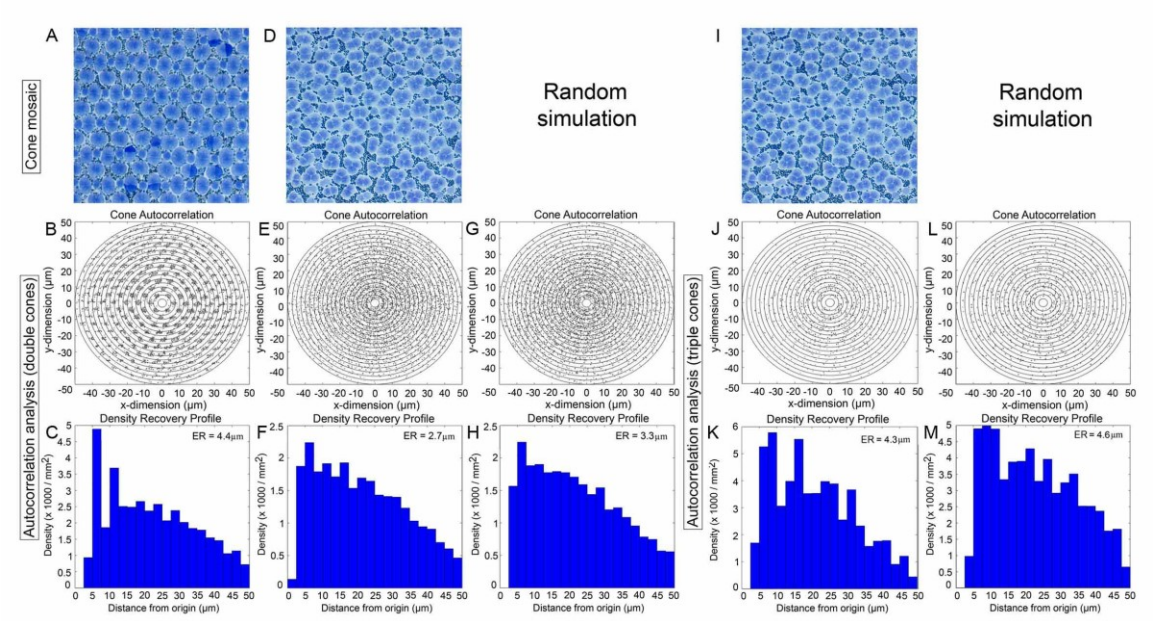

Figure 2.12. Autocorrelogram and density recovery profile for the double cone (B,C,E,F) and triple cone (J,K) distributions shown in Figure 2.8, as well as the random distributions associated with the double cone (G,H) or triple cone (L,M) in the triple cone area.

Note: Presentation of data as per Figure 2.11.

2.3.7. Genomic identification and phylogenetic analyses of Atlantic halibut opsins

Queries of the Atlantic halibut genome predicted seven opsin genes corresponding to five opsin classes: SWS1, SWS2, RH1, RH2, and LWS (Table A2). Two genes were predicted for *rh2* and *sws2*, whereas one gene was predicted for each of the other opsin classes. Coding sequences corresponding to *rh2*, *sws2*, and *lws* were located on chromosome 5; sequences for *sws1* and *rh1* were located on chromosomes 23 and 7, respectively (Fig. A1).

Compared to the annotated genomes of turbot and zebrafish, the positions of the predicted opsins and their flanking genes were in similar orientations (Fig. A1 A-D).

Predicted *rh2* opsins were located in tandem and were flanked by *slc66a22.2* and *synaptoporin* (*synpr*) (Fig. A1 A). Initially, the annotated genome predicted three *rh2* coding sequences; however, one of these sequences (accession: XP_034442263.1) was incorrectly annotated as it had an unusual six exon structure and overlapped the regions of two other *rh2* sequences (Table A2, Fig. A2 A). We hypothesized that this incorrect sequence corresponded to a *rh2* pseudogene, with only the first three exons being correctly annotated and did not consider it in further analyses (Fig. A2 B).

The *sws2-lws* gene cluster on chromosome 5 was flanked by *hcfla* and *gnl3l*, consistent with similar genomic regions in turbot and zebrafish (Fig. A1 B). Within this cluster, two *sws2* genes were separated by a *sws2* pseudogene.

Previously reported Atlantic halibut opsins (Helvik *et al*., 2001b) were used as queries in BLASTp analyses to confirm the classes of the predicted opsins (Tables A6-7). Sequence similarities in the range of 38 – 63% were observed between predicted opsins and those of a different class, whereas opsins of the same class were ≥ 80% identical (Table A3). Predicted opsins with > 99% sequence identity to opsins of their same class were determined to be the same as previously published opsins (Helvik *et al*., 2001b). These opsins included SWS1 (100%), SWS2 (accession: XP_034440595.1) (99%), RH1 (100%), RH2 (accession: XP_034442261.1) (100%), and LWS (99%) (Table A7). A lower percent identity for the other SWS2 (accession: XP_034441481.1) (75%) and RH2 (accession: XP_034442262.1) (86%) opsins suggested that these were novel opsins in Atlantic halibut.

Based on phylogenetic analyses, Atlantic halibut opsins were classified as SWS1, SWS2A (accession: XP_034440595.1), SWS2B (accession: XP_034441481.1), RH1, RH2B (accession: XP_034442261.1), RH2C (accession: XP_034442262.1), and LWS are referred to as such for the remainder of the manuscript (Fig. 2.13). No modifications at known amino acid tuning sites were found for SWS1, SWS2B, RH2B, or RH2C with respect to other flatfishes (Tables A8- A10). An A292S amino acid substitution for Atlantic halibut SWS2A differed from other flatfish (Table A9). Marbled sole and Atlantic halibut LWS share an A164S substitution (Fig. 2.13; Table A11). Some heterogeneity across flatfish was observed for RH1 sites 124 and 300; Atlantic halibut, spotted halibut and barfin flounder all had a valine residue at site 300, but Atlantic halibut differed from these other two flatfish with an A124G substitution (Table A12). However,

this A124G substitution does not impact the λ_{max} of the corresponding visual pigment (Musilova *et al*., 2019).

Except for SWS2A, the λ_{max} of reconstituted barfin flounder opsins (Kasagi *et al*., 2015) corresponded well with some of our microspectrophotometry records of associated visual pigments and were therefore used as references for inferring the λ_{max} of Atlantic halibut opsins when bound to retinal as the chromophore. Therefore, the λ_{max} values of these opsins were predicted to be around 367 nm (SWS1), 416 nm (SWS2B), 494 nm (RH1), 506 nm (RH2B), and 490 nm (RH2C) (Table A13). For SWS2A the corresponding opsin from Japanese flounder was used (Kasagi *et al*., 2018). The A292S substitution for SWS2A suggested a -8 nm shift (Takahashi & Ebrey, 2003) and a predicted λ_{max} near 458 nm. Based on the A164S substitution (Takahashi & Ebrey, 2003), LWS was predicted to have a λ_{max} in the range 554-558 nm.

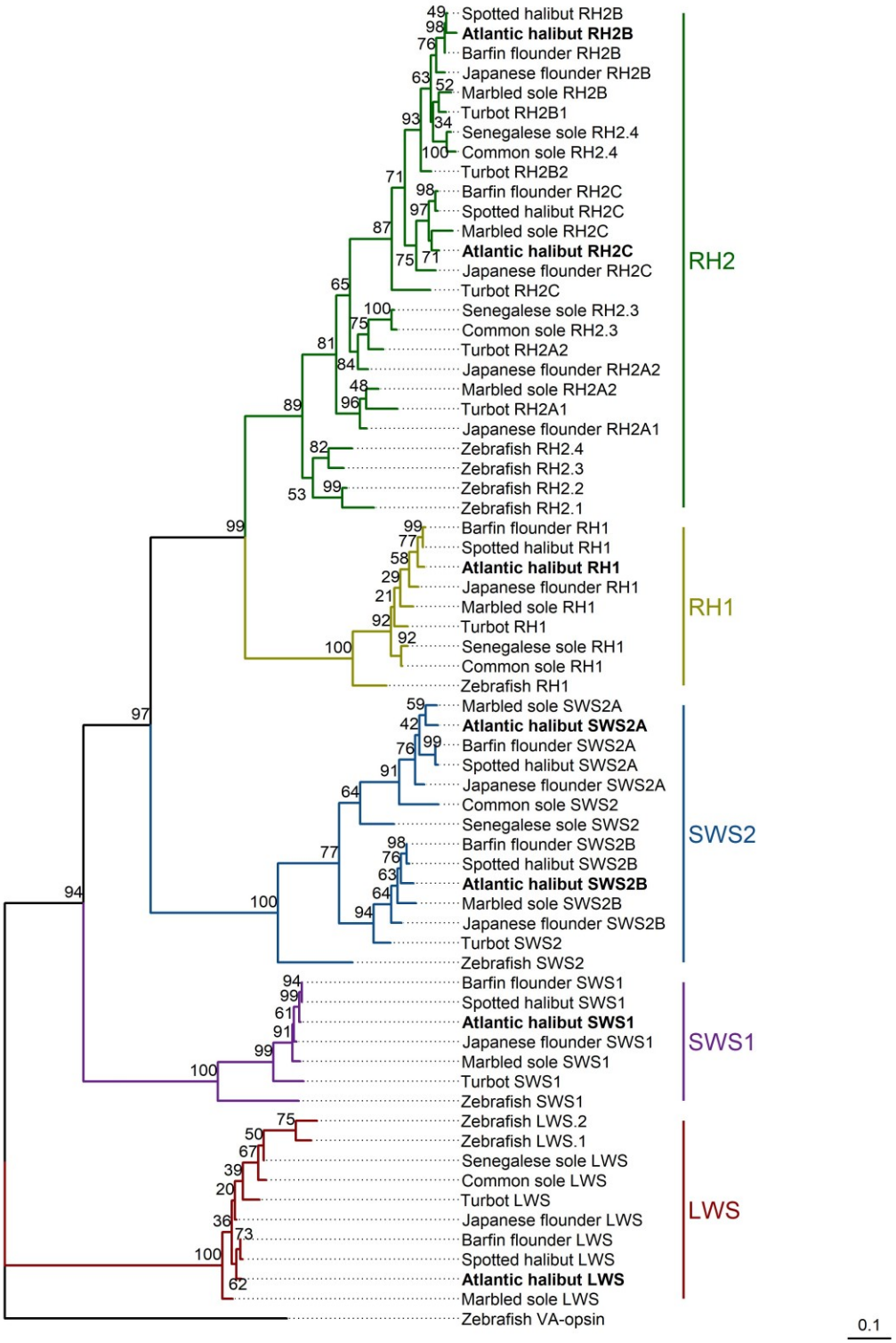

Figure 2.13. Maximum likelihood tree of flatfish and zebrafish amino acid sequences for five opsin classes: SWS1, SWS2, RH1, RH2, and LWS. Bootstrap values (*n* = 100) are located next to the branches and predicted opsins for Atlantic halibut are bolded. See Table A1 for accession numbers used.

2.4. Discussion

2.4.1. Spatiotemporal dynamics of photoreceptor distributions

The retina of Atlantic halibut undergoing eye migration experienced major changes in photoreceptor types and distributions. The single cone type organized in honeycomb mosaic reported at the end of the yolk sac period (40 days post-hatching) (Kvenseth *et al*., 1996) started to reorganize to incorporate double cones (Kvenseth *et al*., 1996) as part of square mosaics (Fig. 2.2) toward the beginning of eye migration. The youngest halibut examined in this study, whose eye migration had barely started, had two regions of the retina, the centroventronasal and centrodorsotemporal, that contained double cones and square mosaics. At later developmental stages, the square mosaic began to appear in the centroventrotemporal retina and, by the end of eye migration, was present throughout the retina. This progression, which swept from ventronasal and dorsotemporal regions to ventrotemporal and, lastly, to the dorsonasal retina contrasts with a previous report stating that the start of the square mosaic was most advanced at the periphery near the *ora serrata* (at 70 days post hatching) and reached the centre of the retina by 100 days post-hatching (Kvenseth *et al*., 1996).

The seeming controversy between our study and previous work (Kvenseth *et al*., 1996) can be resolved by realizing that there are two independent mechanisms that create double cones and the square mosaic in the retinas of flatfishes (Hoke *et al*., 2006). One, common to all fishes, operates at the peripheral growth zone (*ora serrata*) through differentiation of progenitor cells into photoreceptors that become part of established (adult) mosaics, like the square mosaic (Kunz *et al*., 1994). The other appears to occur only among fishes with indirect development. Here, there seems to be a re-arrangement of existing cones in central parts of the retina (present prior to the onset of metamorphosis (Hoke *et al*., 2006)) that leads to square mosaic lattices with substantially more jitter than those forming directly at the periphery, as per our study. In other words, previous authors (Kvenseth *et al*., 1996) did not disambiguate between these two mechanisms leading to potential confusion over the progression of square mosaic formation in the non-peripheral retina prior to the start of metamorphosis.

The progression of double cone and square mosaic appearance reported here agrees with similar observations in winter flounder where two patches of retina, located

in the ventronasal and dorsotemporal regions, were the first to express new opsin transcripts simultaneously (i.e., were present in all samples examined) from the start of metamorphosis (Hoke *et al*., 2006). As in our study, these authors observed that, at the start of eye migration, the ventronasal and dorsotemporal quadrants had double cones as part of emerging square mosaics whereas the dorsonasal and ventrotemporal quadrants had single cones in honeycomb formation (Hoke *et al*., 2006).

Another major discrepancy between our study and previous work (Kvenseth *et al*., 1996) pertains to the appearance of triple cones in the central retina as metamorphosis progressed. Upon completion of eye migration, these cones occupied a large area of central retina as part of random distributions along with double and single cones, whose distributions were also random. Triple cones have never been reported during metamorphosis of flatfishes (Evans & Fernald, 2003; Kvenseth *et al*., 1996; Evans *et al*., 1993; Hoke *et al*., 2006) but are present in the centrodorsal retina of several fish species during metamorphosis (Shand *et al*., 1999b; Shand *et al*., 2001; Zhang *et al*., 2019). Some fishes, which are demersal or live in low light environments as adults, retain a high density of triple cones in a restricted area of centrodorsotemporal retina (Frau *et al*., 2020) often located next to a fovea (Fritsch *et al*., 2017). Other, nocturnal fishes, like some species of holocentrids, also have triple cones. They are primarily located in regions of high cone density, along a central meridian, but constitute less than 0.5% of the total cone population (de Busserolles *et al*., 2021).

Based on the appearance of triple cones around the time when double cones and square mosaics start forming in the retinas of some marine fishes, it has been hypothesized that triple cones may be part of a transitional mosaic between the larval honeycomb mosaic and the adult square mosaic (Shand *et al*., 1999b). Two observations suggest otherwise, however. First, in Atlantic halibut, triple cones were rare in the ventral retina and scarce in the nasal compared to the temporal retina. If triple cones were part of a necessary transitional mosaic leading to the square mosaic, then the ventral and nasal regions of the central retina would not have developed such a mosaic or, at least, not fully. Second, triple cones are retained in the centrodorsotemporal retina of adults of other fish species (Frau *et al*., 2020; Fritsch *et al*., 2017) suggesting a functional role within the random mosaics that they are a part of.

2.4.2. Different square mosaic formation processes in the central and peripheral retina

Our results support two different mechanisms of square mosaic formation in the retina of Atlantic halibut during metamorphosis. At 720 ATU, the centrodorsonasal and centroventrotemporal areas had only singles cones and these were arranged in honeycomb formation. As a square mosaic was present in these regions of the retina by the end of metamorphosis, and no new cones are known to differentiate in the main retina of flatfishes (Hoke *et al*., 2006), existing single cones must have coalesced to form the square mosaic (a conclusion previously reached for the winter flounder by other authors (Evans & Fernald, 1993; Hoke *et al*., 2006)). Electron microscopy evidence suggests such cone fusion occurs in the black bream, *Acanthopagrus butcheri*, and the West Australian dhufish, *Glaucosoma hebraicum*, two marine fishes that also undergo metamorphosis (Shand *et al*., 1999b; Shand *et al*., 2001).

Near the periphery, the regularity of the square lattice contrasted with the jitter present in multiple square mosaic regions of the central retina. At the growth zone, the square mosaic contained corner cones (Fig. B1), and these disappeared with distance from the periphery, as has been shown for the Atlantic salmon, *Salmo salar* (Kunz *et al*., 1994). These observations suggest a direct path of square mosaic formation, as established for other fishes.

2.4.3. Topographical changes in visual acuity match foraging ecology

In the non-peripheral retina, spatial resolving power, our theoretical measure of visual acuity, was greatest in the ventrotemporal retina of the youngest Atlantic halibut examined. At the end of metamorphosis, the area of highest resolving power had shifted to the dorsotemporal retina. The values computed were nearly identical to those published for the plaice, *Pleuronectes platessa*, another flatfish, where spatial resolving power (independently derived from measures of radially-oriented central retina) was ~0.5º at the start of metamorphosis and ~0.3º by the end (Neave, 1984).

The shift in area of greatest resolving power conforms with the foraging needs of the fish as it transforms from a bilaterally symmetric larva to a flattened, demersal juvenile. Pelagic fishes, including larvae, often have the highest cone densities in the ventrotemporal retina and strike at prey that contrast against the water background

located in front of them or slightly above (Novales Flamarique, 2013; Novales Flamarique, 2016; Novales Flamarique, 2019). Demersal fishes, on the other hand, often strike at prey that contrasts against the bottom of the water body (Holmes & Gibson, 1983). As such, the observed shift in area of greatest resolving power would be expected to maximize prey capture, the strongest determinant of fish growth and survival.

2.4.4. A potential role for the triple cone in achromatic target detection

That the highest visual acuity in the post-metamorphic fish coincided with the area of densest triple cone presence suggests that the random mosaic associated with triple cones is not an unintentional by-product of development but serves a specific function. The adults of other demersal fishes have a similar triple cone area in the centrodorsotemporal retina, in the vicinity of where the highest cone densities are found (Fritsch *et al*., 2017; Frau *et al*., 2020). Spatial analyses of flatfish mosaics show that greater cone packing can be achieved through a combination of different cone morphologies (including the triple cone) compared to that from the square mosaic (Frau *et al*., 2020). It has been argued, however, that a regular mosaic should provide better chromatic visual acuity due to the regular distribution of spectral inputs across the visual field (Frau *et al*., 2020; Fernald, 1981; van der Meer, 1992). For a fish that lives in habitats with low light, visual acuity based on chromatic contrast may not be as important as improving photon catch and, potentially, achromatic detection of targets.

In the random mosaic region, the ratio of the sum of triple and double cones to single cones is the same (~2) as that of double to single cones in nearby square mosaic regions. As such, the total ratio of longer to shorter wavelength input should be similar regardless of the mosaic, the major difference being the regularity of chromatic input. Based on these observations and the greater cone packing achievable with the random mosaic (Frau *et al*., 2020), we propose that triple cones serve an achromatic area of high visual acuity. Because of the ventral position of the optic nerve head, the area of random mosaic appears to view the forward horizon. It may therefore represent a specialized region for the early detection of large groundfish predators, like many species of elasmobranchs, that cruise the ocean floor in search of demersal prey. Such

predators lack significant colour and would be readily detected achromatically by improving photon catch.

2.4.5. Visual pigment co-expression: a potential shift toward longer wavelength absorbance

Absorbance measurements from post-metamorphic retinas indicated the presence of at least two opsins, with associated visual pigments peaking at 431 nm and 457 nm, among the single cone population. The λ_{max} and bandwidth at half maximum of the rod visual pigment (mean ± SD = 4170 ± 234 cm^{-1}, n=20) suggested retinal (the aldehyde of vitamin A_1) as the only chromophore in the retina (Hárosi, 1994), as has been measured by High Performance Liquid Chromatography in starry flounder, *Platichthys stellatus* (Iwanicki *et al*., 2017; Savelli *et al*., 2018). Co-expression of the S(431) pigment with another visual pigment [potentially the M(500) or M(514)] in a given single cone was common and may illustrate a progressive switch toward the longer wavelength-associated opsin as the juvenile moves to greater depths. A progression toward longer visual pigments occurs in multiple cone types of the juvenile starry flounder (Savelli *et al*., 2018).

2.4.6. Visual opsin repertoire of Atlantic halibut

The predicted proteins from the Atlantic halibut genome provided evidence for seven visual opsin genes. Phylogenetic and tuning site analyses revealed that these opsins correspond to SWS1, SWS2A, SWS2B, RH1, RH2B, RH2C, and LWS. This expands the previous opsin repertoire known for Atlantic halibut which included SWS1, SWS2, RH1, RH2, and LWS (Helvik *et al*., 2001b). The updated opsin repertoire is consistent with those of other flatfish species, with six visual opsins reported for the common sole (*Solea solea*) and the Senegalese sole (*Solea senegalensis*) (Frau *et al*., 2020), eight for starry flounder (Iwanicki *et al*., 2017) and marbled sole (Sato *et al*., 2021), and nine for turbot (Wang *et al*., 2021). In particular, expansion of the *rh2* repertoire in Atlantic halibut follows findings in other flatfishes where *rh2b* and *rh2c* genes are common and *rh2a* is often absent or present as a pseudogene (Kasagi *et al*., 2015; Kasagi *et al*., 2018; Frau *et al*., 2020; Sato *et al*., 2021; Wang *et al*., 2021).

Both the number of predicted opsins and the surmised λ_{max} of their visual pigments when bound to retinal only partially matched microspectrophotometric records. The predicted SWS2A opsin matched the S(457) visual pigment, RH1 corresponded to the rod(491) visual pigment, and the LWS opsin matched the L(550) visual pigment. The S and M pigments found by microspectrophotometry were not a good match for the SWS2B or RH2 opsins. Previous work comparing the λ_{max} of M visual pigments in the starry flounder (Iwanicki *et al*., 2017) and the common sole (Frau *et al*., 2020) to those of barfin flounder (Kasagi *et al*., 2015) or marbled sole (Sato *et al*., 2021) (the latter two sets measured from opsin-retinal reconstitutions or predicted from opsin tuning sites, respectively) showed that the *in-vivo* measured pigments were significantly long wavelength shifted with respect to *in-vitro* determinations or predictions. With some opsins, this was the case despite having identical amino acids at all tuning sites between species (Kasagi *et al*., 2015; Frau *et al*., 2020b). These results suggest that alternative tuning sites or interactions between multiple tuning sites play important roles in determining the λ_{max} of S and M visual pigments in flatfishes.

2.4.7. Conclusion

Retinal transformation at metamorphosis in Atlantic halibut is a complex process that prepares the animal for the visual ecology demands of a demersal life style. Photoreceptor organization changes from a honeycomb mosaic consisting of single cones to two novel formations: the square mosaic, which occupies most of the post-metamorphic retina, and a random mosaic consisting of single, double and triple cones located in a restricted region of the dorsotemporal retina. In parallel, a square mosaic of greater regularity forms directly from progenitor cells in the peripheral growth zone, and both mosaics coalesce during metamorphosis. The central region of greatest visual acuity shifts from the ventrotemporal to the dorsotemporal retina in accordance with the change in foraging behaviour that accompanies the transition from pelagic to benthic lifestyle. The retina has the potential for colour vision containing a minimum of six cone visual pigments and one rod visual pigment. Such composition resembles that of other flatfishes that have been studied which show abundant expression of multiple S and M visual pigments, but diminished expression of UV and L visual pigments with age.

2.5. References

Bao, B., Ke, Z., Xing, J., Peatman, E., Liu, Z., Xie, C., Xu, B., Gai, J., Gong, X., & Yang, G. (2011). Proliferating cells in suborbital tissue drive eye migration in flatfish. *Developmental Biology*, *351*(1), 200–207.

Benzekri, H., Armesto, P., Cousin, X., Rovira, M., Crespo, D., Merlo, M. A., Mazurais, D., Bautista, R., Guerrero-Fernández, D., & Fernandez-Pozo, N. (2014). De novo assembly, characterization and functional annotation of Senegalese sole (*Solea senegalensis*) and common sole (*Solea solea*) transcriptomes: Integration in a database and design of a microarray. *Bmc Genomics*, *15*(1), 1–18.

Cacei, M., & Cacheris, W. (1984). Fitting curves to data (the Simplex algorithm is the answer). *Byte. 5*, 340–360.

Cheng, C. L., Flamarique, I. N., Hárosi, F. I., Rickers-Haunerland, J., & Haunerland, N. H. (2006). Photoreceptor layer of salmonid fishes: Transformation and loss of single cones in juvenile fish. *Journal of Comparative Neurology*, *495*(2), 213–235.

Davies, W. I., Tamai, T. K., Zheng, L., Fu, J. K., Rihel, J., Foster, R. G., Whitmore, D., & Hankins, M. W. (2015). An extended family of novel vertebrate photopigments is widely expressed and displays a diversity of function. *Genome Research*, *25*(11), 1666–1679.

de Busserolles, F., Cortesi, F., Fogg, L., Stieb, S. M., Luehrmann, M., & Marshall, N. J. (2021). The visual ecology of Holocentridae, a nocturnal coral reef fish family with a deep-sea-like multibank retina. *Journal of Experimental Biology*, *224*(1), jeb233098.

Einfeldt, A. L., Kess, T., Messmer, A., Duffy, S., Wringe, B. F., Fisher, J., den Heyer, C., Bradbury, I. R., Ruzzante, D. E., & Bentzen, P. (2021). Chromosome level reference of Atlantic halibut *Hippoglossus hippoglossus* provides insight into the evolution of sexual determination systems. *Molecular Ecology Resources*, *21*(5), 1686–1696.

Evans, B. I., & Fernald, R. D. (1993). Retinal transformation at metamorphosis in the winter flounder (*Pseudopleuronectes americanus*). *Visual Neuroscience*, *10*(6), 1055–1064.

Evans, B. I., Hárosi, F. I., & Fernald, R. D. (1993). Photoreceptor spectral absorbance in larval and adult winter flounder (*Pseudopleuronectes americanus*). *Visual Neuroscience*, *10*(6), 1065–1071.

Fernald, R. D. (1981). Chromatic organization of a cichlid fish retina. *Vision Research*, *21*(12), 1749–1753.

Figueras, A., Robledo, D., Corvelo, A., Hermida, M., Pereiro, P., Rubiolo, J. A., Gómez-Garrido, J., Carreté, L., Bello, X., & Gut, M. (2016). Whole genome sequencing of turbot (*Scophthalmus maximus*; Pleuronectiformes): A fish adapted to demersal life. *DNA Research*, *23*(3), 181–192.

Frau, S., Novales Flamarique, I., Keeley, P. W., Reese, B. E., & Muñoz-Cueto, J. A. (2020). Straying from the flatfish retinal plan: Cone photoreceptor patterning in the common sole (*Solea solea*) and the Senegalese sole (*Solea senegalensis*). *Journal of Comparative Neurology*, *528*(14), 2283–2307.

Fritsch, R., Collin, S. P., & Michiels, N. K. (2017). Anatomical analysis of the retinal specializations to a crypto-benthic, micro-predatory lifestyle in the Mediterranean triplefin blenny *Tripterygion delaisi*. *Frontiers in Neuroanatomy*, *11*, 122.

Geffen, A., Van der Veer, H., & Nash, R. (2007). The cost of metamorphosis in flatfishes. *Journal of Sea Research*, *58*(1), 35–45.

Hárosi, F. I. (1987). Cynomolgus and rhesus monkey visual pigments. Application of Fourier transform smoothing and statistical techniques to the determination of spectral parameters. *The Journal of General Physiology*, *89*(5), 717–743.

Hárosi, F. I. (1994). An analysis of two spectral properties of vertebrate visual pigments. *Vision Research*, *34*(11), 1359–1367.

Harrison, K. J., Crécy-Lagard, V. de, & Zallot, R. (2018). Gene Graphics: A genomic neighborhood data visualization web application. *Bioinformatics*, *34*(8), 1406–1408.

Helvik, J. V., Drivenes, Ø., Næss, T. H., Fjose, A. & Seo, H.-C. (2001). Molecular cloning and characterization of five opsin genes from the marine flatfish Atlantic halibut (*Hippoglossus hippoglossus*). *Visual Neuroscience*, *18*(5), 767–780.

Hoke, K. L., Evans, B. I., & Fernald, R. D. (2006). Remodeling of the cone photoreceptor mosaic during metamorphosis of flounder (*Pseudopleuronectes americanus*). *Brain, Behavior and Evolution*, *68*(4), 241–254.

Holmes, R., & Gibson, R. (1983). A comparison of predatory behaviour in flatfish. *Animal Behaviour*, *31*(4), 1244–1255.

Iwanicki, T. W., Novales Flamarique, I., Ausió, J., Morris, E., & Taylor, J. S. (2017). Fine-tuning light sensitivity in the starry flounder (*Platichthys stellatus*) retina: Regional variation in photoreceptor cell morphology and opsin gene expression. *Journal of Comparative Neurology*, *525*(10), 2328–2342.

Kasagi, S., Mizusawa, K., Murakami, N., Andoh, T., Furufuji, S., Kawamura, S., & Takahashi, A. (2015). Molecular and functional characterization of opsins in barfin flounder (*Verasper moseri*). *Gene*, *556*(2), 182–191.

Kasagi, S., Mizusawa, K., & Takahashi, A. (2018). Green-shifting of SWS 2A opsin sensitivity and loss of function of RH 2-A opsin in flounders, genus Verasper. *Ecology and Evolution*, *8*(2), 1399–1410.

Keeley, P. W., Eglen, S. J., & Reese, B. E. (2020). From random to regular: Variation in the patterning of retinal mosaics. *Journal of Comparative Neurology*, *528*(13), 2135–2160.

Kumar, S., Stecher, G., Li, M., Knyaz, C., & Tamura, K. (2018). MEGA X: molecular evolutionary genetics analysis across computing platforms. *Molecular Biology and Evolution*, *35*(6), 1547.

Kunz, Y., Wildenburg, G., Goodrich, L., & Callaghan, E. (1994). The fate of ultraviolet receptors in the retina of the Atlantic salmon (Salmo salar). *Vision Research*, *34*(11), 1375–1383.

Kvenseth, A., Pittman, K., & Helvik, J. (1996). Eye development in Atlantic halibut (*Hippoglossus hippoglossus*): Differentiation and development of the retina from early yolk sac stages through metamorphosis. *Canadian Journal of Fisheries and Aquatic Sciences*, *53*(11), 2524–2532.

Larkin, M. A., Blackshields, G., Brown, N. P., Chenna, R., McGettigan, P. A., McWilliam, H., Valentin, F., Wallace, I. M., Wilm, A., & Lopez, R. (2007). Clustal W and Clustal X version 2.0. *Bioinformatics*, *23*(21), 2947–2948.

Musilova, Z., Cortesi, F., Matschiner, M., Davies, W. I., Patel, J. S., Stieb, S. M., de Busserolles, F., Malmstrøm, M., Tørresen, O. K., & Brown, C. J. (2019). Vision using multiple distinct rod opsins in deep-sea fishes. *Science*, *364*(6440), 588–592.

Nakamura, Y., Mori, K., Saitoh, K., Oshima, K., Mekuchi, M., Sugaya, T., Shigenobu, Y., Ojima, N., Muta, S., & Fujiwara, A. (2013). Evolutionary changes of multiple visual pigment genes in the complete genome of Pacific bluefin tuna. *Proceedings of the National Academy of Sciences*, *110*(27), 11061–11066.

Neave, D. (1984). The development of visual acuity in larval plaice and turbot. *J. Exp. Mar. Biol. Ecol.*, *78*, 167–175.

Novales Flamarique, I.N., & Hárosi, F. I. (2000). Photoreceptors, visual pigments, and ellipsosomes in the killifish, *Fundulus heteroclitus*: A microspectrophotometric and histological study. *Visual Neuroscience*, *17*(3), 403–420.

Novales Flamarique, I. N., & Hárosi, F. I. (2002). Visual pigments and dichroism of anchovy cones: A model system for polarization detection. *Visual Neuroscience*, *19*(4), 467–473.

Novales Flamarique, I. (2013). Opsin switch reveals function of the ultraviolet cone in fish foraging. *Proceedings of the Royal Society B: Biological Sciences*, *280*(1752), 20122490.

Novales Flamarique, I. (2016). Diminished foraging performance of a mutant zebrafish with reduced population of ultraviolet cones. *Proceedings of the Royal Society B: Biological Sciences*, *283*(1826), 20160058.

Novales Flamarique, I. (2019). Swimming behaviour tunes fish polarization vision to double prey sighting distance. *Scientific Reports*, *9*(1), 1–8.

Palacios, A. G., Goldsmith, T. H., & Bernard, G. D. (1996). Sensitivity of cones from a cyprinid fish (*Danio aequipinnatus*) to ultraviolet and visible light. *Visual Neuroscience*, *13*(3), 411–421.

Palczewski, K., Kumasaka, T., Hori, T., Behnke, C. A., Motoshima, H., Fox, B. A., Le Trong, I., Teller, D. C., Okada, T., & Stenkamp, R. E. (2000). Crystal structure of rhodopsin: AG protein-coupled receptor. *Science*, *289*(5480), 739–745.

R Core Team. (2021). R: A language and environment for statistical computing. R Foundation for Statistical Computing, Vienna, Austria. URL https://www.R-project.org/.

RStudio Team. (2021). RStudio: Integrated Development Environment for R. RStudio, PBC, Boston, MA URL http://www.rstudio.com/.

Reese, B. E., & Keeley, P. W. (2015). Design principles and developmental mechanisms underlying retinal mosaics. *Biological Reviews*, *90*(3), 854–876.

Sato, I., Kasagi, S., Takahashi, A., & Mizusawa, K. (2021). Expression dynamics of visual opsin genes in marbled sole *Pseudopleuronectes yokohamae* during metamorphosis from the larval to the juvenile stage. *Gene*, *787*, 145622.

Savelli, I., Flamarique, I. N., Iwanicki, T., & Taylor, J. S. (2018). Parallel opsin switches in multiple cone types of the starry flounder retina: Tuning visual pigment composition for a demersal life style. *Scientific Reports*, *8*(1), 1–10.

Shand, J., Archer, M. A., & Collin, S. P. (1999). Ontogenetic changes in the retinal photoreceptor mosaic in a fish, the black bream, *Acanthopagrus butcheri*. *Journal of Comparative Neurology*, *412*(2), 203–217.

Shand, J., ARCHER, M. A., THOMAS, N., & CLEARY, J. (2001). Retinal development of West Australian dhufish, *Glaucosoma hebraicum*. *Visual Neuroscience*, *18*(5), 711.

Sirovich, L., & Abramov, I. (1977). Photopigments and pseudo-pigments. *Vision Research*, *17*(1), 5–16.

Suzuki, T., & Tanaka, M. (2014). Development and regulation of external asymmetry during flatfish metamorphosis in. *Flatfishes: Biology and Exploitation*, 463–493.

Takahashi, Y., & Ebrey, T. G. (2003). Molecular basis of spectral tuning in the newt short wavelength sensitive visual pigment. *Biochemistry*, *42*(20), 6025–6034.

Van der Meer, H. (1992). Constructional morphology of photoreceptor patterns in percomorph fish. *Acta Biotheoretica*, *40*(1), 51–85.

Wang, Y., Zhou, L., Wu, L., Song, C., Ma, X., Xu, S., Du, T., Li, X., & Li, J. (2021). Evolutionary ecology of the visual opsin gene sequence and its expression in turbot (*Scophthalmus maximus*). *BMC Ecology and Evolution*, *21*(1), 1–12.

Yokoyama, S. (2008). Evolution of dim-light and color vision pigments. *Annu. Rev. Genomics Hum. Genet.*, *9*, 259–282.

Yu, G., Smith, D. K., Zhu, H., Guan, Y., & Lam, T. T. (2017). ggtree: An R package for visualization and annotation of phylogenetic trees with their covariates and other associated data. *Methods in Ecology and Evolution*, *8*(1), 28–36.

Zhang, R., Zhao, J., Hao, Y., Cao, X., Zhao, Y., & Tang, S. (2019). Retinal development in mandarinfish *Siniperca chuatsi* and morphological analysis of the photoreceptor layer. *Journal of Fish Biology*, *95*(3), 903–917.

Chapter 3.

Chromatic organization of retinal photoreceptors during eye migration of Atlantic halibut (*Hippoglossus hippoglossus*)

This chapter was adapted from Bolstad, K., & Novales Flamarique, I. (2022b). Chromatic organization of retinal photoreceptors during eye migration of Atlantic halibut (*Hippoglossus hippoglossus*). *Journal of Comparative Neurology*, 1-25.

Abstract

The expression of different opsin types during eye migration has not been examined despite its importance in understanding photoreceptor plasticity and whether cell fate (in terms of spectral phenotype) could influence square mosaic formation. Here, we probed the retina of Atlantic halibut undergoing eye migration for opsin expression using two antibodies, AHblue and AB5407, that labeled short wavelength sensitive 2A (SWS2A) opsin and longer wavelength (predominantly middle wavelength sensitive, RH2) opsins, respectively. Throughout the retina, double and triple cones labeled with AB5407 exclusively, whereas the vast majority of single cones labeled with AHblue. A minority (<5%) of single cones in the square mosaic of the centroventral retina labeled with AB5407. In regions of mosaic transition and near peripheral growth zones, some single cones co-expressed at least two opsins as they labeled with both antibodies. Short wavelength (SWS2A expressing, or S) cones formed a non-random mosaic gradient from central to dorsal retina in a region dominated by the larval single cone mosaic. Our results demonstrate the expression of at least two opsins throughout the post-metamorphic retina and suggest opsin switching as a mechanism to create new cone spectral phenotypes. In addition, the S cone gradient at the onset of eye migration may underlie a plastic, cell induction mechanism by which a cone's phenotype determines that of its neighbors and the formation of the square mosaic.

3.1. Introduction

During eye migration, the retina of Atlantic halibut hosts multiple mosaic types as a function of topographical location and developmental stage; these changes in the spatial organization of photoreceptors correspond to shifts in visual acuity during metamorphosis that match changes in foraging ecology (Bolstad & Novales Flamarique, 2022a; Chapter 2). In addition to different visual acuity demands prior to and post-metamorphosis, the transition of flatfish from a pelagic to a benthic environment expose them to different light conditions, and thus, may necessitate a change in the chromatic (opsin) expression of photoreceptors.

Corresponding changes in opsin expression with metamorphosis are found in winter flounder: *in-situ* hybridization experiments demonstrated that larval retinal photoreceptors express a single opsin transcript (*rh2*), some of which are replaced in the post-metamorphic retina which expresses four opsin transcripts (*sws2*, *rh2*, *lws*, and *rh1*) (Hoke *et al*., 2006). Within these post-metamorphic retinas, *sws2* expression was confined to single cones, and *rh2* and *lws* were each confined to one member of a double cone. In contrast to the findings in winter flounder, *in-situ* hybridization observations from Atlantic halibut larvae toward the end of yolk sac absorption (i.e., 40 days post-hatching, or about 30 days prior to the start of eye migration) showed expression of four opsin transcripts (*sws1*, *sws2*, *rh2* and *lws*) in the single cone retina (Helvik *et al*., 2001b). The vast majority (> 90%) of cones expressed *rh2* whereas *sws2* and *lws* were only found in about 10% of photoreceptors. Regardless of frequency, *sws2*, *rh2*, and *lws* were found throughout the retina, while *sws1* was confined to the ventral retina (Helvik *et al*., 2001a; Forsell *et al*., 2001). Later analysis of the juvenile retina (2 year old fish) showed *rh2* and *lws* localized to separate double cones in the square mosaic (Helvik *et al*., 2001b). To obtain this square mosaic patterning, Helvik *et al*. (2001a) argue that some *rh2* expressing photoreceptors must acquire a different spectral phenotype. Further, microspectrophotometry data in the juvenile suggests co-localization of an S (431 nm) and M visual pigment in most single cones (Bolstad & Novales Flamarique, 2022a; Chapter 2), however, the chromatic organization of photoreceptors during eye migration is unknown in Atlantic halibut. Additionally, chromatic organization has not been assessed at a protein level in any flatfish.

In Chapter 2, I propose that the triple cones found in the centrodorsotemporal retina in Atlantic halibut may be important for achromatic target detection, but the spectral phenotype of the cones in this area have not yet been characterized.

This chapter examines the chromatic organization of photoreceptors during eye migration of Atlantic halibut by histochemical and spatial (topographical) analyses. The work was performed on the same cohort of fish previously analyzed for photoreceptor morphological organization and visual pigment content (Bolstad & Novales Flamarique, 2022a; Chapter 2). By exploring opsin expression of photoreceptors, this study reveals potential mechanisms of mosaic re-organization including spectral phenotype plasticity in flatfishes.

3.2. Methods

The fish examined are from the same cohort discussed in Chapter 2, As such, all methods related to fish collection can be found there.

3.2.1. Immunohistochemistry

Whole bodies of euthanized fish were fixed (4% paraformaldehyde in 0.08 M PBS, pH 7.4) at 4^{o}C for a minimum of 72 hrs. For a given fish, the head was processed as a whole or the eyes were extracted from it and processed individually, keeping track of the left and right eye. Following several rinses in 0.08 M PBS, the tissue was cryoprotected in sucrose solution (25% sucrose, 20% optimal cutting temperature [OCT] medium in 0.08 M PBS) and embedded in 100% OCT medium (Cedar Lane Laboratories). The resulting blocks were cryosectioned in 7-10 µm steps in either tangential (for individual eyes) or coronal (for heads) planes (Fig. 2.1) to reveal the cone mosaic or photoreceptors along their lengths in the medial retina, respectively. Serial sections were deposited cyclically on poly-L-lysine coated slides and used for immunohistochemical detection of opsins. This entailed blocking the sections with a 1:20 solution of normal donkey serum:PBTA (PBTA: 0.5% bovine serum albumin in 0.08 M PBS with 0.1% Triton X-100 and 0.1% sodium azide) overnight at 4°C, followed by another overnight incubation in a solution containing one or two primary antibodies in PBTA (1:200). The primary antibodies used were mouse monoclonal 4D2 against bovine RH1 opsin (Molday and MacKenzie, 1983), rabbit AB5407 against human blue (SWS1)

opsin (Chemicon), and a mouse monoclonal antibody (AHblue) against the SWS2A opsin of Atlantic halibut (antigenic site: HGRVMELPEDFWIC) manufactured by GenScript USA (Table 3.1; Bolstad and Novales Flamarique, 2022a; Chapter 2).

Simultaneous incubation with two antibodies for the purpose of detecting two different opsins was only possible with AHblue and AB5407. Antibody AB5407 is known to label SWS2, RH2 and RH1 opsins with varying affinity in rainbow trout, *Onchorhynchus mykiss* (Novales Flamarique et al., 2021), and 4D2 labels RH2 and RH1 opsins in multiple fishes (Novales Flamarique, 2011). Antibody 1D4 against bovine RH1 opsin (Molday and MacKenzie, 1983) and AB5405 (Chemicon) against human MWS/LWS opsin were also attempted. However, AB5405 resulted in no labeling and 1D4 gave the same labeling pattern as 4D2 and AB5407 so they were not pursued further. Antibody 4D2 was independently used to quantify AB5407-labelled cells.

Following primary antibody incubation, the slides were rinsed multiple times in PBTA and exposed to secondary antibody solution (1:200 in PBTA) overnight at 4°C. The secondary antibodies contained cyanine fluorophores and consisted of donkey antirabbit or antimouse Cy2 or Cy 3 (Jackson Immunoresearch). Parallel, control experiments were also conducted without the primary or secondary antibodies. After several washes in PBTA, cover slips were put on the slides with 5% n-propyl-gallate in glycerol as the mounting medium. They were viewed with the E-600 Nikon microscope equipped for DIC and fluorescence imaging. Photographs were obtained with a DXM-100 digital camera at 30x (20x/0.50 objective) or 90x (60x/1.40 objective) total magnification. When necessary, multiple images were merged using Volocity Quantitation software (Quorum Technologies, Canada) to illustrate multi-labelling patterns. Observations were carried out on eight retinas (four left eye and four right eye in origin) cut tangentially and five heads cut radially, with four tangentially-cut retinas (two from left eyes and two from right eyes) analyzed for densities of cones labeled by AHblue or AB5407, and 4D2. The AHblue-derived S cone densities were used in the spatial analyses.

Table 3.1. List of primary antibodies.

Antibody	Immunogen	Host species	Source	Main target in retinas of fishes
AHblue (RRID:AB_2922945)	HGRVMELPEDFWIC *of* Atlantic halibut SWS2 opsin	Mouse	Bolstad & Novales Flamarique (2022b)	SWS2 opsin (Atlantic halibut)
4D2 (RRID:AB_2315273)	C terminal (4D2 epitope) of bovine rod outer segment	Mouse	Molday & MacKenzie (1983)	RH2 opsin (lesser affinity to RH1) (Atlantic salmon, zebrafish, northern anchovy)
AB5407 (RRID:AB_177457)	Human recombinant SWS1 (blue) opsin	Rabbit	Chemicon (AB5407)	RH2 and SWS2 opsins (lesser affinity to RH1)

3.2.2. Morphometric analyses

These analyses were undertaken to resolve the spatial organizations of AH-blue labelled cones within different mosaic types and how they compared to those when the entire population of single cones (Bolstad & Novales Flamarique, 2022a; Chapter 2) was considered. The same spatial statistics were used as in Chapter 2, with focus placed on the antibody (AHblue) labelled cones for S cones.

3.3. Results

3.3.1. Photoreceptor opsin expression

By combining tangential/oblique sections from isolated retinas (Fig. 2.1 E; Fig 3.1; Fig. 3.2) and coronal sections of the head through various regions of the eye with respect to the lens (Fig. 2.1E; Fig. C1- C3; Fig. 3.3- 3.7), the chromatic organization of cone photoreceptors was explored, simultaneously, with two antibodies (AHblue and AB5407) and, independently, with 4D2 (co-localized with AB5407, Fig. 3.2 A-H). In the retina at 773 ATU, the honeycomb mosaic (Fig. 3.1 A) showed a minority of single cones that labelled with AHblue (denoting SWS2 opsin expression; red fluorescence) among a

majority of single cones that labelled with AB5407 (denoting expression of a longer wavelength opsin, likely overwhelmingly RH2; green fluorescence) (Fig. 3.1 B). Cones expressing SWS2 (i.e., short wavelength sensitive, S, cones) were always surrounded by AB5407 labelled neighbours (Fig. 3.1 B; Fig. 3.2 I-L). Further from the centre of the retina, S cones often had three rows of AB5407 labelled single cones separating each other along one dimension (see rows between S cones within adjacent white hexagons in Fig. 3.1 B). Closer to the centre of the retina, this approximate spacing rule for a given S cone tended to occur with respect to all nearest homotypic cells (see lower right area of Fig. 3.1 B). Correspondingly, the ratio of AB5407 labelled cones to S cones increased significantly (ANOVA $F_{1,8} = 7.14$, $p = 0.028$) from a mean ± SD (n=4) of 11 ± 2.5 in the central retina to 22 ± 7.4 in the centrodorsal retina.

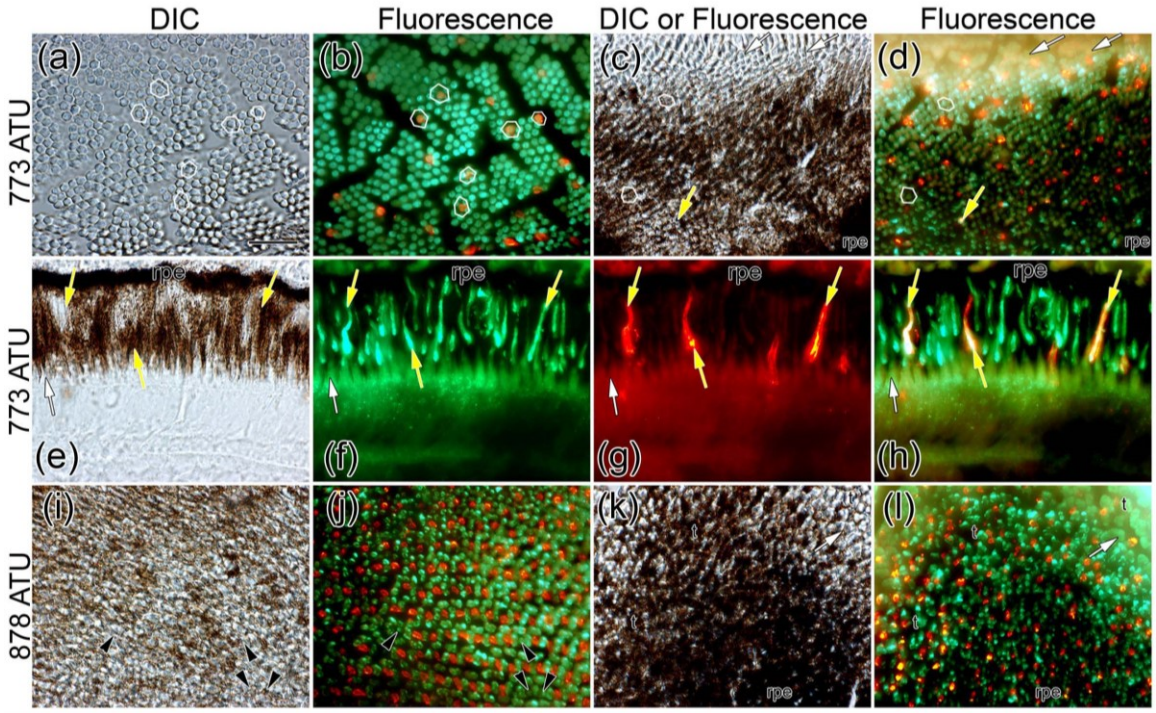

Figure 3.1. Micrographs of tangential or radial cryosections (DIC and corresponding fluorescence images) from the retina of Atlantic halibut undergoing eye migration.

Note: Symbols indicate the same structures in corresponding sets of images. Two primary antibodies were used (AB5407, green fluorescence, and AHblue, red-yellow fluorescence) with AB5407 labelling RH2 and LWS opsins and AH blue labelling SWS2 opsin ((a),(b)) Tangential micrographs from the central retina at 773 ATU showing a minority of single cones labelled with antibody AHblue (red-yellow fluorescence) among a majority labelled with antibody AB5407 (green fluorescence). The white hexagons (b) around SWS2 expressing cones link six AB5407 labelled neighbours (visible or extrapolated where gaps are found in the medium). ((c),(d)) Tangential micrographs from a transitional area in the centroventronasal retina at 773 ATU where double cones (top)

encounter the honeycomb mosaic (lower area with white hexagons). Double cones and most single cones label with AB5407; some single cones label with AHblue and one single cone co-expresses different opsin types as it labels with both antibodies (white fluorescence, yellow arrow). White arrows point to double cone partitioning membranes in this and other panels. ((e)-(h)) Radial micrographs showing co-expressing cones (yellow arrows) in the centroventronasal retina at 773 ATU. Sequential micrographs show green (f) and red (g) fluorescence, and the merged image (h). ((i),(j)) Tangential micrographs from the central retina at 878 ATU showing a square mosaic where double cones label with AB5407 and the overwhelming majority of single cones label with AHblue. Some single cones label with AB5407 (black arrowheads). ((k),(l)) Tangential micrographs from the centrodorsotemporal retina at 878 ATU showing triple (t) and double cones that label with AB5407 and single cones labelling with AHblue. Abbreviations: rpe, retinal pigment epithelium. Scale bar in (a) = 10 μm applies to ((b)-(l)).

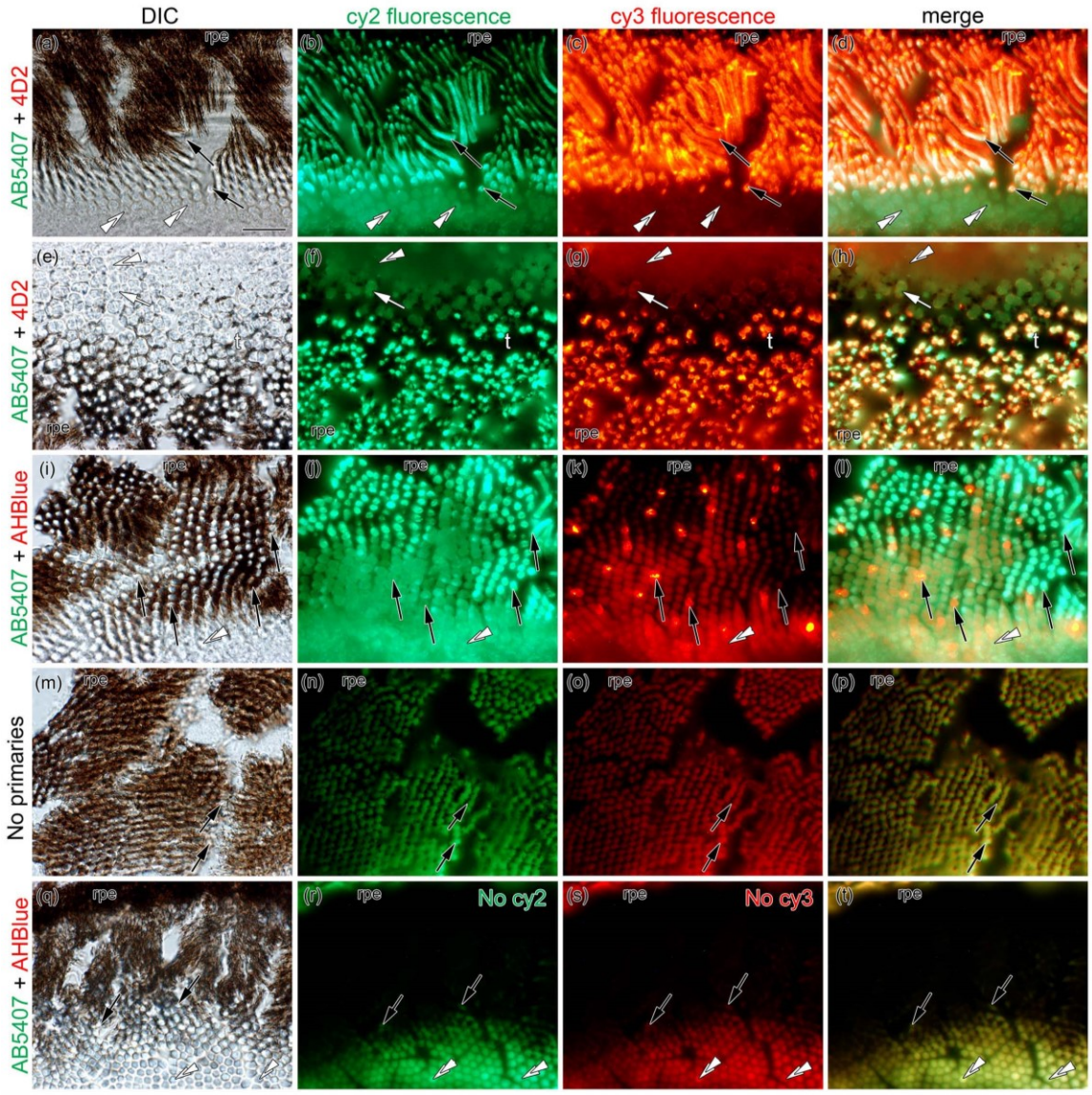

Figure 3.2. Micrographs of cryosections (DIC and corresponding fluorescence images) from the retina of one Atlantic halibut at 773 ATU showing labelling patterns by the two combinations of antibodies used in the study (AB5407 and AHBlue or AB5407 and 4D2) and controls.

Note: Symbols indicate the same structures in corresponding sets of images. ((a)-(d)) Section showing the honeycomb mosaic (a) where the outer segments of single cones labelled by AB5407 (b) are also labelled by 4D2 (c) as seen by the white colour in the merged image (d). The inner segments of cones (double white arrowheads) are not labelled as evidenced by the much lower background fluorescence compared to that of the outer segments (black arrows). ((e)-(h)) Same presentation as per ((a)-(d)) but for a region of the retina with triple cones (t) and double cones (white arrow points to a double cone partition). Both antibodies label the outer segments of double and triple cones. ((i)-(l)) Section of the honeycomb mosaic showing label with AB5407 and AHBlue; each antibody labels a different population of single cones. ((m)-(p)) Control section of the honeycomb mosaic showing low background fluorescence when primary antibodies (i.e., AB5407, AHBlue or 4D2) are excluded from the procedure. ((q)-(t)) Control section of

the honeycomb mosaic showing minute background fluorescence (primarily restricted to the inner segments) when primary antibodies (in this case AB5407 and AHBlue) are included but secondary antibodies (cy2 and cy3) are excluded from the procedure. Abbreviation: rpe, retinal pigment epithelium. Scale bar in (a) = 10 μm applies to all panels.

In regions of transition between the honeycomb mosaic and adjacent areas with double cones, S cones became more equidistant with proximity to the region of double cones (Fig. 3.1 C,D). On occasion, cones labelling with both antibodies, thereby co-expressing a minimum of two different opsins, were present near transition areas (Fig. 3.1 C-H) and closer to peripheral growth zones (Fig. 3.3 A,B; Fig. 3.7 A,B). In radial sections, co-expressing cones were identified by the co-localization of fluorescence to outer segments with the same shape (Fig. 3.1 E-H).

Regions with square mosaic formations had both double cone members that labelled with AB5407 whereas the majority of single cones labelled with AHblue (Fig. 3.1 I,J; shown for a retina at 878 ATU). In the central retina, a minority (3.5 ± 1.4 % of the single cone population, n=4) were not S cones but labelled with AB5407 (Fig. 3.1 J; black arrowheads). In areas with triple cones, both double and triple cones labelled exclusively with AB5407 and single cones with AHblue. Thus, all areas of the retina expressed a minimum of two opsins among the cone population. Labelling trends were the same for left and right eye retinas. Control retinas (i.e., those that had not undergone primary or secondary antibody incubation) showed only minor background autofluorescence and this was primarily concentrated in the inner segments (Fig. 3.2 M-T) as is often the case with paraformaldehyde fixation.

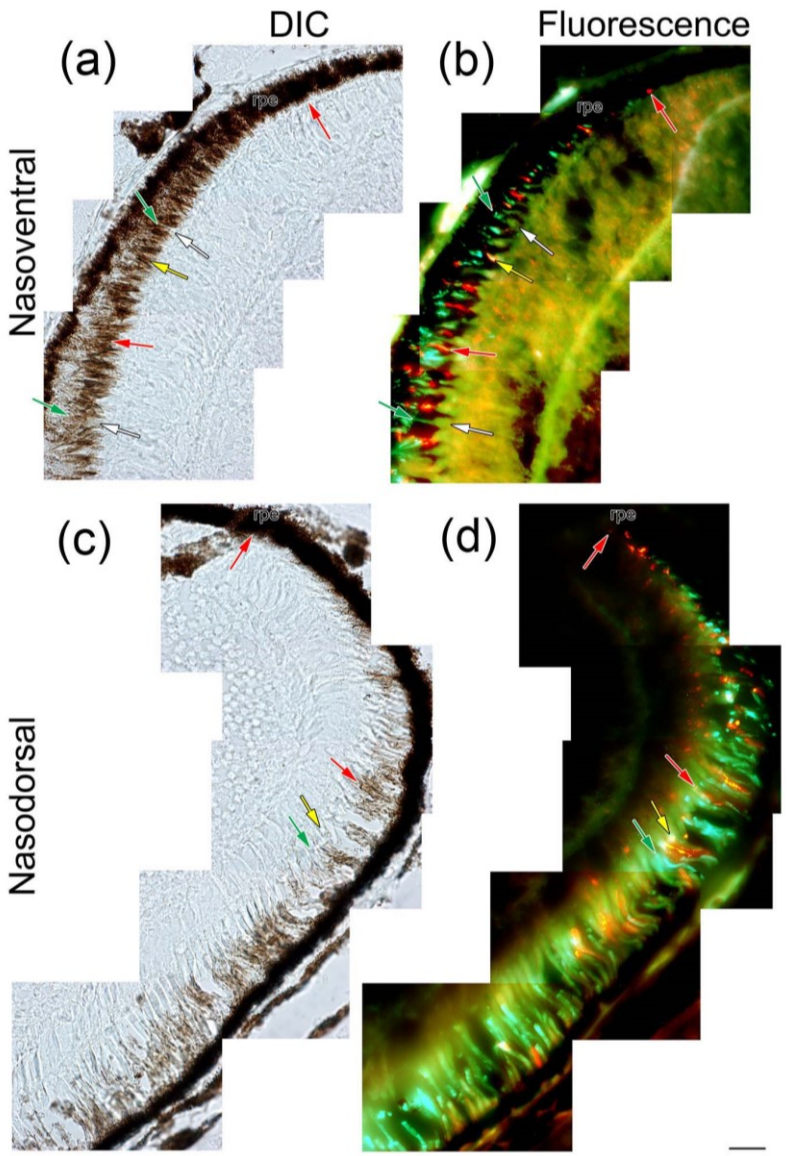

Figure 3.3. Micrographs of radial cryosections (DIC and corresponding fluorescence images) showing the most ventral ((a),(b)) and most dorsal ((c),(d)) regions of the nasal retina shown in Figure C1.

Note: Symbols indicate the same structures in corresponding sets of images. ((a),(b)) The ventral periphery exhibits single and double cones (a) with prominent labelling of double cones by AB5407 (green fluorescence, green arrows) and single cones by AHblue (red-yellow fluorescence, red arrows); the occasional single cone labels with both antibodies (yellow arrow) (b). ((c),(d)) The dorsal periphery shows single cones (c) labelled with either AB5407 (green fluorescence, green arrows) or AHblue (red-yellow fluorescence, red arrows), with instances of double labelling at the base of some single cone outer segments (yellow arrow) (d). As opposed to the labelling throughout the ventral periphery (b), the frequency of cones labelled by AHblue in the dorsal periphery diminishes toward the central retina (d). In both peripheral growth zones, AHblue is the first antibody to label differentiating cones ((b),(d)). White arrows point to double cone partitions. Scale bar at the bottom right = 10 µm and applies to ((a)-(d)).

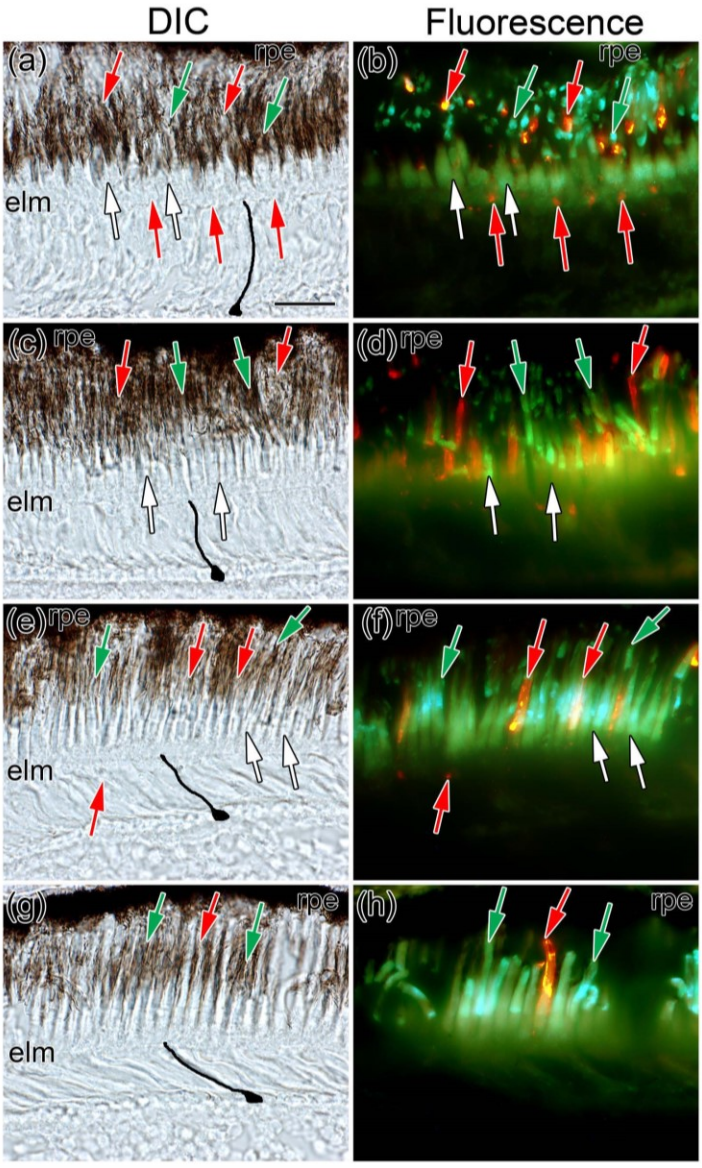

Figure 3.4. Micrographs of radial cryosections (DIC and corresponding fluorescence images) spanning various regions from the nasal retina illustrated in Figure C1.

Note: Symbols indicate the same structures in corresponding sets of images. ((a),(b)) Centroventral retina showing single and double cones (a) and widespread labelling of outer segments by AHblue (red-yellow fluorescence, red arrows) and AB5407 (green fluorescence, green arrows) (b). Antibody AHblue also labels inner segments of single cones, particularly the myoid region near the external limiting membrane (elm). ((c),(d)) Central retina showing tightly packed cones and pronounced labelling of outer segments by AHblue and AB5407. ((e),(f)) Centrodorsal retina showing similar cone diversity and packing to that in the central retina ((c),(d)) but single cone labelling by AHblue is reduced (f). ((g),(h)) Dorsal retina showing only single cones (g) and labelling by AHblue restricted to one cone (h). A representative cone axon starting near the elm and ending at the terminal has been traced in black in each DIC image ((a),(c),(e),(g)) illustrating a progressive axonal bend from centroventral to dorsal retina. White arrows point to double cone partitions. Scale bar in (a) = 10 μm applies to ((b)-(h)).

The general trends deduced from analyses of tangential sections were corroborated and further resolved with radial sections. For instance, coronal cuts of the head at 773 ATU revealed extensive double cone presence in the ventral half of the retina within a population of cones that were generally shorter than those in the upper half (Fig. 3.3- 3.6). This region of the retina labelled prominently with both antibodies, from periphery to centre (Figure 3.3 A,B; Fig. 3.4 A-D; Fig. 3.5 A,B; Fig. 3.6 A-D). The central region contained slender, highly packed cones with extensive labelling by both antibodies (Fig. 3.4 C-F; Fig. 3.6 C-F) and the occasional presence of triple cones (Fig. 3.6 C). Cones in the dorsal retina showed little taper and there was a stretch centered around the mid-dorsal retina where double cones were absent (Fig. C1-C2; Fig. 3.4 G; Fig. 3.6 G). Nasal to the lens, this area devoid of double cones extended all the way to the periphery (Fig. 3.5 C,D). At the level of the lens, however, double cones started to appear closer to the peripheral growth zone (Fig. 3.5 C,D).

As opposed to the persistent pattern of AHblue label throughout the ventral retina (Fig. 3.3 B; Fig. 3.4 B,D; Fig. 3.5 B; Fig. 3.6 B,D), the frequency of SWS2 opsin expressing cells diminished from the centrodorsal to mid-dorsal retina (i.e., the stretch with low, if any, double cone presence) but increased again near the peripheral growth zone (Fig. 3.3 D; Fig. 3.4 F,H; Fig. 3.5 D; Fig. 3.6 F,H). The mid-dorsal retina was also characterized by a pronounced bend of cone axons compared to other regions of the retina (Fig. 3.4 A,C,E,G; Fig. 3.6 A,C,E,G). In peripheral growth zones, the first antibody to label differentiating photoreceptors was AHblue (Fig. 3.3; Fig. 3.5). Temporal to the lens (Fig. C3), the occurrence of double cones and regular S cone patterning in oblique sections suggested the widespread presence of square mosaics (Fig. 3.7 A-N). Closer to the distal temporal retina, a transition area was observed where a jittered square mosaic abutted onto the honeycomb mosaic (Fig. 3.7 O,P).

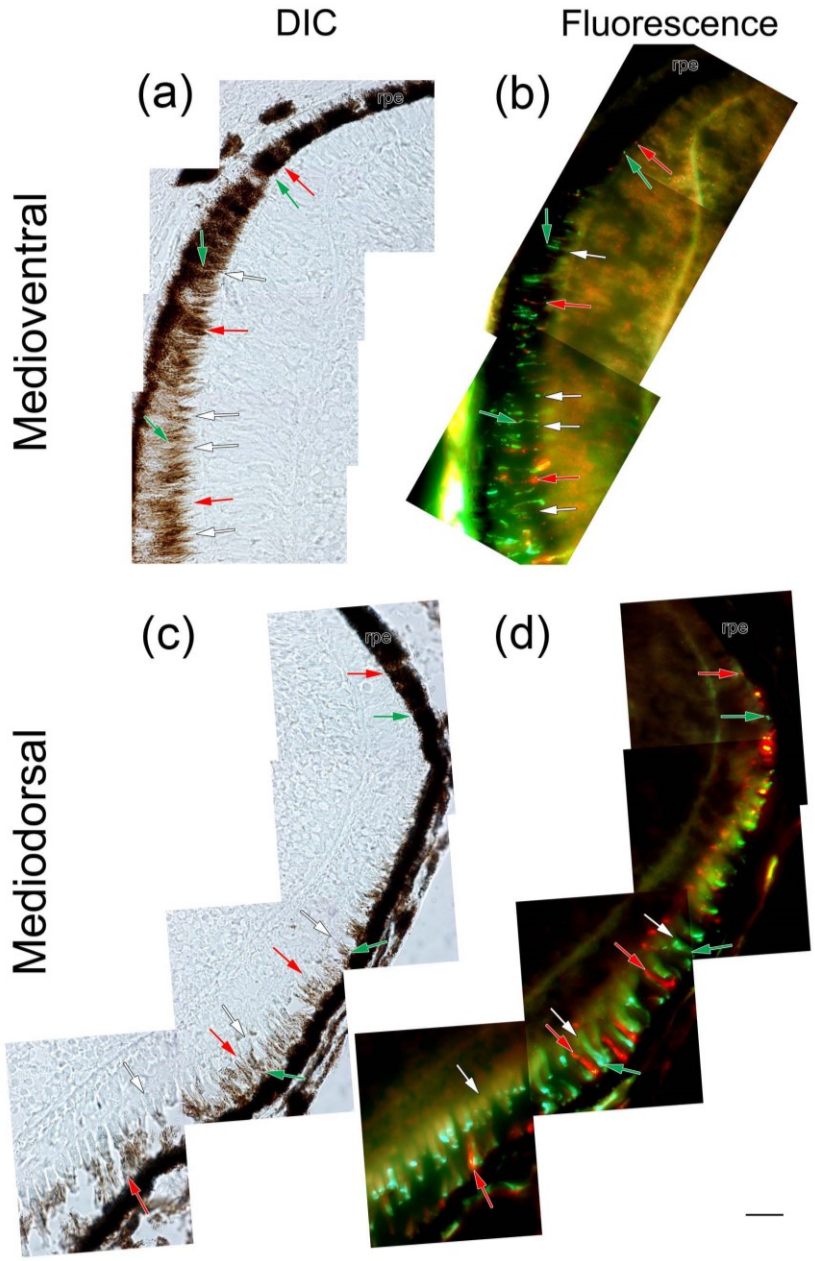

Figure 3.5. Micrographs of radial cryosections (DIC and corresponding fluorescence images) showing the most ventral ((a),(b)) and most dorsal ((c),(d)) regions of the medial retina illustrated in Figure C2.

Note: Symbols indicate the same structures in corresponding sets of images. ((a)-(d)) Both the ventral and dorsal peripheral retinal regions consist of single and double cones ((a),(c)) with the latter cone type labelled by AB5407 (green arrows) and the former by AHblue (red arrows)((b),(d)). As per the nasal retina (Figure 3.4), labelling by AHblue decreases from periphery toward centre in the dorsal retina (d) but not in the ventral retina (b). The first antibody to label differentiating cones in both peripheral growth zones is AHblue ((b),(d)). White arrows point to double cone partitions. The scale bar at the bottom right = 10 µm and applies to ((a)-(d)).

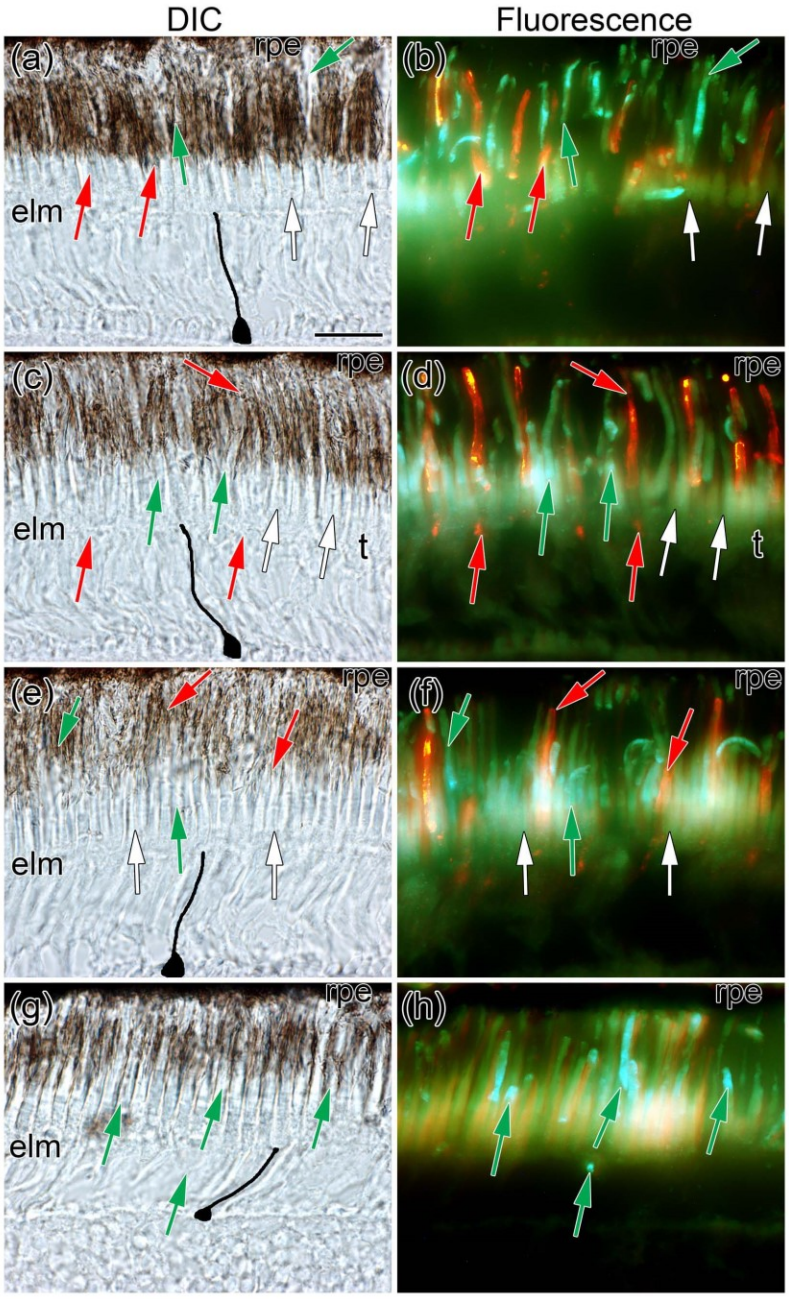

Figure 3.6. Micrographs of radial cryosections (DIC and corresponding fluorescence images) spanning various regions from the medial retina illustrated in Figure C2.

Note: Symbols indicate the same structures in corresponding sets of images. ((a)-(h)) Single and double cones are present throughout the centroventral to central retina ((a),(c),(e)) and some triple cones (t) can also be discerned in the central retina (c). Double and triple cones label with antibody AB5407 (green arrows) and single cones with AHblue (red arrows)((b),(d),(f)). ((g),(h)) Region from the mid-dorsal retina showing only single cones (g), and these label with AB5407 (h). A representative cone axon traced in black in each DIC image ((a),(c),(e),(g)) illustrates a greater axonal bend in the dorsal retina. White arrows point to double cone partitions. Scale bar in (A) = 10 µm applies to ((b)-(h)).

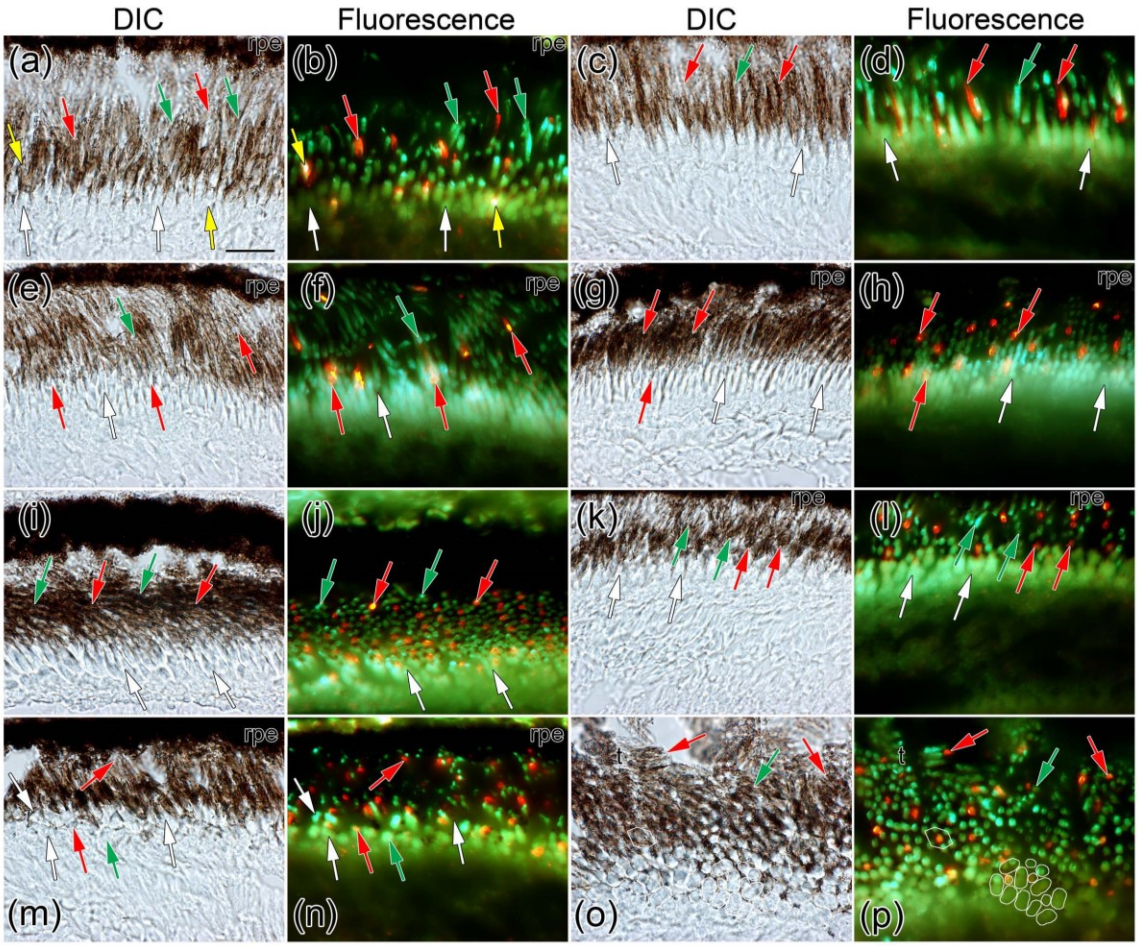

Figure 3.7. Micrographs of oblique cryosections (DIC and corresponding fluorescence images) showing various regions of the temporal retina illustrated in Figure C3.

Note: Symbols indicate the same structures in corresponding sets of images. ((a)-(d)) The ventral retina shows single and double cones ((a),(c)) with the latter cone type labelled by AB5407 (green arrows) and the former by AHblue (red arrows)((b),(d)). Closer to the ventral peripheral growth zone, some single cones label with both antibodies (yellow arrows) (b). ((e)-(h)) In areas closest to the central retina, cones are tightly packed ((e),(g)) and there is prominent labelling by both AB5407 and AHblue ((f),(h)). ((i)-(n)) In more dorsal areas, both the disposition of double cones ((m),(n)) and the periodic labelling by AHblue ((j),(l),(n)) reveal a square mosaic. ((o),(p)) Centrodorsotemporal retina from a coronal section temporal to that illustrated in Figure C3. This is a transitional area between honeycomb and square mosaic with the occasional triple cone (t). The inner segment contour of a few double cones and single cones have been traced in white near the transition zone. White arrows point to double cone partitions. The scale bar in (a) = 10 μm applies to ((b)-(p)).

3.3.2. Overview of the chromatic organization of cone mosaics

Figure 3.8 shows the chromatic organization of mosaic types during eye migration as deduced from antibody labelling by AHBlue and AB5407 (and the co-labelling 4D2), differential staining of double cone inner segments (e.g., Fig. 3.1 C,E), and visual pigment absorbance measurements from single and double cones in juvenile fish (Bolstad & Novales Flamarique, 2022a; Chapter 2). At 720 ATU, a square mosaic of varying jitter is present in the ventronasal and centrodorsotemporal retina; additionally, a highly regular square mosaic consisting of smaller cones occurs in areas near the periphery (Fig. 3.8 A). The double cones contain RH2 opsins except for a minority in the ventral retina (<1% of the total cone population) where one member likely expresses LWS opsin. This is deduced from differential staining of the two members that make up a double cone whereby, in other fishes (Novales Flamarique, 2001, 2002), the ellipsoid of the L member of an L/M pair stains darker than the M member with Richardson's solution (Bolstad & Novales Flamarique, 2022a; Chapter 2). Single centre cones express SWS2 opsins throughout the retina and a minority express RH2 opsins. Some single (corner) cones, found only in the ventral retina, may express SWS1 opsin (as deduced from *sws1* riboprobe labelling of rare single cones in the pre-metamorphic larva and in the 2 year old juvenile, Helvik *et al*., 2001a,b; Forsell *et al*., 2001). The rest of the retina shows single cones in honeycomb mosaic formation with the vast majority containing RH2 opsins and some expressing SWS2 opsin, but with reduced SWS2 expression toward the dorsal distal retina. In the ventro-temporal retina, there could be rare instances of single cones in the honeycomb mosaic that express SWS1 opsin, as suggested by the *sws1* transcripts detected at other stages (Helvik *et al*., 2001a,b; Forsell *et al*., 2001).

At 773 and 825 ATU, the square mosaic is present throughout the ventral retina and triple cones are found in the central region though they are primarily concentrated in the centrodorsotemporal retina (Fig. 3.8 B). Triple cones, like double cones, express RH2 opsins. Differential staining between triple cone inner segments was not found with Richardson's solution suggesting a lack of LWS opsin expression (Bolstad & Novales Flamarique, 2022a; Chapter 2). Single cones in areas with triple cones express SWS2 opsins. The honeycomb mosaic occupies primarily the dorsonasal retina, stretching to the nasal periphery. The majority of single cones in the honeycomb mosaic express RH2 opsins. Along the medial retina, from central to dorsal periphery, single cones of the

honeycomb mosaic form a gradient of diminishing SWS2 opsin expression. These S cones (that are part of the honeycomb mosaic) approach the density found in adjacent square mosaics near the central retina and then progressively decrease in number until they are absent in the mid-to-upper dorsal retina, re-appearing near the periphery but as part of square mosaics.

At 878 ATU, the entire retina is populated by the square mosaic with the exception of a centrodorsotemporal region that contains random arrangements of triple, double and single cones (Fig. 3.8 C; Bolstad & Novales Flamarique, 2022a; Chapter 2). As per other stages, double and triple cones express RH2 opsins and single centre cones express SWS2 opsins. A minority (<1%) of ventral double cones have one member that expresses LWS opsin as deduced from visual pigment measurements and differential staining of cone ellipsoids. Some corner cones may express SWS1 opsin (based on the very faint labelling with an *sws1* riboprobe obtained previously for two cones in a 2 year old fish, Helvik *et al*., 2001b). If such cones exist, however, they must be rare as no corresponding visual pigment was found by microspectrophotometry (Bolstad & Novales Flamarique, 2022a).

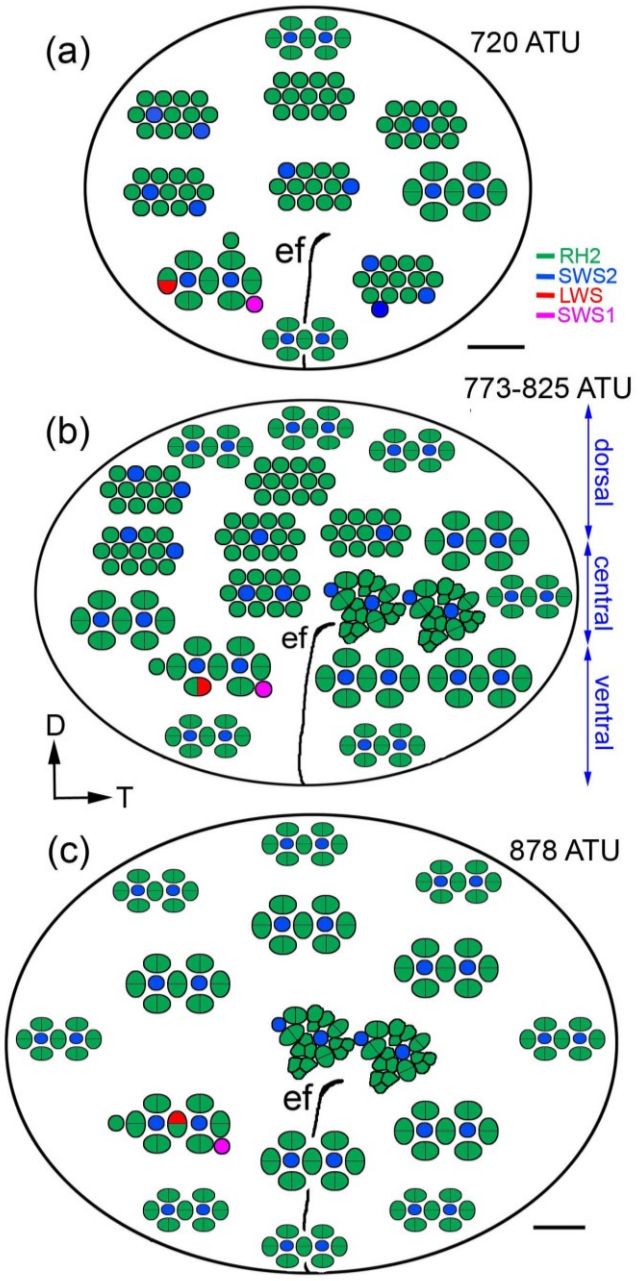

Figure 3.8. Schematics illustrating approximate positions of mosaic types and their opsin expression during eye migration of Atlantic halibut.

Note: (a) At 720 ATU, the retina shows a combination of honeycomb and square mosaics. Most cones in the honeycomb mosaic express RH2 opsins (green) and a minority express SWS2 opsins (blue). The latter (S cones) decrease in number toward the distal dorsal retina. Square mosaics of varying regularity are present in the ventronasal and centrodorsotemporal regions of the retina and another square mosaic, more regular and consisting of smaller cones, is present in peripheral areas. The square mosaic unit is made up of four double cones surrounding a single centre cone. Double cones express RH2 opsins (M/M pairs) but for a minority in the ventral retina that express LWS opsin (red) (L/M pairs). Centre cones express SWS2 opsins with the exception of a few in the ventral retina that express RH2 (or, potentially, SWS1) opsins.

Rare corner cones, present in the ventral retina may express SWS1 opsin (pink). (b) At 773 and 825 ATU, the retina has an additional, random mosaic consisting of single, double and triple cones throughout much of the central meridian but concentrated in the centrodorsotemporal retina. Single cones in this mosaic express SWS2 opsins whereas double and triple cones express RH2 opsins. The square mosaic occupies a progressively greater area of retina compared to the honeycomb mosaic. The approximate regions of dorsal, central and ventral retina corresponding to those in Figure 2.1(e) are indicated in blue on the right. (c) At 878 ATU, the square mosaic is present throughout the majority of the retina except for a centrodorsotemporal area dominated by the random mosaic of single, double and triple cones. Abbreviations: ef, embryonic fissure. In (b) the direction axes point to the dorsal (D) and temporal (T) retina; the legend shows the correspondence between opsins and colours. Scale bars in (a) and (c) = 0.2 mm applies to the retinal contours.

3.3.3. Spatial analyses of cone distributions, autocorrelations, and Density Recovery Profiles

The greatest S cone regularities were associated with lattice mosaics, as expected from their characteristically high periodicity (Fig. 3.9 A-E). The lowest ones belonged to S cones in mosaics with triple cones (Fig. 3.9 O-S) and intermediate ones were associated with S cones of the honeycomb mosaic (Fig. 3.5 F-J). The latter result differs from that when all single cones are considered (Bolstad & Novales Flamarique, 2022a; Chapter 2) revealing differential regularity with spectral cone identity. Of the S cones that were not part of square mosaics, only those that were part of the honeycomb mosaic (e.g., Fig. 3.9 F-J) had distributions with statistics significantly greater than those obtained from random simulations with corresponding mean density and constrained by soma size, i.e., 2.2 μm (mean ± SD regularity of S cone and corresponding random distributions were 4.9 ± 0.69 and 2.5 ± 0.42, respectively, by nearest neighbour analysis, and 5.2 ± 0.76 and 2.3 ± 0.45, respectively, by Voronoi domain analysis; $F_{4,24}$ and p for regularity derived by nearest neighbour analysis and Voronoi domain analysis were, respectively, 86 and <0.0001, and 110 and <0.0001).

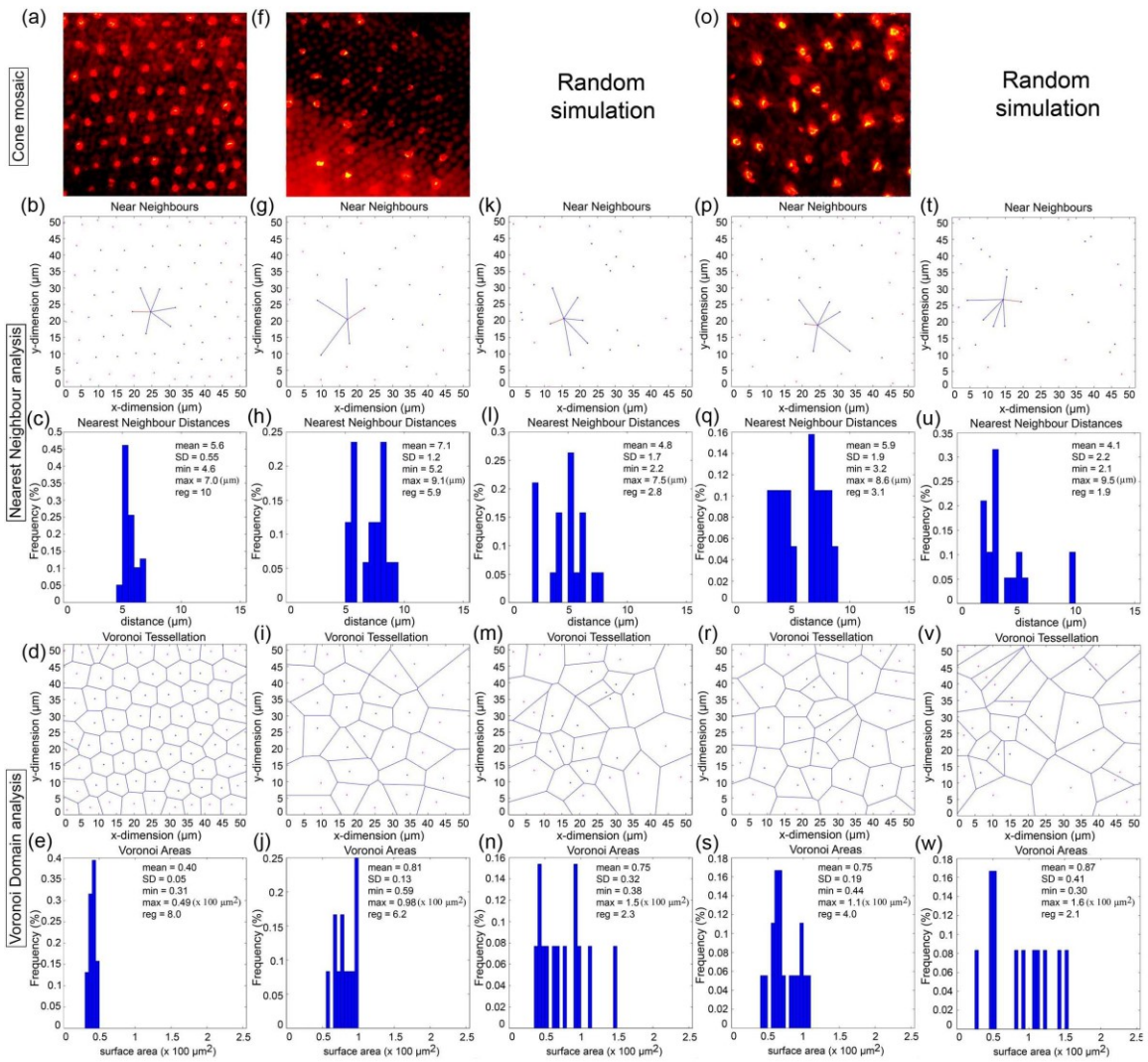

Figure 3.9. Spatial analysis of SWS2 opsin expressing single (S) cones (red-yellow labeling with AHblue) from representative mosaics in the retina of Atlantic halibut at 825 ATU.

Note: ((a)-(e)) Cone mosaic from the centroventral retina (a). Nearest neighbour analysis illustrating the near neighbours of a single cone, including its nearest neighbour in red (b) and their frequency distribution (c) [statistics (in μm) are the mean nearest neighbour distance, its standard deviation (SD), the minimum (min) and maximum (max) nearest neighbour distances, and the regularity index = mean/SD]; Voronoi tessellation of double cone domains (d) and their frequency distribution (e) [statistics (in 100 μm^2) are the mean area (domain), its standard deviation (SD), the minimum (min) and maximum (max) areas, and the regularity index = mean/SD]. ((f)-(j)) Same presentation of data as per ((a)-(e)) but for the centrodorsonasal retina. ((k)-(n)) Same presentation of data as per ((g)-(j)) but for a random distribution of points matched for density with that in (f) and constrained by single cone soma size. ((o)-(s)) Same presentation of data as per ((a)-(e)) but for the centrodorsotemporal retina. ((t)-(w)) Same presentation of data as per ((p)-(s)) but for a random distribution of points matched for density with that in (o) and constrained by single cone soma size.

Only S cones associated with the square mosaic (Fig. 3.10 A) had autocorrelograms with periodic foci characteristic of a lattice (Fig. 3.10 B); no such periodicity was observed with respect to non-square mosaics (Fig. 3.10 D,E,I,J). This result differs from that when all single cones are considered given the high regularity of the honeycomb mosaic in its entirety (Bolstad & Novales Flamarique, 2022a; Chapter 2). The density recovery profile of S cones in the square mosaic exceeded twice the diameter of a single cone (Fig. 3.10 C), as may have been expected from the presence of a double cone between nearest S cones (Fig. 3.1 E). In mosaics with triple cones, S cone autocorrelations (Fig. 3.10 J) produced effective radii (Fig. 3.10 K) that were statistically similar or lower than those obtained from simulations of random distributions (Fig. 3.10 L,M). In contrast, the effective radius of S cones in the honeycomb mosaic was significantly greater (mean ± SD = 5.7 ± 1.0) than that obtained from random distributions (3.0 ± 1.4) ($F_{4,24}$ = 12.3, p = 0.002) (Fig. 3.10 F,G,H).

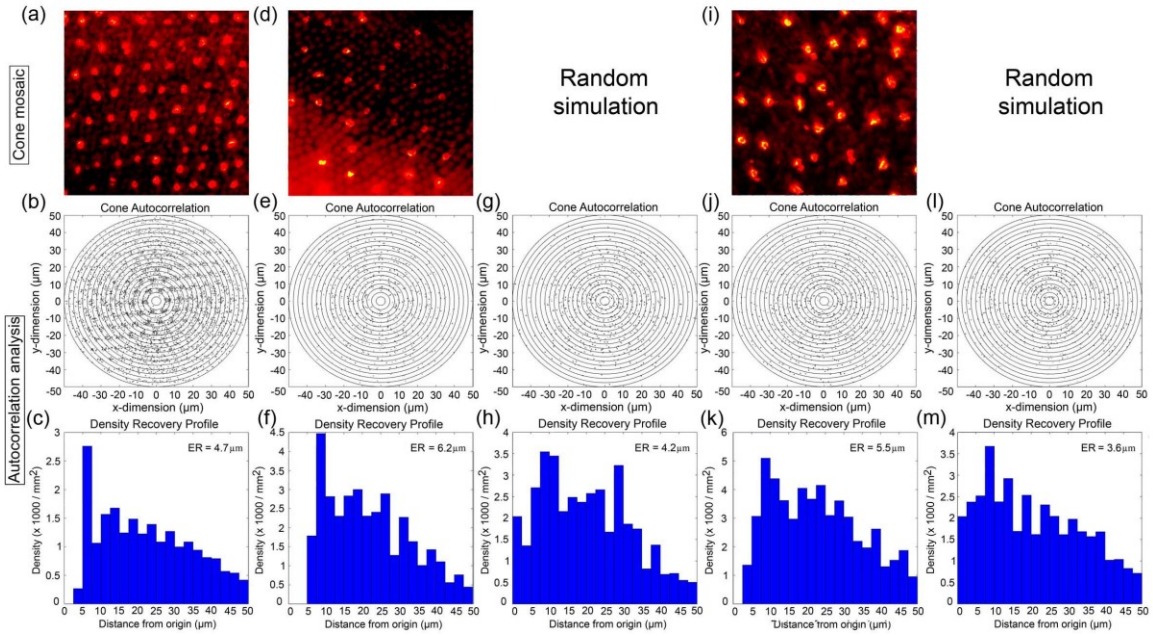

Figure 3.10. Autocorrelogram and associated density recovery profile for the distributions shown in Figure 3.9.

Note: The ER is the effective radius (or exclusion zone) which represents the size of the null region at the centre of the autocorrelogram.

3.4. Discussion

3.4.1. Chromatic organization of cone photoreceptors

The pre-metamorphic larva of Atlantic halibut at the end of yolk sac absorption has a honeycomb mosaic retina where single cones express transcripts belonging to all cone opsin classes (*sws1*, *sws2*, *rh2* and *lws*; Helvik et al. 2001a). The majority of these cones (> 90%) express *rh2* transcript whereas less than 10% express *sws2* or *lws* transcripts, though all these transcript types are distributed throughout the retina (Helvik *et a*l., 2001a). In accordance with these findings, our observations show that single cones of the honeycomb mosaic were overwhelmingly labelled by AB5407 and 4D2 which bind RH2 opsins. Short wavelength (SWS2 expressing, or S) cones in the honeycomb mosaic were, however, not ubiquitous throughout the retina. Their presence decreased from central to dorsal periphery and they were absent (no label with AHblue) in a region in the mid to upper dorsal retina. This retinal area did not show structural links between inner segments of neighbouring single cones which, in other fishes, marks the creation of novel cone types, such as double and triple cones (Shand *et al*., 1999, 2001).

In areas with square mosaics, S cones occupied the central position in the mosaic unit. Double cones labelled with AB5407 and 4D2 indicating expression of RH2 opsins. These results concur with microspectrophotometry measurements showing that single cones possessed overwhelmingly S visual pigments and double cones had, primarily, M visual pigments (Bolstad & Novales Flamarique, 2022a; Chapter 2). A minority (4 of 40 double cones measured by microspectrophotometry) were L/M pairs and these were found in the ventral retina, a region where up to 10% of the double cone population has members of a pair that stain differently from each other with Richardson's solution (Bolstad & Novales Flamarique, 2022a; Chapter 2). If this dye has the same properties in the retina of Atlantic halibut as in salmonid fishes (Novales Flamarique, 2001, 2002, Cheng *et al*., 2006), then L/M cones were present primarily in the ventral retina, constituted less than 1 % of the overall double cone population, and were randomly distributed.

A minority (< 5%) of single cones in square mosaics of the centroventral retina did not label with AHblue but, instead, labelled with AB5407. These cones would

therefore express RH2 opsins and may be the result of an imperfect chromatic re-arrangement process transforming the honeycomb mosaic into the square lattice (Bolstad & Novales Flamarique, 2022a; Chapter 2). Single cones that express RH2 opsins are found in other fishes that have square mosaics without corner cones. In these species, however, the double cones are L/L pairs (e.g., the freshwater sunfishes, Dearry & Barlow, 1987; Novales Flamarique & Hawryshyn 1997).

Corner cones were rare and only found in the ventral retina; some of them may have expressed SWS1 opsin, especially at the start of eye migration as *sws1* transcripts were detected in the pre-metamorphic larva (Helvik *et al*., 2001a). However, our inability to measure UV visual pigment in single cones (Bolstad & Novales Flamarique, 2022a; Chapter 2) suggests that there must be very few in the postmetamorphic retina. This appears to be the case in other flatfishes as well (Kasagi *et al*., 2015; Savelli *et al*., 2018; Sato *et al*., 2021).

In regions with random mosaics, double and triple cones expressed RH2 opsins, as they labelled with AB5407 and 4D2. The single cones in these mosaics were, overwhelmingly, S cones, since they labelled with AHblue. Some single cones, located near regions of mosaic transition, co-expressed at least two opsins (as they labelled with both AB5407 and AHBlue) suggesting a changeover from a larval RH2 opsin to a post-metamorphic SWS2 opsin. Such opsin switches are thought to occur during development of winter flounder (Evans *et al*., 1993; Hoke *et al*., 2006) where a single M visual pigment present pre-metamorphosis is replaced by three (S, M, and L) visual pigments, that are novel, post-metamorphosis (Evans *et al*., 1993).

3.4.2. Potential dynamics of square mosaic formation in the retina

In the main (non-peripheral) retina before completion of eye migration, S cones formed a gradient from the central retina, with established square mosaic, to the dorsal retina, characterized by the larval honeycomb mosaic. S cone patterning within the honeycomb mosaic was not random but resembled that of single centre cones closer to the central retina (near the transition region with the square mosaic) and progressively sparser versions further toward the dorsal periphery (i.e., a ratio of 2 for AB5407 labelled cones to S cones in the centrodorsal compared to the central retina). No S cones were

present starting in the mid dorsal retina until the vicinity of the peripheral growth zone, where S cones were again detected but as part of square mosaics.

This gradient-like patterning of honeycomb mosaic S cones together with the observed instances of opsin co-expression, and variable jitter of square mosaics in the main retina (Bolstad & Novales Flamarique, 2022a, Chapter 2), suggests a potential scheme of cell reorganization for square mosaic formation. According to this scheme, individual cones in the larval honeycomb mosaic would switch opsin expression from RH2 to SWS2 while maintaining a minimum distance between them (as suggested by the effective radius of the autocorrelation plots). These cells would then act as markers for surrounding single cones to start coalescing, forming double cones and re-orienting, as necessary. Such a process would be plastic and require differential adhesion between cone types as well as the possibility of short distance migrations, as is common during mammalian retinal development (Reese & Galli-Resta, 2002). The form of communication between neighbouring photoreceptors in establishing the final lattice is not known but gap junctions are present between cone pedicles (O'Brien *et al*., 2004; Li *et al*., 2009) and electrical signalling can also occur through horizontal cells (Wagner, 1975). In addition, temporary contacts between inner segments (Shand *et al*., 1999, 2001) or between accessory outer segments (Bolstad & Novales Flamarique, 2022a; Chapter 2) could also influence the process.

3.4.3. Conclusion

The retina of Atlantic halibut undergoes major changes in opsin expression during metamorphosis that set up a chromatically organized square mosaic lattice throughout most of the juvenile retina. This study informs on potential mechanisms to achieve this in the main (non-peripheral) retina through opsin switching within individual, differentiated cones (surmised from opsin co-expression findings), and the possibility that cone spectral phenotype (as per the S cone gradient in the dorsal retina) may influence square mosaic formation. The random distribution of single, double, and triple cones in the centrodorsotemporal retina suggests that different developmental mechanisms guide photoreceptor formation in this region of the retina.

3.5. References

Bolstad, K., & Novales Flamarique, I. (2022a). Photoreceptor distributions, visual pigments and the opsin repertoire of Atlantic halibut (*Hippoglossus hippoglossus*). *Scientific Reports*, *12*(1), 1–24.

Cheng, C. L., Flamarique, I. N., Hárosi, F. I., Rickers-Haunerland, J., & Haunerland, N. H. (2006). Photoreceptor layer of salmonid fishes: Transformation and loss of single cones in juvenile fish. *Journal of Comparative Neurology*, *495*(2), 213–235.

Dearry, A., & Barlow Jr, R. (1987). Circadian rhythms in the green sunfish retina. *The Journal of General Physiology*, *89*(5), 745–770.

Evans, B. I., Hárosi, F. I., & Fernald, R. D. (1993). Photoreceptor spectral absorbance in larval and adult winter flounder (*Pseudopleuronectes americanus*). *Visual Neuroscience*, *10*(6), 1065–1071.

Forsell, J., Ekström, P., Flamarique, I. N., & Holmqvist, B. (2001). Expression of pineal ultraviolet-and green-like opsins in the pineal organ and retina of teleosts. *Journal of Experimental Biology*, *204*(14), 2517–2525.

Helvik, J. V., Drivenes, Ø., Harboe, T., & Seo, H.-C. (2001). Topography of different photoreceptor cell types in the larval retina of Atlantic halibut (Hippoglossus hippoglossus). *Journal of Experimental Biology*, *204*(14), 2553–2559.

Helvik, J. V., Drivenes, Ø., Næss, T. H., Fjose, A. & Seo, H.-C. (2001). Molecular cloning and characterization of five opsin genes from the marine flatfish Atlantic halibut (*Hippoglossus hippoglossus*). *Visual Neuroscience*, *18*(5), 767–780.

Hoke, K. L., Evans, B. I., & Fernald, R. D. (2006). Remodeling of the cone photoreceptor mosaic during metamorphosis of flounder (*Pseudopleuronectes americanus*). *Brain, Behavior and Evolution*, *68*(4), 241–254.

Kasagi, S., Mizusawa, K., Murakami, N., Andoh, T., Furufuji, S., Kawamura, S., & Takahashi, A. (2015). Molecular and functional characterization of opsins in barfin flounder (*Verasper moseri*). *Gene*, *556*(2), 182–191.

Li, H., Chuang, A. Z., & O'Brien, J. (2009). Photoreceptor coupling is controlled by connexin 35 phosphorylation in zebrafish retina. *Journal of Neuroscience*, *29*(48), 15178–15186.

Molday, R., & MacKenzie, D. (1983). Monoclonal antibodies to rhodopsin: Characterization, cross-reactivity, and application as structural probes. *Biochemistry*, *22*(3), 653–660.

Novales Flamarique, I. N. (2002). Partial re-incorporation of corner cones in the retina of the Atlantic salmon (*Salmo salar*). *Vision Research*, *42*(25), 2737–2745.

Novales Flamarique, I. N., & Hawryshyn, C. W. (1997). No evidence of polarization sensitivity in freshwater sunfish from multi-unit optic nerve recordings. *Vision Research*, *37*(8), 967–973.

Novales Flamarique, I. (2011). Unique photoreceptor arrangements in a fish with polarized light discrimination. *Journal of Comparative Neurology*, *519*(4), 714–737.

Novales Flamarique, I., Fujihara, R., Yazawa, R., Bolstad, K., Gowen, B., & Yoshizaki, G. (2021). Disrupted eye and head development in rainbow trout with reduced ultraviolet (*sws1*) opsin expression. *Journal of Comparative Neurology 529*, 3013–3031.

O'Brien, J., Nguyen, H. B., & Mills, S. L. (2004). Cone photoreceptors in bass retina use two connexins to mediate electrical coupling. *Journal of Neuroscience*, *24*(24), 5632–5642.

Reese, B. E., & Galli-Resta, L. (2002). The role of tangential dispersion in retinal mosaic formation. *Progress in Retinal and Eye Research*, *21*(2), 153–168.

Sato, I., Kasagi, S., Takahashi, A., & Mizusawa, K. (2021). Expression dynamics of visual opsin genes in marbled sole *Pseudopleuronectes yokohamae* during metamorphosis from the larval to the juvenile stage. *Gene*, *787*, 145622.

Savelli, I., & Flamarique, I. N. (2018). Variation in opsin transcript expression explains intraretinal differences in spectral sensitivity of the northern anchovy. *Visual Neuroscience*, *35*.

Savelli, I., Flamarique, I. N., Iwanicki, T., & Taylor, J. S. (2018). Parallel opsin switches in multiple cone types of the starry flounder retina: Tuning visual pigment composition for a demersal life style. *Scientific Reports*, *8*(1), 1–10.

Shand, J., Archer, M. A., & Collin, S. P. (1999). Ontogenetic changes in the retinal photoreceptor mosaic in a fish, the black bream, *Acanthopagrus butcheri*. *Journal of Comparative Neurology*, *412*(2), 203–217.

Shand, J., Archer, M. A., Thomas, N., & Cleary, J. (2001). Retinal development of West Australian dhufish, *Glaucosoma hebraicum*. *Visual Neuroscience*, *18*(5), 711.

Wagner, H.-J. (1975). Comparative analysis of the patterns of receptor and horizontal cells in teleost fishes. In *Vision in fishes* (pp. 517–524). Springer.

Wagner, H.-J. (1990). Retinal structure of fishes. In *The visual system of fish* (pp. 109–157). Springer.

Chapter 4.

General Discussion

In my thesis I examined the retina development of Atlantic halibut during metamorphosis to gain a better understanding of the flatfish retina development, and the potential mechanisms contributing to square mosaic formation.

In Chapter 2, I characterized the spatiotemporal re-organization of photoreceptors, which operates by different mechanisms in the peripheral and central retinas. In addition to the formation of a square mosaic, I characterized a triple cone domain that forms in the centrodorsaltemporal retina, which may play a role in achromatic target detection. I propose that Atlantic halibut have seven visual opsins (*sws1*, *sws2a*, *sws2b*, *rh1*, *rh2b*, *rh2c*, and *lws*).

In Chapter 3, I illustrated that the retina is transformed chromatically as well as morphologically during eye migration. This chromatic re-organization is achieved through opsin switching, suggesting plastic phenotypes of photoreceptors during development. Here I discuss how these retinal transformations prepare the larval halibut for life as a demersal predator and suggest areas for future research.

Section 4.1.1. was adapted from the discussion section in Bolstad, K., & Novales Flamarique, I. (2022b). Chromatic organization of retinal photoreceptors during eye migration of Atlantic halibut (*Hippoglossus hippoglossus*). *Journal of Comparative Neurology*, 1-25.

4.1.1. An evolving area of high visual acuity during metamorphosis

Based on theoretical determinations using ocular dimensions and cone densities, the surmised region of greatest visual acuity progresses from ventrotemporal to dorsotemporal retina during eye migration (Bolstad & Novales Flamarique, 2022a; Chapter 2). Overall, visual acuity increases during this transition, similar to other flatfishes such as plaice (*Pleuronectes platessa*) and turbot (*Scopthalmus maximus*) (Neave, 1984).

At the start of eye migration, halibut larvae are catching prey located in their upper frontal field, much like the larval zebrafish (Yoshimatsu *et al*., 2020). During this stage, larval halibut retinas are characterized by a honeycomb mosaic comprised of single cones, most of which express the RH2 opsin (Bolstad & Novales Flamarique, 2022a,b; Chapters 2 and 3). This honeycomb characterizes the area of greatest visual acuity in the larval retina, yet this mosaic lacks latticed SWS2 cone expression and as such, these larvae are likely detecting prey achromatically, as light reflects off these targets. The single cones in this mosaic are tightly packed, which is common in luminosity based visual systems (Frau *et al*., 2020).

Towards the end of metamorphosis and into the juvenile stage, the halibut begins to search for prey located on the ocean floor (Holmes & Gibson, 1983), where the background is more complex than in the water column and a colour-based, high visual acuity detection system would be favored. This demand is met through the chromatically regular square mosaic of the juvenile retina (Bolstad & Novales Flamarique, 2022b; Chapter 3). Further, the area of greatest visual acuity in the juvenile retina is located inside of the achromatic triple cone domain (centrodorsotemporal region), which may be important for target detection (Bolstad & Novales Flamarique, 2022a; Chapter 2). This combined retinal organization is reminiscent of those found in Starry flounder (Iwanicki *et al*., 2017), and flatfishes in the genus *Solea* (Frau *et al*., 2020), and suggests that both regions of the retina may have evolved as an important system for visually mediated predation as part of a demersal life style.

4.1.2. Discerning the role of SWS2 expression during square mosaic formation: a role for future research

In Chapter 3, I provide evidence for a photoreceptor gradient for the SWS2A opsin in the developing retina, as well as co-expression of RH2 and SWS2 opsins within the same photoreceptors. I suggest that these SWS2A expressing photoreceptors act as a marker for the formation of the square mosaic, however, future studies would need to assess how reduced expression of the SWS2A opsin might impact photoreceptor organization during eye migration.

In barfin flounder and marbled sole, both *sws2a* and *sws2b* are expressed in the larval stage, with *sws2a* expression increasing with age and the opposite occurring for

sws2b (Kasagi *et al*., 2015; Sato *et al*., 2021). Given that these opsins are both expressed during the larval stage, and change expression during development, they may play unique roles during photoreceptor rearrangement, but to date, no studies have assessed the spatial expression of these opsins histologically. Gene knockout or knockdown studies should target *sws2a* and *sws2b* in Atlantic halibut and determine the roles of their protein products during retinal development.

Further, Crumbs protein 2b (Cr2b) is hypothesized to play a role in retinal mosaic formation; this protein is found around SWS2, RH2, and LWS expressing cones (Zou *et al*., 2012), and knockout of this gene leads to a disorganized photoreceptor mosaic in zebrafish retinas (Hao *et al*., 2012). Along with assessing the role of SWS2 opsins during retinal development, future studies should examine whether SWS2 and Cr2b interact to form the square mosaic.

4.1.3. Expression dynamics of predicted opsins: future investigations of patterns with ontogeny and spatial complexity

In Chapter 3, I provided evidence for a chromatically organized retina in Atlantic halibut at the level of SWS2A and RH2. The two subtypes of RH2, RH2B and RH2C were not differentiated between, yet their proposed maximum absorbances differ (RH2B ~506 nm; RH2C ~490 nm), which may have functional consequences during development. While teleosts may switch to the longer-wavelength opsins during development (Novales Flamarique, 2013; Temple *et al*., 2008), Kasagi *et al*. (2015) show that *rh2b* and *rh2c* are both highly expressed in the larval retina. Given that the honeycomb mosaic is present during this stage in Atlantic halibut (Bolstad & Novales Flamarique, 2022a; Chapter 2), expression of more than one subfamily during this stage could add further spatial complexity to the larval retina and may have implications for achromatic detection vs. color- contrast vision (Dalton *et al*., 2017; Iwanicki *et al*., 2017). Future research should quantify the temporal and spatial expression of these opsins during Atlantic halibut retinal development.

4.2. References

Bolstad, K., & Novales Flamarique, I. (2022a). Photoreceptor distributions, visual pigments and the opsin repertoire of Atlantic halibut (*Hippoglossus hippoglossus*). *Scientific Reports*, *12*: 8062.

Bolstad, K., & Novales Flamarique, I. (2022b). Chromatic organization of retinal photoreceptors during eye migration of Atlantic halibut (*Hippoglossus hippoglossus*). *Journal of Comparative Neurology*, 1-25.

Dalton, B. E., De Busserolles, F., Marshall, N. J., & Carleton, K. L. (2017). Retinal specialization through spatially varying cell densities and opsin coexpression in cichlid fish. *Journal of Experimental Biology*, *220*(2), 266–277.

Frau, S., Novales Flamarique, I., Keeley, P. W., Reese, B. E., & Muñoz-Cueto, J. A. (2020). Straying from the flatfish retinal plan: Cone photoreceptor patterning in the common sole (*Solea solea*) and the Senegalese sole (*Solea senegalensis*). *Journal of Comparative Neurology*, *528*(14), 2283–2307.

Holmes, R., & Gibson, R. (1983). A comparison of predatory behaviour in flatfish. *Animal Behaviour*, *31*(4), 1244–1255.

Hao, Q., Zheng, M., Weng, K., Hao, Y., Zhou, Y., Lin, Y., Gao, F., Kou, Z., Kawamura, S., & Yao, K. (2021). Crumbs proteins stabilize the cone mosaics of photoreceptors and improve vision in zebrafish. *Journal of Genetics and Genomics*, *48*(1), 52–62.

Iwanicki, T. W., Novales Flamarique, I., Ausió, J., Morris, E., & Taylor, J. S. (2017). Fine-tuning light sensitivity in the starry flounder (Platichthys stellatus) retina: Regional variation in photoreceptor cell morphology and opsin gene expression. *Journal of Comparative Neurology*, *525*(10), 2328–2342.

Kasagi, S., Mizusawa, K., Murakami, N., Andoh, T., Furufuji, S., Kawamura, S., & Takahashi, A. (2015). Molecular and functional characterization of opsins in barfin flounder (*Verasper moseri*). *Gene*, *556*(2), 182–191.

Neave, D. (1984). The development of visual acuity in larval plaice and turbot. *J. Exp. Mar. Biol. Ecol.*, *78*, 167–175.

Novales Flamarique, I. (2013). Opsin switch reveals function of the ultraviolet cone in fish foraging. *Proceedings of the Royal Society B: Biological Sciences*, *280*(1752), 20122490.

Sato, I., Kasagi, S., Takahashi, A., & Mizusawa, K. (2021). Expression dynamics of visual opsin genes in marbled sole *Pseudopleuronectes yokohamae* during metamorphosis from the larval to the juvenile stage. *Gene*, *787*, 145622.

Temple, S., Veldhoen, K., Phelan, J., Veldhoen, N., & Hawryshyn, C. (2008). Ontogenetic changes in photoreceptor opsin gene expression in coho salmon (*Oncorhynchus kisutch*, Walbaum). *Journal of Experimental Biology*, *211*(24), 3879–3888.

Yoshimatsu, T., Schröder, C., Nevala, N. E., Berens, P., & Baden, T. (2020). Fovea-like photoreceptor specializations underlie single UV cone driven prey-capture behavior in zebrafish. *Neuron*, *107*(2), 320–337.

Zou, J., Wang, X., & Wei, X. (2012). *Crb* apical polarity proteins maintain zebrafish retinal cone mosaics via intercellular binding of their extracellular domains. *Developmental Cell*, *22*(6), 1261–1274.

Appendix A.

Opsin Prediction in Atlantic halibut

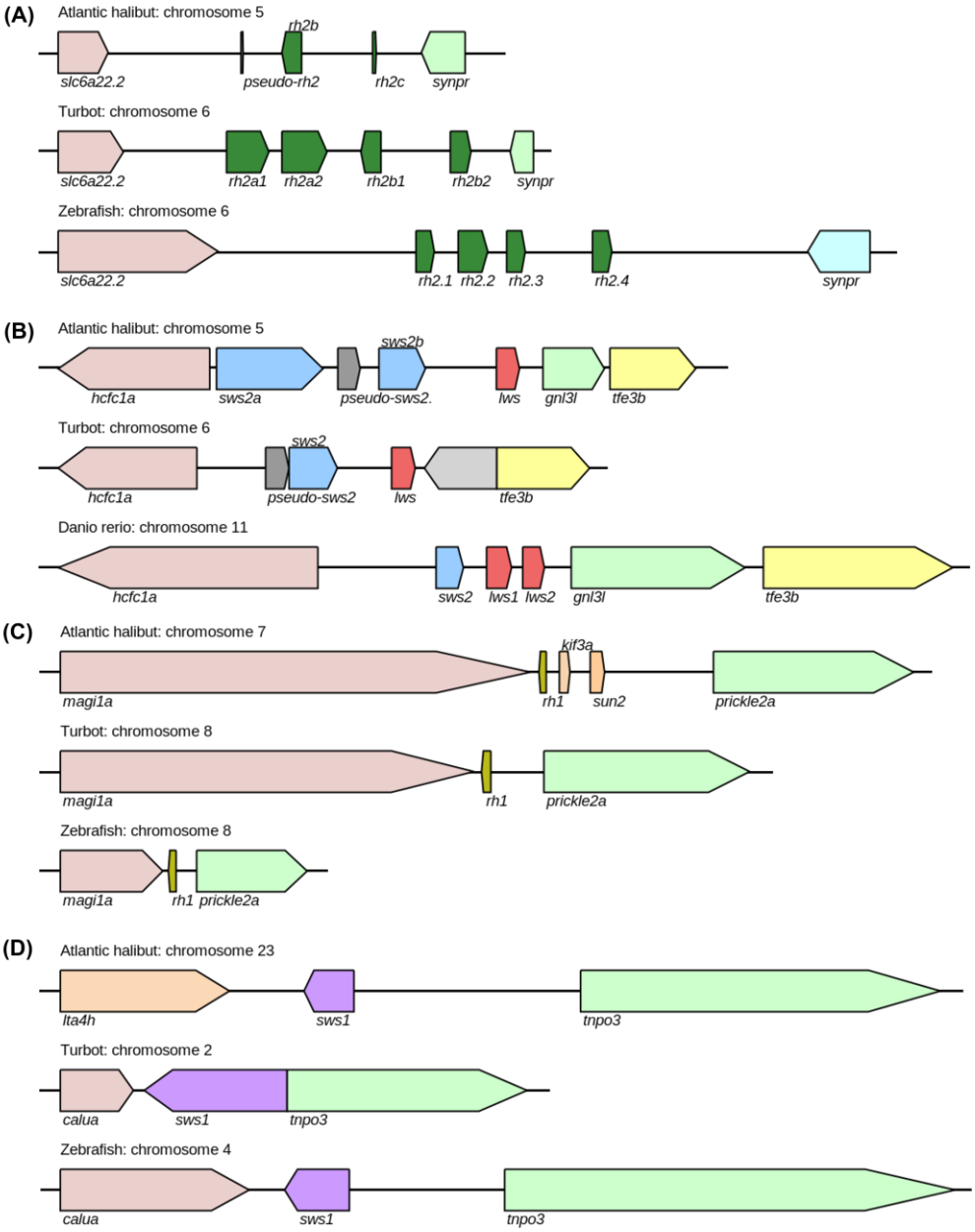

Figure A1. Locations of predicted opsin coding sequences and their immediate flanking genes in Atlantic halibut (*Hippoglossus hippoglossus*) compared to turbot (*Scophthalmus maximus*) and zebrafish (*Danio rerio*) for (A) *rh2* (B) *sws2* and *lws*, (C) *rh1*, and (D) *sws1*.

Note: The *sws2-lws* gene cluster in turbot does not include *gnl3l* as the immediate flanking gene in the current NCBI annotation, rather an uncharacterized protein (shown in grey). As such, for the *sws2-lws* gene cluster, two downstream flanking genes were shown.

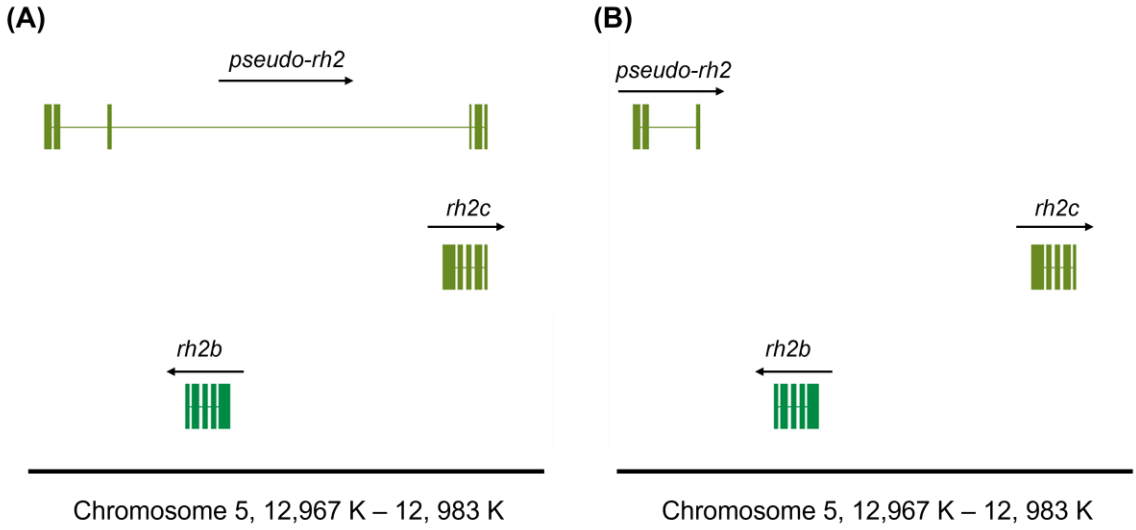

Figure A2. Predicted rh2 sequences in Atlantic halibut.
Note: (A) One of the predicted sequences (XP_034442261.1; *pseudo-rh2*) overlaps with the other two *rh2* sequences (accessions: XP_034442261.1 and XP_034442262.1) and has six exons, which is unusual for teleost *rh2* opsins. As such, we hypothesize that this sequence is a *pseudo-rh2* gene. (B) Refined *rh2* sequence structures, where only the first three exons of the *pseudo-rh2* sequence is retained. Opsin names included in this figure follow those that were assigned after phylogenetic analysis.

Table A1. NCBI and SoleaDB protein accession numbers used in this study.
Note: Previously predicted opsins[1] from Atlantic halibut (*Hippoglossus hippoglossus*) are also included.

Organism	Common name	Opsin name	Protein accession
Danio rerio	Zebrafish	SWS1	NP_571394.1
		SWS2	NP_571267.1
		RH1	NP_571159.1
		RH2.1	NP_571328.2
		RH2.2	NP_878311.1
		RH2.3	NP_878312.1
		RH2.4	NP_571329.1
		LWS.1	NP_001300644.1
		LWS.2	NP_001002443.1
Hippoglossus hippoglossus[1]	Atlantic halibut	SWS1	AAM17917.1
		SWS2	AAM17920.1
		RH1	AAM17918.1
		RH2	AAM17916.1
		LWS	AAM17921.1
Paralichthys olivaceus	Japanese flounder	SWS1	BAW35575.1
		SWS2A	BAW35586
		SWS2B	BAW35589
		RH1	BAW35583.1
		RH2A1	BAW79257.1
		RH2A2	BAW79258.1
		RH2B	BAW35578.1
		RH2C	BAW35580.1
		LWS	BAW35572.1
Pseudopleuronectes yokohamae	Marbled sole	SWS1	BCL84791.1
		SWS2A	BCL84789.1
		SWS2B	BCL84790.1
		RH1	BCL84792.1
		RH2A	BCL84786.1
		RH2B	BCL84787.1
		RH2C	BCL84788.1
		LWS	BCL84785.1
Scophthalmus maximus	Turbot	SWS1	AWO98359.1
		SWS2	AWP03347.1
		RH1	QDY91961
		RH2A1	QDY91963.1
		RH2A2	QDY91964.1
		RH2B1	QDY91965.1
		RH2B2	QDY91966.1

Organism	Common name	Opsin name	Protein accession
		RH2C	QDY91967.1
		LWS	AAQ02802.1
Solea senegalensis	Senegalese sole	SWS2	solea_v4.0_unigene481685
		RH1	solea_v4.1_unigene22024
		RH2.3	solea_v4.0_unigene28898
		RH2.4	solea_v4.0_unigene416478
		LWS	solea_v4.0_unigene34221
Solea solea	Common sole	SWS2	solea_solea_v1.1_unigene342597
		RH1	solea_solea_v1.1_unigene42150
		RH2.3	solea_solea_v1.0_unigene71547
		RH2.4	solea_solea_v1.0_unigene94070
		LWS	solea_solea_v1.1_unigene189057
Verasper variegatus	Spotted halibut	SWS1	BAW35573.1
		SWS2A	BAW35584
		SWS2B	BAW35587
		RH1	BAW35581.1
		RH2B	BAW35576.1
		RH2C	BAW35579.1
		LWS	BAW35570.1
Verasper moseri	Barfin flounder	SWS1	BAO93915.1
		SWS2A	BAO93916
		SWS2B	BAO93917
		RH1	BAO93912.1
		RH2B	BAO93913.1
		RH2C	BAO93914.1
		LWS	BAO93911.1

[1]Einfeldt, A. L., Kess, T., Messmer, A., Duffy, S., Wringe, B. F., Fisher, J., den Heyer, C., Bradbury, I. R., Ruzzante, D. E., & Bentzen, P. (2021). Chromosome level reference of Atlantic halibut *Hippoglossus hippoglossus* provides insight into the evolution of sexual determination systems. *Molecular Ecology Resources*, *21*(5), 1686–1696.

Table A2. Predicted opsins from the Atlantic halibut reference genome[1] generated from BLASTp queries of zebrafish opsins (e-value < 1e-5, percent identity ≥50%).

Note: Included in the table are the opsin subclasses assigned after phylogenetic analysis.

Opsin class	Opsin subclass	Protein accession	CDS chromosome: location	Gene ID
SWS1	SWS1	XP_034434209.1	23 (complement): 18,346,408 to 18,348,321	*opn1sw1*
SWS2	SWS2A	XP_034440595.1	5: 23,451,385 to 23,452,968	*LOC117761093*
	SWS2B	XP_034441481.1	5: 23,458,711 to 23,462,900	*LOC117761574*
RH1	RH1	XP_034445498.1	7 (complement): 19,548,054 to 19,549,112	*LOC117764105*
RH2	RH2B	XP_034442261.1	5 (complement): 12,972,356 to 12,973,875	*LOC117761967*
	RH2C	XP_034442262.1	5: 12,981,421 to 12,982,946	*LOC117761968*
	pseudo-RH2	XP_034442263.1	5: 12,967,537 to 12,982,946	
LWS	LWS	XP_034441780.1	5: 23,469,900 to 23,471,991	*LOC117761719*

[1]Einfeldt, A. L., Kess, T., Messmer, A., Duffy, S., Wringe, B. F., Fisher, J., den Heyer, C., Bradbury, I. R., Ruzzante, D. E., & Bentzen, P. (2021). Chromosome level reference of Atlantic halibut *Hippoglossus hippoglossus* provides insight into the evolution of sexual determination systems. *Molecular Ecology Resources*, *21*(5), 1686–1696.

Table A3. Opsins initially predicted by BLASTp queries of the Atlantic halibut reference genome[1] with zebrafish opsins.

Note: These predicted proteins were eliminated from further analyses after examination of their sequence structure and location. Note that the predicted opsin corresponding to RH1 (accession: XP_034447460.1) is actually an exo-rhodopsin protein but was initially classified as an RH1-like protein.

Opsin class	Protein accession	Reason for elimination
SWS1	XP_034434208.1	Two SWS1 proteins are predicted from the same region of the genome. Compared to zebrafish SWS1, this protein has a lower percent identity (62%) and query cover (81%) than the other protein (73% and 97%, respectively).
SWS2	XP_034440596.1	Two SWS2 proteins are predicted from the same genomic region. The proteins have comparable percent identities and query covers to Zebrafish SWS2, but the sequence corresponding to this protein has a 5' UTR region approximately 8.4 Mbp upstream of the first exon.
RH1	XP_034447460.1	Contains introns similar to exo-rhodopsin (*exorh)*, found in pineal glands of teleosts such as zebrafish[2] and Atlantic halibut[3].

[1]Einfeldt, A. L., Kess, T., Messmer, A., Duffy, S., Wringe, B. F., Fisher, J., den Heyer, C., Bradbury, I. R., Ruzzante, D. E., & Bentzen, P. (2021). Chromosome level reference of Atlantic halibut *Hippoglossus hippoglossus* provides insight into the evolution of sexual determination systems. *Molecular Ecology Resources*, *21*(5), 1686–1696.

[2]Eilertsen, M., Drivenes, Ø., Edvardsen, R. B., Bradley, C. A., Ebbesson, L. O., & Helvik, J. V. (2014). Exorhodopsin and melanopsin systems in the pineal complex and brain at early developmental stages of Atlantic halibut (*Hippoglossus hippoglossus*). *Journal of Comparative Neurology*, *522*(18), 4003–4022.

[3]Mano, H., Kojima, D., & Fukada, Y. (1999). Exo-rhodopsin: A novel rhodopsin expressed in the zebrafish pineal gland. *Molecular Brain Research*, *73*(1–2), 110–118.

Table A4. Predicted opsin proteins from Atlantic halibut compared to corresponding visual opsins in zebrafish and nonvisual opsins from Atlantic halibut and zebrafish.

Note: Disulfide bridges are noted by C110 and C187, the chromophore binding site by K296, counterion residue at site 113, and motifs at sites 134-136[1]. See Tables A1 and A5 for accession numbers. Predicted opsin names follow those assigned after phylogenetic analysis.

Opsin class	Species	C110	E113 or Y113	ERW 134-136	C187	K296
SWS1	Atlantic halibut SWS1	C	E	ERY	C	K
	Zebrafish	C	E	ERY	C	K
SWS2	Atlantic halibut SWS2A	C	E	ERW	C	K
	Atlantic halibut SWS2B	C	E	ERW	C	K
	Zebrafish	C	E	ERW	C	K
RH1	Atlantic halibut RH1	C	E	ERW	C	K
	Zebrafish RH1	C	E	ERW	C	K
RH2	Atlantic halibut RH2B	C	E	ERY	C	K
	Atlantic halibut RH2C	C	E	ERY	C	K
	Zebrafish RH2.1	C	E	ERY	C	K
	Zebrafish RH2.2	C	E	ERY	C	K
	Zebrafish RH2.3	C	E	ERY	C	K
	Zebrafish RH2.4	C	E	ERY	C	K
LWS	Atlantic halibut LWS	C	E	ERW	C	K
	Zebrafish LWS.1	C	E	ERW	C	K
	Zebrafish LWS.2	C	E	ERW	C	K
OPN4M1/ Melanopsin-1	Atlantic halibut	C	Y	DRY	C	K
	Zebrafish	C	Y	DRY	C	K
OPN4XB	Atlantic halibut	C	Y	DRY	C	K
OPN4XB	Zebrafish	C	Y	DRY	C	K
TMT OPN3A	Atlantic halibut	C	Y	ERY	C	K
	Zebrafish	C	Y	ERY	C	K

[1] Davies, W. I., Tamai, T. K., Zheng, L., Fu, J. K., Rihel, J., Foster, R. G., Whitmore, D., & Hankins, M. W. (2015). An extended family of novel vertebrate photopigments is widely expressed and displays a diversity of function. *Genome Research*, *25*(11), 1666–1679.

Table A5. Non- visual opsin protein accession numbers obtained from NCBI.

Nonvisual opsin name	Species	Protein accession
OPN4M1/ melanopsin-1	Atlantic halibut	AIG92840.1
	Zebrafish	ADN39430.1
OPN4XB	Atlantic halibut	XP_034451267.1
	Zebrafish	NP_001245152.1
Teleost multiple tissue opsin 3a (TMT OPN3A)	Atlantic halibut	XP_034453944.1
	Zebrafish	NP_001269303.1
VA opsin	Zebrafish	NP_571661.1

Table A6. Predicted opsin proteins compared to published opsin proteins from Atlantic halibut[1].

Note: Predicted opsin names follow those assigned after phylogenetic analysis.

Published opsin	Predicted opsin	Opsin accession	No. of amino acids	Percent identity	Query cover (%)	E-value
SWS1	SWS1	XP_034434209.1	339	100	100	0
SWS2	SWS2A	XP_034440595.1	353	99	100	0
	SWS2B	XP_034441481.1	353	75	100	0
RH1	RH1	XP_034445498.1	352	100	100	0
RH2	RH2B	XP_034442261.1	352	100	100	0
	RH2C	XP_034442262.1	352	86	100	0
LWS	LWS	XP_034441780.1	357	99	100	0

[1]Helvik, J. V., Drivenes, Ø., Næss, T. H., Fjose, A. & Seo, H.-C. (2001). Molecular cloning and characterization of five opsin genes from the marine flatfish Atlantic halibut (*Hippoglossus hippoglossus*). *Visual Neuroscience*, *18*(5), 767–780.

Table A7. Amino acid sequence identity between predicted and published[1] Atlantic halibut opsins.

Note: Predicted opsins with an identity ≥ 70% to published opsins are bolded. Predicted opsin names follow those assigned after phylogenetic analysis.

Predicted opsins	Published Atlantic halibut opsins				
	SWS1	SWS2	RH1	RH2	LWS
SWS1	**100**	46	47	48	45
SWS2A	47	**99**	49	54	42
SWS2B	46	**75**	50	52	41
RH1	46	50	**100**	62	38
RH2B	48	53	61	**100**	45
RH2C	50	53	61	**86**	45
LWS	45	42	39	45	**99**

[1]Helvik, J. V., Drivenes, Ø., Næss, T. H., Fjose, A. & Seo, H.-C. (2001). Molecular cloning and characterization of five opsin genes from the marine flatfish Atlantic halibut (*Hippoglossus hippoglossus*). *Visual Neuroscience*, *18*(5), 767–780.

Table A8. Key amino acid tuning sites for *sws1* opsins[1-3].

Note: All amino acid sites reported are standardized to bovine rhodopsin.

Opsin name	Species	46	49	52	86	90	93	114	118
Predicted	Atlantic halibut SWS1	S	F	T	F	S	Q	S	S
SWS1	Japanese flounder	S	F	T	F	S	Q	S	S
	Spotted halibut	S	F	T	F	S	Q	S	S
	Barfin flounder	S	F	T	F	S	Q	S	S
	Marbled sole	C	F	T	F	S	Q	S	S
	Turbot	F	F	T	F	S	Q	A	S
	Zebrafish	F	I	T	F	S	Q	A	S

[1]Yokoyama, S. (2008). Evolution of dim-light and color vision pigments. *Annu. Rev. Genomics Hum. Genet*., *9*, 259–282.

[2]Nakamura, Y., Mori, K., Saitoh, K., Oshima, K., Mekuchi, M., Sugaya, T., Shigenobu, Y., Ojima, N., Muta, S., & Fujiwara, A. (2013). Evolutionary changes of multiple visual pigment genes in the complete genome of Pacific bluefin tuna. *Proceedings of the National Academy of Sciences*, *110*(27), 11061–11066.

[3] Wang, Y., Zhou, L., Wu, L., Song, C., Ma, X., Xu, S., Du, T., Li, X., & Li, J. (2021). Evolutionary ecology of the visual opsin gene sequence and its expression in turbot (*Scophthalmus maximus*). *BMC Ecology and Evolution*, *21*(1), 1–12.

Table A9. Key amino acid tuning sites for *sws2* opsins[1,2].
Note: All amino acid sites reported are standardized to bovine rhodopsin.

Opsin Name	Species	46	52	91	93	94	116	269	292
Predicted	Atlantic halibut SWS2A	F	T	S	V	G	M	A	S
	Atlantic halibut SWS2B	F	T	S	T	C	T	A	S
SWS2A	Japanese flounder	F	T	S	V	G	M	A	A
	Spotted halibut	F	T	S	V	G	M	T	A
	Barfin flounder	F	T	S	V	G	M	T	A
	Marbled sole	F	T	S	V	G	M	A	A
SWS2B	Japanese flounder	F	T	S	T	C	T	A	S
	Spotted halibut	F	T	S	T	C	T	A	S
	Barfin flounder	F	T	S	T	C	T	A	S
	Marbled sole	F	S	S	T	C	T	A	S
SWS2	Common sole	I	S	T	V	G	M	A	A
	Senegalese sole	F	T	S	T	A	M	T	S
	Turbot	F	T	S	T	C	S	A	S
	Zebrafish	F	T	S	V	A	T	A	S

[1]Yokoyama, S. (2008). Evolution of dim-light and color vision pigments. *Annu. Rev. Genomics Hum. Genet*., *9*, 259–282.

[2]Nakamura, Y., Mori, K., Saitoh, K., Oshima, K., Mekuchi, M., Sugaya, T., Shigenobu, Y., Ojima, N., Muta, S., & Fujiwara, A. (2013). Evolutionary changes of multiple visual pigment genes in the complete genome of Pacific bluefin tuna. *Proceedings of the National Academy of Sciences*, *110*(27), 11061–11066.

Table A10. Key amino acid tuning sites for *rh2* opsins[1-3].
Note: All amino acid sites reported are standardized to bovine rhodopsin.

Opsin name	Species	49	52	97	122	207	292
Predicted	Atlantic halibut RH2B	C	T	S	E	M	A
	Atlantic halibut RH2C	C	T	T	Q	L	A
RH2A1	Japanese flounder	C	F	S	Q	M	A
	Turbot	C	F	S	Q	L	A
RH2A2	Japanese flounder	C	F	T	Q	M	A
	Turbot	C	F	T	Q	M	A
RH2A	Marbled sole	C	T	S	Q	M	A
RH2B1	Turbot	C	T	S	E	M	A
RH2B2	Turbot	C	T	S	E	M	A
RH2B	Japanese flounder	C	T	S	E	M	A
	Spotted halibut	C	T	S	E	M	A
	Barfin flounder	C	T	S	E	M	A
	Marbled sole	C	T	S	E	M	A
RH2C	Japanese flounder	C	T	S	Q	L	A
	Spotted halibut	C	T	T	Q	L	A
	Barfin flounder	C	T	T	Q	L	A
	Marbled sole	C	T	T	Q	L	A
	Turbot	C	T	S	Q	L	A
RH2.1	Zebrafish	I	F	C	Q	M	A
RH2.2	Zebrafish	C	L	C	Q	M	A
RH2.3	Zebrafish	C	F	T	Q	M	A
	Common sole	C	L	T	Q	M	A
	Senegalese sole	S	L	T	Q	M	A
RH2.4	Zebrafish	C	F	T	E	M	A
	Common sole	C	T	S	E	M	A
	Senegalese sole	C	T	S	E	M	A

[1]Yokoyama, S. (2008). Evolution of dim-light and color vision pigments. *Annu. Rev. Genomics Hum. Genet*., *9*, 259–282.

[2]Nakamura, Y., Mori, K., Saitoh, K., Oshima, K., Mekuchi, M., Sugaya, T., Shigenobu, Y., Ojima, N., Muta, S., & Fujiwara, A. (2013). Evolutionary changes of multiple visual pigment genes in the complete genome of Pacific bluefin tuna. *Proceedings of the National Academy of Sciences*, *110*(27), 11061–11066.

[3] Wang, Y., Zhou, L., Wu, L., Song, C., Ma, X., Xu, S., Du, T., Li, X., & Li, J. (2021). Evolutionary ecology of the visual opsin gene sequence and its expression in turbot (*Scophthalmus maximus*). *BMC Ecology and Evolution*, *21*(1), 1–12.

Table A11. Key amino acid tuning sites for *lws* opsins[1-3].
Note: All amino acid sites reported are standardized to bovine rhodopsin.

Opsin name	Species	164	181	261	269	292
Predicted	Atlantic halibut LWS	S	H	Y	T	A
LWS	Japanese flounder	A	H	Y	T	A
	Spotted halibut	A	H	Y	T	A
	Barfin flounder	A	H	Y	T	A
	Marbled sole	S	H	Y	T	A
	Turbot	P	H	Y	T	A
	Common sole	A	H	Y	T	A
	Senegalese sole	A	H	Y	T	A
LWS.1	Zebrafish	A	H	Y	T	A
LWS.2	Zebrafish	A	H	F	T	A

[1]Yokoyama, S. (2008). Evolution of dim-light and color vision pigments. *Annu. Rev. Genomics Hum. Genet*., *9*, 259–282.

[2]Nakamura, Y., Mori, K., Saitoh, K., Oshima, K., Mekuchi, M., Sugaya, T., Shigenobu, Y., Ojima, N., Muta, S., & Fujiwara, A. (2013). Evolutionary changes of multiple visual pigment genes in the complete genome of Pacific bluefin tuna. *Proceedings of the National Academy of Sciences*, *110*(27), 11061–11066.

[3] Wang, Y., Zhou, L., Wu, L., Song, C., Ma, X., Xu, S., Du, T., Li, X., & Li, J. (2021). Evolutionary ecology of the visual opsin gene sequence and its expression in turbot (*Scophthalmus maximus*). *BMC Ecology and Evolution*, *21*(1), 1–12.

Table A12. Key amino acid tuning sites for *rh1* opsins[1-4].
Note: All amino acid sites reported are standardized to bovine rhodopsin. The following acronyms are used for each species: AH (Atlantic halibut), JF (Japanese flounder), SH (Spotted halibut), BF (Barfin flounder), MS (Marbled sole), TB (Turbot), CS (Common sole), SS (Senegalese sole).

Opsin name	Predicted AH RH1	Rh1 JF	SH	BF	MS	TB	CS	SS	ZB
83	N	N	N	N	D	N	N	N	D
90	G	G	G	G	G	G	G	G	G
96	Y	Y	Y	Y	Y	Y	Y	Y	Y
102	Y	Y	Y	Y	Y	Y	Y	Y	Y
113	E	E	E	E	E	E	E	E	E
118	T	T	T	T	T	T	T	T	T
122	E	E	E	E	E	E	E	E	E
124	G	A	A	A	S	G	G	A	G
132	A	A	A	A	A	A	A	A	A
164	A	A	A	A	A	A	A	A	A
183	M	M	M	M	M	M	M	M	M
194	R	R	R	R	R	R	R	R	R
195	A	A	A	A	A	A	A	A	T
207	M	M	M	M	M	M	M	M	M
208	F	F	F	F	F	F	F	F	F
211	H	H	H	H	H	H	H	H	H
214	I	I	I	I	I	I	I	I	I

Opsin name	Predicted AH RH1	Rh1 JF	SH	BF	MS	TB	CS	SS	ZB
253	M	M	M	M	M	M	M	M	M
261	F	F	F	F	F	F	F	F	F
265	W	W	W	W	W	W	W	W	W
269	A	A	A	A	A	A	A	A	A
289	T	T	T	T	T	T	T	T	T
292	A	A	A	A	A	A	A	A	A
295	A	A	A	A	A	A	A	A	A
299	A	S	A	A	A	S	S	S	A
300	V	I	V	V	I	I	I	I	V

[1]Yokoyama, S. (2008). Evolution of dim-light and color vision pigments. *Annu. Rev. Genomics Hum. Genet*., *9*, 259–282.

[2]Nakamura, Y., Mori, K., Saitoh, K., Oshima, K., Mekuchi, M., Sugaya, T., Shigenobu, Y., Ojima, N., Muta, S., & Fujiwara, A. (2013). Evolutionary changes of multiple visual pigment genes in the complete genome of Pacific bluefin tuna. *Proceedings of the National Academy of Sciences*, *110*(27), 11061–11066.

[3] Wang, Y., Zhou, L., Wu, L., Song, C., Ma, X., Xu, S., Du, T., Li, X., & Li, J. (2021). Evolutionary ecology of the visual opsin gene sequence and its expression in turbot (*Scophthalmus maximus*). *BMC Ecology and Evolution*, *21*(1), 1–12.

[4] Musilova, Z., Cortesi, F., Matschiner, M., Davies, W. I., Patel, J. S., Stieb, S. M., de Busserolles, F., Malmstrøm, M., Tørresen, O. K., & Brown, C. J. (2019). Vision using multiple distinct rod opsins in deep-sea fishes. *Science*, *364*(6440), 588–592.

Table A13. Predicted λmax for Atlantic halibut visual opsins based off of variable amino acid tuning sites.

Note: Residue number is standardized to bovine rhodopsin.

Opsin Name	Reference λmax (nm)	Amino acid substitutions at tuning sites (±nm shift in λ_{max})	Predicted λmax (nm)
SWS1	367 nm[1]	--	~367 nm
SWS2A	465.6 nm[2]	A292S (-8 nm)[3]	~457.6 nm
SWS2B	416 nm[1]	--	~ 416 nm
RH1	494 nm[1]	--	~494 nm
RH2B	506 nm[1]	--	~506 nm
RH2C	490 nm[1]	--	~490 nm
LWS	552 nm[1]	A164S (2-6 nm)[3]	~554-558 nm

1Kasagi, S., Mizusawa, K., Murakami, N., Andoh, T., Furufuji, S., Kawamura, S., & Takahashi, A. (2015). Molecular and functional characterization of opsins in barfin flounder (*Verasper moseri*). *Gene*, *556*(2), 182–191.

2Kasagi, S., Mizusawa, K., & Takahashi, A. (2018). Green-shifting of SWS 2A opsin sensitivity and loss of function of RH 2-A opsin in flounders, genus *Verasper*. *Ecology and Evolution*, *8*(2), 1399–1410.

3Takahashi, Y., & Ebrey, T. G. (2003). Molecular basis of spectral tuning in the newt short wavelength sensitive visual pigment. *Biochemistry*, *42*(20), 6025–6034.

Appendix B.

Atlantic halibut peripheral photoreceptor mosaic

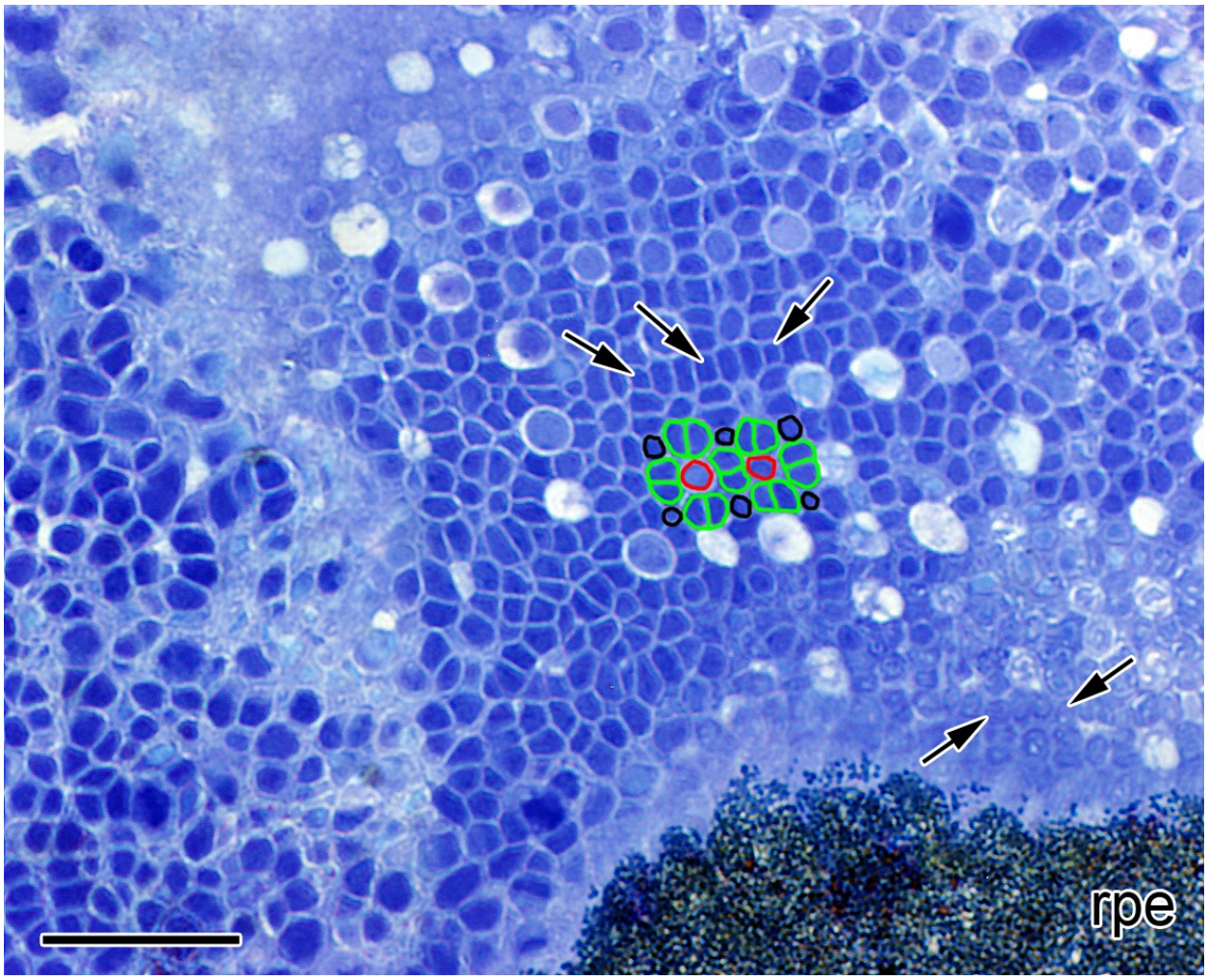

Figure A3. Micrograph of Atlantic halibut retinal peripheral growth zone.

Note: The contours of two unit mosaics are traced showing double cones (green), single centre cones (red) and single corner cones (black). Black arrows point to other single corner cones. Abbreviation: rpe, retinal pigment epithelium. Magnification bar = 10μm.

Appendix C.

Reconstructed retinal micrographs of Atlantic halibut at 773 ATU

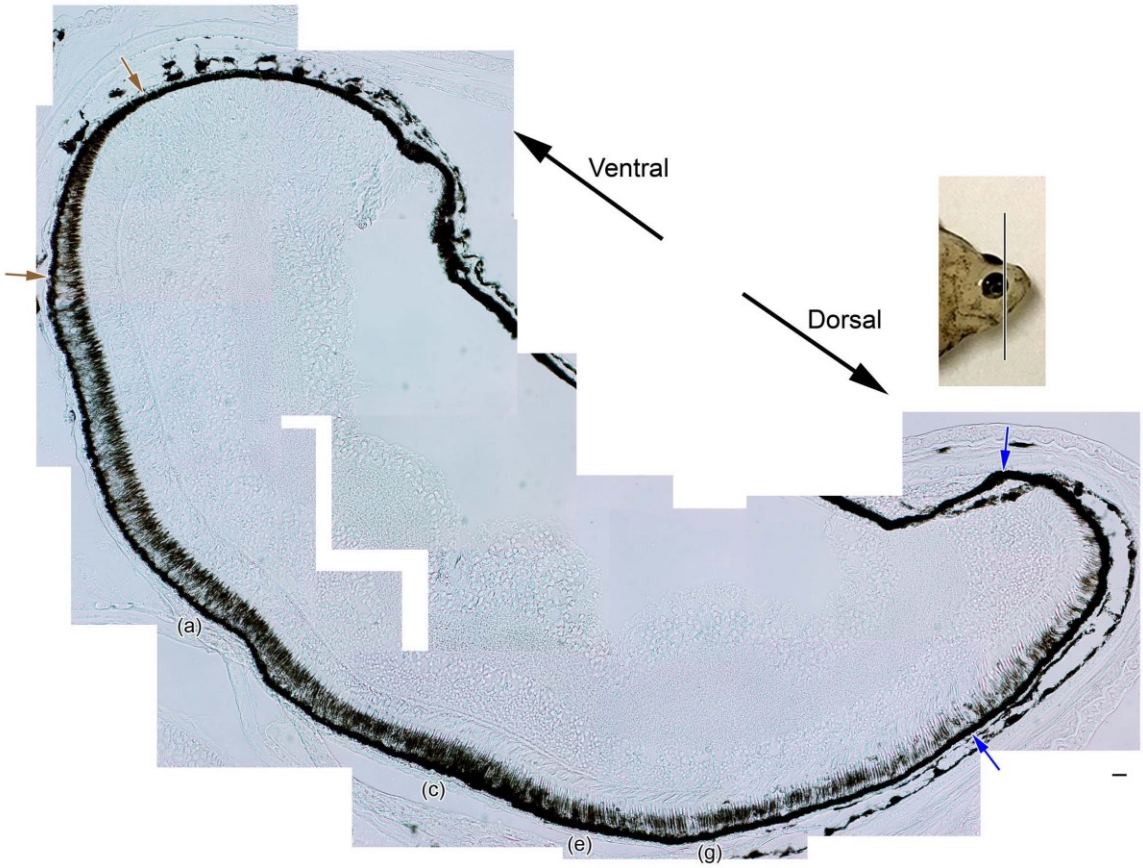

Figure C1. Reconstructed retina from a coronal cut of the head of Atlantic halibut, nasal to the lens, at 773 ATU.

Note: The photograph of the fish head on the right side shows the level of cut (vertical line). The ventral retina has double cones whereas the upper dorsal retina shows primarily single cones. A highly packed area of cones spans the central part of the retina. The most ventral region (stretch between the two brown arrows) and the most dorsal region (stretch between the two blue arrows) are shown at higher magnification in Figure 3.4. Letters ((a),(c),(e),(g)) mark corresponding areas shown at higher magnification in Figure 3.5. The scale bar at the bottom right = 10 µm.

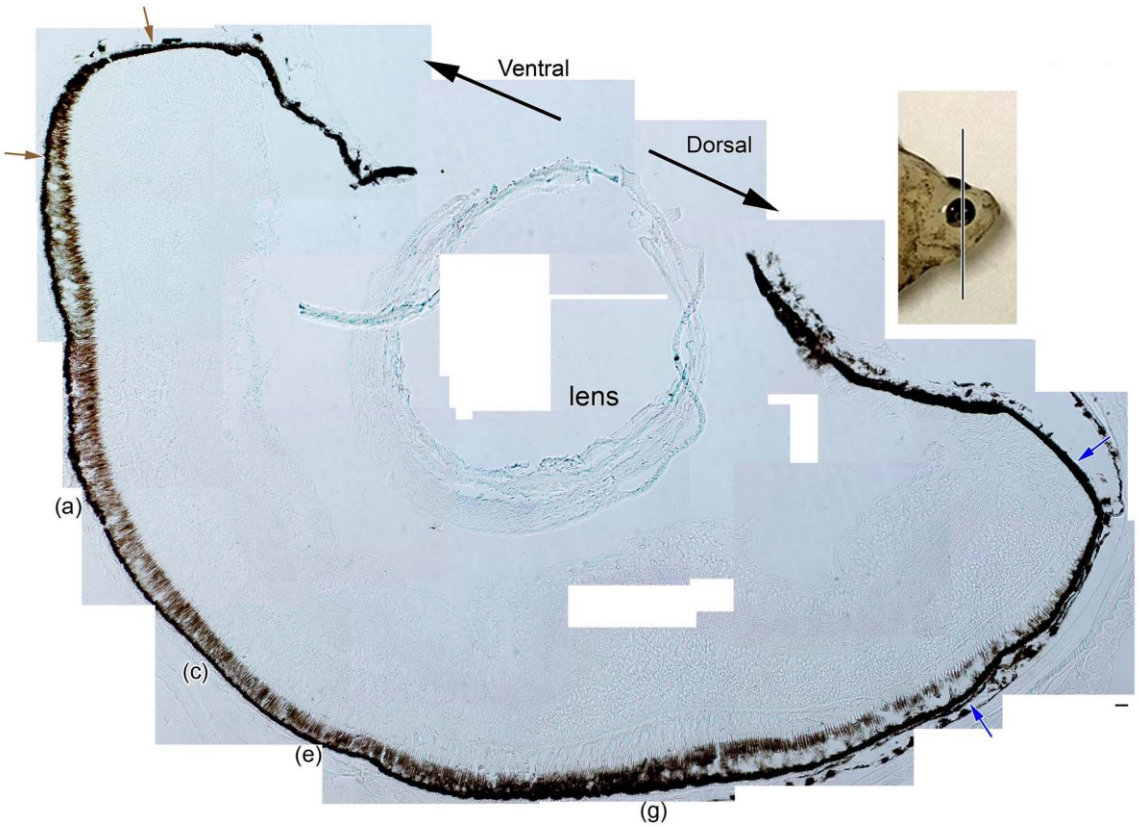

Figure C2. Reconstructed retina from a coronal cut of the head of Atlantic halibut at 773 ATU at the level of the lens.

Note: The photograph of the fish head on the right side shows the level of cut (vertical line). Similar patterns to those in Figure C1 in terms of cone types and packing from ventral to dorsal retina are present with the exception that double cones are prominent in the dorsal periphery and triple cones occur in the central retina. The most ventral region (stretch between the two brown arrows) and the most dorsal region (stretch between the two blue arrows) are shown at higher magnification in Figure 3.6. Letters ((a),(c),(e),(g)) mark corresponding areas shown at higher magnification in Figure 3.7. The scale bar at the bottom right = 10 µm.

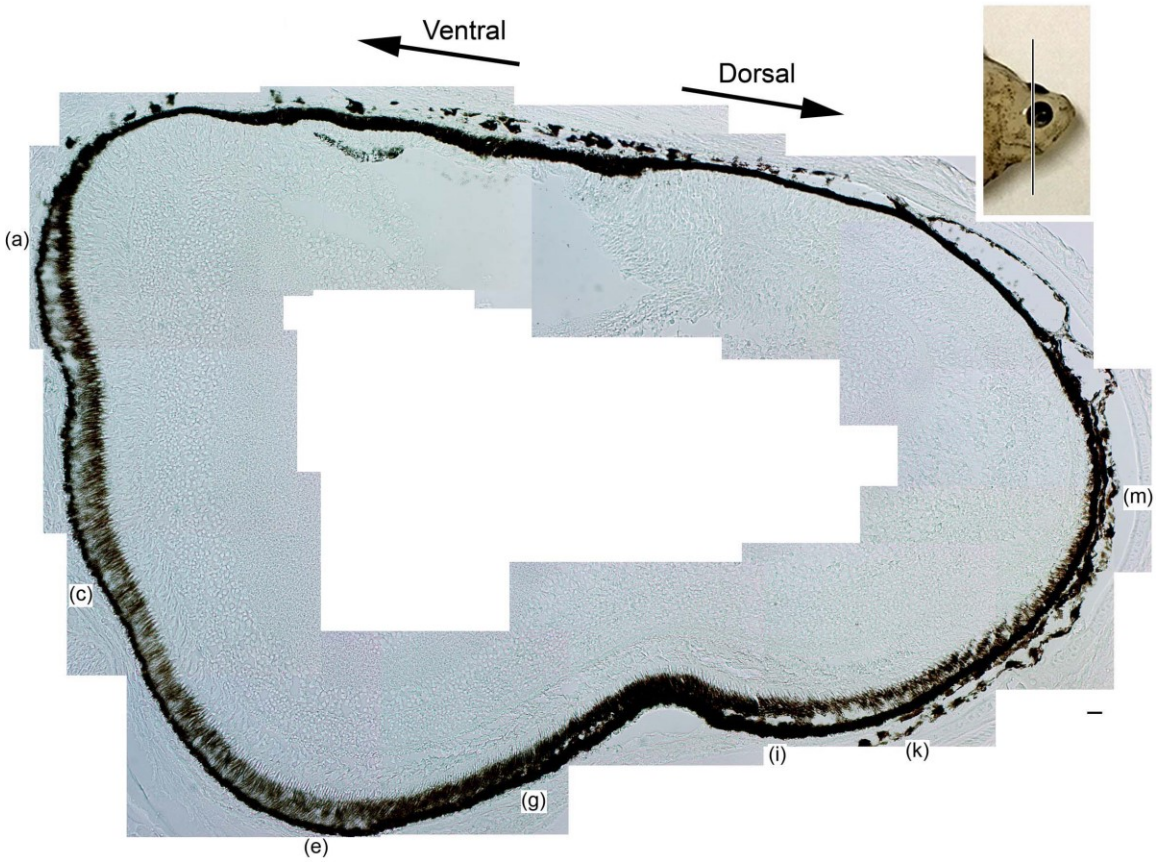

Figure C3. Reconstructed retina from a coronal cut of the head of Atlantic halibut, temporal to the lens, at 773 ATU.

Note: The photograph of the fish head on the right side shows the level of cut (vertical line). Double cones are present throughout this region of retina. Letters ((a),(c),(e),(g),(i),(k),(m)) mark corresponding areas shown at higher magnification in Figure 3.8. The scale bar at the bottom right = 10 µm.